Unveiling long-term changes in river flow regimes across Northern Italy

BY

Arman MOHAMMADI

ENVIRONMENTAL AND LAND ENGINEERING-CLIMATE CHANGE

Department of Environment, Land and Infrastructure Engineering

This thesis is presented as part of the requirements for the

Award of the degree of the Master of Science

Supervisors:

Dr. Paola MAZZOGLIO

Prof. Alberto VIGLIONE

Dr. Miriam BERTOLA

October 2025

Declaration

This project report is submitted in partial fulfillment of the requirements for the degree of Master of Engineering in Environmental and Land Engineering.
I declare that this thesis was composed by me, that the work contained herein is my own, except where explicitly stated otherwise in the text, and that it has not been submitted, in whole or in part, for any other degree or professional qualification.

Arman Mohammadi

This thesis was conducted under the supervision of Dr. Paola Mazzoglio, Prof. Alberto Viglione from Politecnico di Torino and Dr. Miriam Bertola from Technische Universität Wien.

Abstract

This thesis investigates long term changes in river discharge across 22 Piedmont catchments in northwestern Italy and tests their consistency with trends in precipitation, temperature, and potential evapotranspiration (PET). Daily flows were aggregated to annual, seasonal, and monthly scales. Trends were assessed with the Mann–Kendall (MK) test and Sen's slope.

Summer low flows decline clearly during the July and August minima. This marks stronger drought stress. These declines persist into early autumn. High-flow indicators do not rise uniformly; annual and seasonal maxima do not show a clear trend, so flood change appears less systematic in the Piedmont than in nearby Mediterranean basins. Temperature and PET increase strongly at all time scales, with the steepest slopes in summer. Precipitation is weak and spatially variable, with modest summer declines and no consistent autumn rise.

These signals identify warming-driven atmospheric demand as the main climatic control on discharge change, with physiography amplifying outcomes. Alpine headwaters show earlier snowmelt and smaller spring to summer contributions. Lowland rivers combine alpine inflows with higher evaporative losses and local demand. Foothill tributaries sit between these two.

The study shows that by applying a nonparametric framework to both hydrological and climatic variables, climate forcing is already reshaping Piedmont river flow regimes. This study adds details through analysis of the trends at monthly resolution to better understand regime changes. The results highlight the need for stronger drought resilience while keeping proportionate flood preparedness.

Acknowledgment

I would like to thank my supervisors, Paola Mazzoglio, Alberto Viglione, and Miriam Bertola at TU Wien, as well as my professors at the DIATI Department at Politecnico di Torino, for their guidance, encouragement, and patient feedback throughout my master's program and this research.

I owe my greatest thanks to my family and close friends for their steady support, patience, and faith in me during the inevitable ups and downs of this project. Any errors or omissions are mine alone.

Contents

List of Figures

List of Tables

Chapter 1

Introduction

1.1 Introduction

River flows have a significant influence on ecological sustainability, resource management, and infrastructure planning. Understanding changes in these flow regimes, especially in the face of climate variability and anthropogenic pressures, is crucial for informed water resource management. Changes in discharge affect both the frequency of droughts and the magnitude of floods, with direct implications for society and the environment. Nowadays, climate change is already altering many hydrological processes across Europe. River discharges are one of these important hydrological series. Long-term studies report decreases in summer low flows (Stahl et al., 2010), earlier snow melt and reduced spring contributions in Alpine basins (Parajka and Blöschl, 2010; Mallucci et al., 2019), and regionally flood regime changes on the European scale (Blöschl et al., 2019).

Northern Italy, particularly Piedmont, is situated on the border that separates the Alpine and Mediterranean regions. The area is consequently subject to several climatic pressures, such as decreases in snow storage and increasing summer evapotranspiration (Brussolo et al., 2022). These make the region highly sensitive to climate variability and change. Meanwhile, its rivers are used for irrigation, power, and supply (Ouassanouan et al., 2022), which adds more reasons to possible flow regime changes. With this background mentioned, there is also a growing need to analyze long-term changes in discharge and their relationships with climatic drivers. Detection of such trends provides a basis for adaptation, drought planning, risk assessment, and water availability planning.

1.2 Problem Statement and Research Gap

Multiple studies have examined long-term hydrological changes in Europe, specifically in Alpine catchments and Northern Italy, and often at annual or seasonal indices and large-scale syntheses (Stahl et al., 2010; Blöschl et al., 2019; Mallucci et al., 2019; Montanari et al., 2023). In Piedmont specifically, existing assessments tend to emphasize annual trends or seasonal totals. Although these are highly informative in the regional context, they may yield little insight into monthly dynamics (Montanari, 2012). This does leave open basic questions about the timing of changes, e.g., whether summer low-flow stress is localized in particular months, and whether flood-related indicators show coherent changes in autumn.

The management relevance of this gap is clear. Planning for droughts, floods, and water availability within the year depends on understanding the direction of change and how it changes within the year. The 2022 Po River drought, reported as the most severe in two centuries, shows how summer deficits can escalate into basin-wide crises when both non-climatic (such as human demand) and climatic forcing effects happen together (Montanari et al., 2023). At the same time, flood responses in Italy are known to be highly regional and conditioned by physiography and the dominant flood-generating mechanisms (Blöschl et al., 2019).

In Piedmont, there is a lack of station-based analysis of trends at a monthly resolution, as well as their relation with climatic driver changes (such as precipitation, temperature, potential evapotranspiration) across physiographic units (Alpine, pre-Alpine (foothill), low-land). Addressing this gap may be a good practice for drought planning, environmental flow management, irrigation plans, and proportionate flood-risk management.

1.3 Structure of the Thesis

To investigate these changes, we need a methodology to detect variations in both discharge and climatic time series. In the next chapter, a summary of the literature on relatively simple and most used trend-detection methodologies, particularly the Mann-Kendall test and the Sen's slope estimator, will be discussed. In Chapter 3, a brief review of previous researches on streamflow trends in Europe and Northern Italy are discussed, drawing on regional studies in Northern Italy and broader comparative studies across Europe. Chapter 4 presents the

data and methodology, and the results of the analysis are presented in Chapter 5. Then relationship between discharge trends and climatic trends across scales will be discussed, and in the final chapter, the key findings and recommendations for future studies are presented.

Chapter 2

Most Used Trend Detection Methods in Hydrology

2.1 Introduction

Hydrological time series are raw observations that can help us understand the responses of river basins to climatic variability and human activities. Some of these time series include mean daily discharge, annual flood peaks, winter and summer low-flow indices, groundwater levels, and water quality indices, among others. To observe any changes in these datasets, we need identification of statistically significant trends in them, for climate change detection (IPCC, 2021), as well as updating design criteria for flood risk management, navigation planning, and water supply planning.

"Trend" is defined as a non-random, systematic change with time in one or a number of attributes of the distribution, such as the central tendency, variability, chosen quantiles, or even timing (Hirsch et al., 1982). Most European measurements are limited to after 1950 and have gaps (Blöschl et al., 2019). Therefore, distinguishing actual trends might be complicated and can lead to a loss of statistical power. In some cases, the existence of serial correlation can artificially rise apparent significance unless we control it (Hamed and Rao, 1998), and also non-stationary human effects such as flow regulation, land use or land cover change, abstraction with time of groundwater, and interbasin transfer can mask or mimic climatic signals (Mallucci et al., 2019; Nunno et al., 2024).

Those challenges need to be addressed. So, hydrologists use a toolkit of methods to identify

monotonic trends, step shifts, and shifts in variability of the hydrological timeseries. Best practice is to implement a quality control protocol that can deal with any serial dependency, to deploy robust rank-based tests such as Mann–Kendall in combination with Sen's slope, and to identify field significance at network scales (Yue and Wang, 2004a). This chapter reviews that landscape by briefly introducing some popular trend detection methods.

2.2 Classical Non-Parametric Tests

Non-parametric rank-based tests are widely used in hydrological trend analysis since they do not assume a certain distribution for the data. They are robust against outliers and work reasonably well with records at coarse precision (Kundzewicz and Robson, 2004). The methodology's core is the Mann–Kendall family of statistics, supplemented with Sen's slope estimator for magnitude and a collection of pre-whitening correction methods for serial dependency.

2.2.1 Mann–Kendall (MK) Test

This method determines whether values tend to be larger at later times than earlier times, without assuming any specific distribution. The MK method counts the balance between increasing and decreasing pairs and standardizes that count. In other words, for each pair (Q_i, Q_j) with $j > i$, vote $+1$ if $Q_j > Q_i$, -1 if $Q_j < Q_i$, and 0 if equal. With no monotonic trend, ups and downs cancel on average; a surplus of positive (increasing) or negative (decreasing) values indicates the direction of the trend (Mann, 1945; Kendall, 1975; Hirsch and Slack, 1984).

Its formal definition is: for $\{Q_1, \ldots, Q_n\}$,

$$S = \sum_{i=1}^{n-1} \sum_{j=i+1}^{n} \operatorname{sgn}(Q_j - Q_i), \quad \operatorname{sgn}(x) = \begin{cases} +1 & x > 0 \\ 0 & x = 0 \\ -1 & x < 0 \end{cases},$$

with variance

$$\operatorname{Var}(S) = \frac{n(n-1)(2n+5) - \sum_k t_k(t_k-1)(2t_k+5)}{18},$$

where t_k is the size of kth tie group. The standardized statistic is

$$Z = \begin{cases} \dfrac{S-1}{\sqrt{\mathrm{Var}(S)}} & S > 0 \\ 0 & S = 0 \\ \dfrac{S+1}{\sqrt{\mathrm{Var}(S)}} & S < 0 \ . \end{cases}$$

For measurements $Q_1, \ldots, Q_n$, the quantity S is sum of signs of all pairwise differences $Q_j - Q_i$ for $j > i$. Under the null hypothesis of no monotonic trend and independence, S has a mean of zero. When calculating the variance, a tie correction is applied, which is important for hydrological records with zeros or rounded data. The standardized score Z is roughly normally distributed for moderate samples. For very short series, exact probabilities are preferred (Helsel and Hirsch, 2002).

Seasonal extension. Pooling across months or seasons can mask the trends that exist in hydrological time series. The Seasonal Kendall test is a common extension (Hirsch et al., 1982) that applies MK separately to each of m seasons (often $m = 12$ months), producing $\{S_s, \mathrm{Var}(S_s)\}_{s=1}^{m}$, and then aggregates to a single overall test:

$$S_{\mathrm{tot}} = \sum_{s=1}^{m} S_s, \qquad \mathrm{Var}_{\mathrm{tot}} = \sum_{s=1}^{m} \mathrm{Var}(S_s),$$

with Z computed from S_{tot} and $\mathrm{Var}_{\mathrm{tot}}$ as above. This keeps power in strongly seasonal settings and reduces cancellation when some months trend upward while others trend downward. In this way, it preserves power while controlling type I error under strong seasonality.

Power and robustness. In hydrology, MK is used as it has high efficiency relative to other methods, such as parametric t-tests for monotonic alternatives. It is robust to outliers and rounding, but loses power for step shifts. In this case, the change-point tests are advisable to use. These kinds of tests are useful when a regime shift is suspected (Yue and Wang, 2004b). MK is paired with Sen's slope to report trend magnitude.

2.2.2 Sen's Slope Estimator

Sen's slope (Sen, 1968) estimates trend magnitude by taking the median of the slopes formed by all ordered pairs in the series.

$$\hat{\beta} = \text{median}\left\{\frac{Q_j - Q_i}{j - i} : 1 \leq i < j \leq n\right\}.$$

The estimator is rank-based and often called the Theil–Sen method. It handles the outliers and non-normal errors and pairs naturally with MK. MK shows the presence of a monotonic trend, and Sen's slope reports how large it is in units of the variable per unit time. Also, some studies report the percentage change per decade, which may be clearer if a relative rate is provided. Confidence intervals use the MK variance to obtain index bounds on the ordered set of $N' = n(n-1)/2$ slopes. Let

$$C_\alpha = Z_{1-\alpha/2}\sqrt{\text{Var}(S)}.$$

Define

$$M_1 = \left\lceil \frac{N' - C_\alpha}{2} \right\rceil, \qquad M_2 = \left\lceil \frac{N' + C_\alpha}{2} \right\rceil,$$

and take the (M_1)th and (M_2)th ordered slopes as the $(1-\alpha)$ interval limits (Sen, 1968; Gilbert, 1987). Reporting $\hat{\beta}$ with its 95% confidence interval shows both statistical and practical significance (e.g.,% per decade).

2.2.3 Handling Serial Correlation

Positive autocorrelation increases the actual variance of the MK statistic. If it is ignored, then p-values tend to be too small (Hamed and Rao, 1998). In the literature review, two fixes are commonly used.

Modified MK. The general modified MK adjusts the Mann–Kendall variance using a variance inflation factor based on estimated autocorrelation. This lowers the chance of detecting a false trend caused by serial dependence (Hamed and Rao, 1998). Other studies estimate autocorrelation on a detrended series, preferably using ranks. In the Modified Mann–Kendall

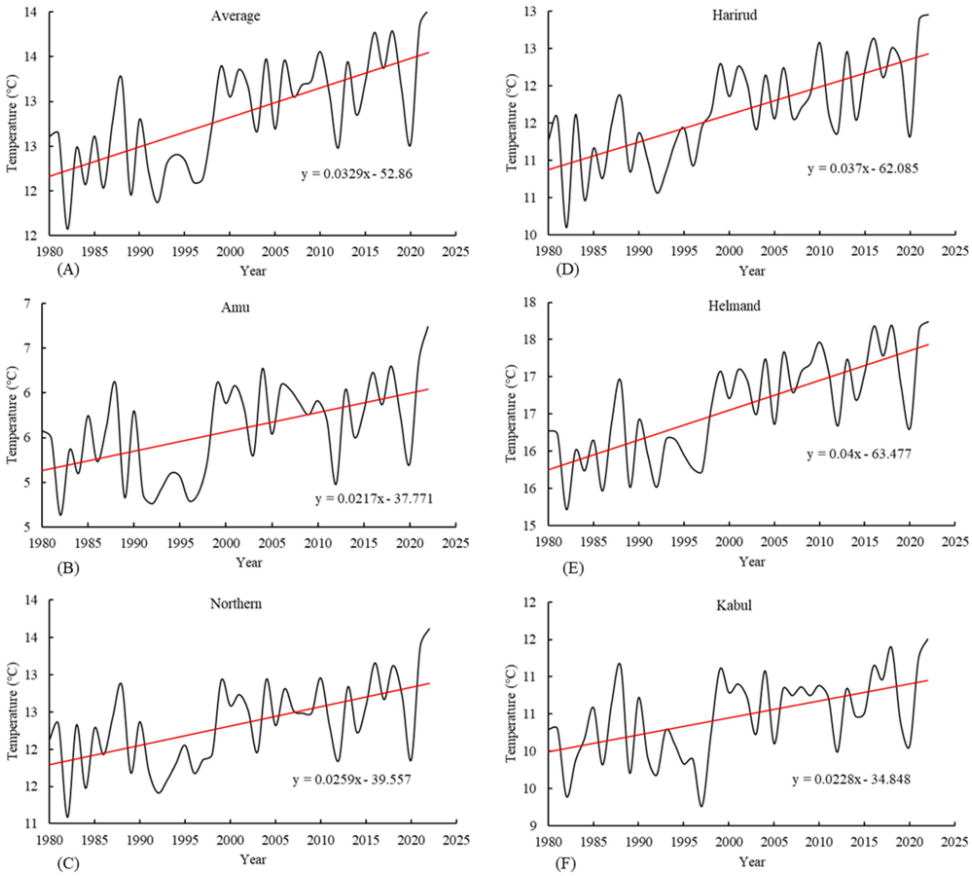

Figure 2.1: Example of Mann–Kendall trend detection with Sen's slope applied to mean annual temperature in six Afghan river basins (1980–2022). Black lines show observed series; red lines indicate Sen's slope trend estimates. Adapted from Akhundzadah (2024).

test using an effective sample size, the nominal n is replaced by an effective size n^* that accounts for short-lag autocorrelation. Assume ρ_k to be the sample autocorrelation at lag k of the (detrended) series, truncated at the largest k with a significant ρ_k. The effective sample size is defined as:

$$n^* = \frac{n}{1 + 2\sum_{k=1}^{K}\left(1 - \frac{k}{n}\right)\rho_k},$$

With this change, the MK variance is multiplied by n/n^*, ($\mathrm{Var}^*(S) = \mathrm{Var}(S) \cdot \frac{n}{n^*}$).The test becomes more conservative (conservative Z) and Sen's slope does not change (Yue and Wang, 2004b).

Trend-free prewhitening (TFPW). TFPW is used to reduce autocorrelation without disturbing the underlying trend of the timeseries, which matters for tests like the Mann–Kendall (MK). The workflow is simple, as follows: estimate a provisional trend and subtract it; apply

prewhitening to the detrended series; then add the trend back. This separates the effect of short-term dependence from the real trend signal. It reduces false positives and can enhance the power to detect changes. As a result, trend detection tests are more reliable when autocorrelation is present (Yue and Wang, 2004b; Collaud Coen et al., 2020).

2.3 Parametric and Regression-Based Approaches

Parametric models specify a functional relationship between time and discharge, or some other hydrological variables. They provide an estimate of the rate of change (on annual, seasonal, and monthly scales) along with intervals or confidence limits. They also allow covariates, transformations, and flexible error forms. In hydrological trend detection studies, simple or log-linear Ordinary Least Squares (OLS) regression, quantile regression, and Generalized Least Squares (GLS) are the methods most frequently used.

2.3.1 Simple and Log-Linear Regression

Simple Linear regression is a common parametric tool in hydrology, easy to interpret, and can quantify how hydrological variables, such as river flow, change with time. It works simply by fitting a straight line that estimates the average rate of change over an assumed timescale, e.g, annual. A straight-line model such as

$$Q_t = \beta_0 + \beta_1 t + \varepsilon_t,$$

where t is time (for example, in years), offers an easily interpreted slope β_1 (change per unit time). It assumes linearity and constant variance, so it works well for detecting overall upward or downward trends in mean flows. Streamflow variance typically increases with magnitude and has a skewed distribution, so logarithmic transformations are often applied before fitting the linear model. Therefore, the residuals meet the normality and homoscedasticity assumptions of the OLS model. When these assumptions hold, the t-test (as a parametric inference tool) on β_1 is robust and often aligns with MK. However, the method is sensitive to outliers and non-normal errors (Draper and Smith, 1998; Helsel and Hirsch, 2002).

2.3.2 Quantile Regression (QR)

Koenker and Bassett (1978) introduced Quantile regression. This method fits specified quantiles (e.g., the 5th, 50th, and 95th percentiles) instead of the mean. Even when the median is steady, QR is an ideal method for detecting divergent trends in low-flow and high-flow tails. This method is not based on normally distributed errors, and it is robust to heteroscedasticity. QR also tends to be less powerful when sample sizes are small (Tarr, 2012).

2.3.3 Generalized Least Squares (GLS)

Generalized least squares (GLS) is a parametric regression method that extends OLS by modeling autocorrelation and changes in variance in the residuals. When residuals are auto-correlated, OLS standard errors are biased. GLS corrects this by explicitly modelling the error covariance structure, usually as an Autoregressive (AR) and Autoregressive Moving Average (ARMA) processes, and produces valid confidence intervals. When errors exhibit complex patterns and are correlated, as is typical in hydrological data, GLS can complement simple linear and quantile regression by providing more reliable inference. (Hamed and Rao, 1998; von Storch and Zwiers, 1999).

2.4 Change Point and Step Shift Detection

When hydrological records contain abrupt regime shifts, monotonic tests like the Mann-Kendall (MK) can lead to misleading results. Therefore, pairing MK with change-point detection tools could be useful. A brief explanation of some of these tools is as follows:

- **Pettitt**: it is nonparametric rank-based, with no distributional assumptions, with good power for a single sudden shift. However it cannot identify multiple breaks. In addition, seasonality and autocorrelation may reduce nominal accuracy (Pettitt, 1979).
- **Buishand range test**: this test is based on cumulative deviations from the mean and assumes independent normal errors. It is commonly used for annual totals (Buishand, 1984).

- **CUSUM (Cumulative Sum) / CUSUMSQ (Cumulative Sum of Squares)**: these tests monitor cumulative sums of deviations and squared deviations. Using the bootstrap significance methods, it accommodates autocorrelation (Alexandersson, 1986).

- **Multiple breaks (Bai–Perron, PELT)**: these are piecewise linear segmentations with model selection criteria that can detect multiple abrupt changes. They should be combined with GLS or robust errors if serial dependence is present (Bai and Perron, 2003; Killick et al., 2012).

These methods enhance our ability to detect and describe shifts in hydrological regimes that result from climate and non-climatic variability.

2.5 Field Significance and Spatial Correlation

In the previous sections, we introduced the most commonly used methods for testing the existence and direction of trends in hydrological records, including river flow records. These tests are designed to detect trends at each gauging station. To determine whether the trend is significant for a broader region or if it is just noise in some stations, we use the field significance method. It is a regional assessment test that measures multiple gauges simultaneously. If each series is tested at $\alpha = 0.05$, about 5% will look significant by chance even when there is no real trend. Neighbouring catchments are also correlated. So we use spatially consistent resampling as a complementary control.

Spatially consistent resampling Gauging stations in the same region tend to be spatially correlated because they share climate, terrain, and flow controls. Therefore, simple aggregation of the significance indicator is not appropriate. To handle this dependence, we can use a spatially consistent resampling method. Assume I_s as the significance indicator

$$I_s = \begin{cases} 1, & \text{if } p_s < \alpha \\ 0, & \text{otherwise} \end{cases} \quad \text{for } s = 1, \ldots, S,$$

where p_s is the p-value at station s and S is the number of stations. The observed fraction of significant stations is

$$F_{\text{obs}} = \frac{1}{S}\sum_{s=1}^{S} I_s.$$

To build the null distribution of F, permute years jointly across all stations, preserving spatial dependence (Livezey and Chen, 1983). With B Monte Carlo resamples, the field p-value is

$$p_{\text{field}} = \frac{1 + \sum_{b=1}^{B} \mathbf{1}(F_b \geq F_{\text{obs}})}{1 + B}.$$

B is the number of Monte Carlo resamples used to approximate the null distribution by resampling.

Field-wide validation is vital for large domains. For spatially clustered stations, local rejections are likely false unless the regional pattern is considered. In mapping flood discharge trends over Europe, Blöschl et al. (2019) identified from a total of 3,738 gauges coherent regional signals despite localized variability (Figure 2.2).

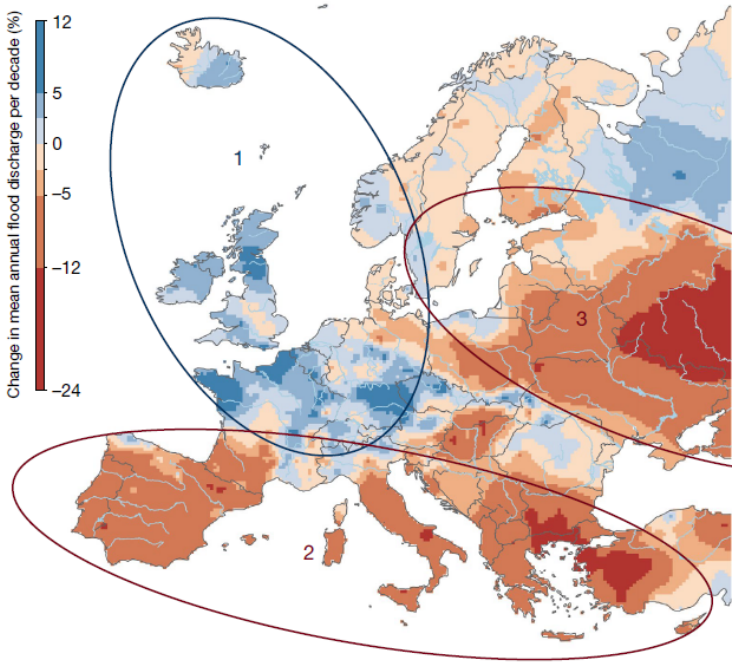

Figure 2.2: Observed regional trends of river flood discharges in Europe (1960–2010). Blue indicates increasing mean annual flood discharges, expressed as a percentage change per decade, and red indicates decreasing mean annual flood discharges. Regions 1–3 mark distinct drivers: 1. Northwestern Europe: increasing rainfall and soil moisture, 2. Southern Europe: decreasing rainfall and increasing evaporation, 3. Eastern Europe: decreasing and earlier snowmelt. Adapted from Blöschl et al. (2019).

2.6 Decision Rationale for This research

We use MK with Sen's slope as the main framework. These methods are non-parametric, handle outliers and rounding, work with some missing data, and are commonly used in European streamflow studies, which lets us compare with earlier work. Trend magnitudes are given by Sen's slope with confidence intervals.

Chapter 3

Previous Research on Streamflow Trends in Europe and Northern Italy

3.1 Introduction

Over the past few decades, substantial research has been conducted on streamflow trends across Europe. These studies range from broad pan-continental assessments to detailed analyses of Alpine, Mediterranean, and Italian catchments. These investigations reveal diverse patterns in river flow regimes, including the magnitude, frequency, and timing of river flows, which are caused by a combination of climatic and non-climatic factors.

This chapter synthesises the existing researches in two parts. The first part provides an overview of observed hydrological changes in Europe and Northern Italy, including general trends in streamflow, floods, and low flows or droughts. The second part provides an overview of the drivers of the changes. These drivers are distinguished as climatic drivers, including trends in rainfall, rise in air temperatures, potential evapotranspiration, and alterations in snow regimes, among others, and non-climatic drivers, including changes in land use, water abstraction, and flow regulation. Together, these two perspectives provide the framework for the trend analysis conducted in this thesis.

3.2 Part 1: Observed Streamflow Trends

The discussion focuses on three themes: general streamflow trends, including annual and seasonal variations, changes in flood magnitude, frequency, and timing, as well as trends in low flows and drought occurrence. The primary focus will be on studies conducted on the continental, Alpine, and Northern Italian scales.

3.2.1 Observed General Streamflow Trends

Starting from a continental scale, Stahl et al. (2010) presented one of the first coordinated assessments of near-natural streamflow trends in Europe. They analysed 441 small catchments from 15 countries for the period of 1962 to 2004 using the Kendall–Theil robust line. Results showed a clear north-south gradient in annual flow, with increases common in northern, western, and central Europe, while decreases prevailed in southern and eastern regions. The monthly view added detail. Winter flows (October to March) rose across much of northern, western, and central Europe. Declines were widespread from April to September. Low flow behaviour also varied by season. In snow-dominated regions such as the Alps, winter low flows generally increased. In most basins with summer minima, summer low flows decreased. Many central European basins also saw earlier summer low flows, consistent with earlier snowmelt and reduced summer baseflow.

Focusing on the Alpine domain, Bard et al. (2015) analysed 177 daily streamflow series from snowmelt-dominated catchments, including sites in Northern Italy. They used indices for low, medium, and snowmelt-related high flows. The results reveal that winter droughts generally became less severe, with shorter durations and smaller deficits. An exception was the snowmelt rainfall regime, where severity increased. Also, snowmelt-driven high flows started earlier and lasted longer. Lower percentiles of the flow-duration curve declined in the southern and eastern Alps. This points to reduced spring and summer flows. In contrast, higher percentiles rose in snowmelt rainfall regimes.

Bocchiola et al. (2014) examined 23 Alpine rivers (including Northern Italy), from 1921 to 2011, and found a broad decline in annual discharge, with additional decreases in spring and summer. They linked these shifts to large-scale climate modes, such as the North Atlantic Oscillation, in conjunction with local patterns of precipitation and temperature. Likewise,

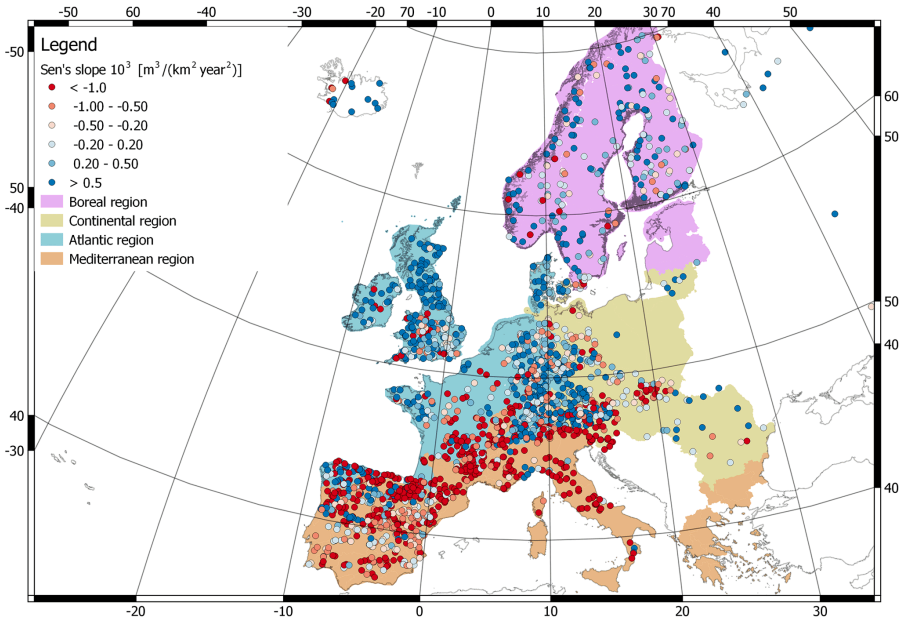

Figure 3.1: Long-term changes in annual streamflow across Europe, 1950–2013. Red points indicate decreasing trends, and blue points indicate increasing trends, estimated using Sen's slope. The map shows a clear north-south gradient, with declines in southern Europe, including Northern Italy, and increases in northern regions. Adapted from Masseroni et al. (2021).

Balistrocchi et al. (2021) reported significant drops in mean annual runoff in the Central Italian Alps, based on records from five major rivers, including multi-century series for the Adda and Adige. They attributed the decline not to precipitation change (annual precipitation trends were not significant) but to higher hydrological losses from rising temperatures and extensive afforestation since the mid-twentieth century.

3.2.2 Observed Flood Trends

At the continental scale, Blöschl et al. (2019) produced the widest spatial analysis of European flood discharges so far, using 3,738 gauging stations (1960–2010). They identified distinct regional patterns in them, including increases in northwestern Europe linked to enhanced precipitation and soil moisture, and decreases in southern and eastern Europe, including Northern Italy, associated with reduced precipitation, higher evapotranspiration, and diminished snowmelt. Figure 2.2 (see Chapter 2, Section 2.5), illustrates these flood patterns in Europe, where Blöschl et al. (2019) mapped annual flood discharge trends across 3,738 European stations (1960–2010). In southern Europe, mean flood discharge showed

about 5% decline per decade, a trend consistent with regional climate drivers. The change aligns with model projections of future flood hazards, highlighting the value of incorporating climate signals into flood risk management.

Bertola et al. (2020) used a nonstationary regional flood-frequency method to distinguish between changes in small (Q_2) and large (Q_{100}) floods at 2,370 stations. Across southern Europe, including northern Italy, significant reductions were apparent for small floods, while weak or no significant trends were observed for large floods. The research attributes these decreases to lower precipitation, increased evapotranspiration, and alterations in soil moisture.

Focusing on Alpine catchments, Mangini et al. (2018) studied Annual Maximum Flood (AMF) and Peak Over Threshold (POT) time series for 629 stations in the period 1965 to 2005. Over the entire Alpine region, including major northern Italian rivers such as the Po and Adige, they found general decreases in flood sizes south of the major Alpine watershed and significant decreases in flood frequencies at all POT thresholds.

Long-term records at Pontelagoscuro on the Po River provide further evidence for Northern Italy. Zanchettin et al. (2014) reported a marked and more than three weeks per century shift toward earlier spring discharge peaks. They found that these changes are mainly driven by a change in precipitation seasonality, characterized by a larger winter share and a higher fraction falling as liquid precipitation. Sakamuri et al. (2025)'s work indicates mixed but generally negative trends in annual maximum precipitation and streamflow for small Po Basin rivers, while large rivers show weakly positive or nonsignificant trends. These results suggest scale dependence in flood trends.

3.2.3 Observed Low Flow and Drought Trends

On the pan-European scale, Stahl et al. (2010) reported persistent spatial patterns of low-flow behavior across 441 near-natural catchments (1962–2004). Winter low flows increased in snow-dominated catchments, such as the Alps and northern Scandinavia, under conditions of milder winters and mid-winter snowmelt. Conversely, summer low flows decreased at most summer-minimum catchments over central and southern Europe, typically occurring earlier in the year. The timing of the 7-day summer low flow was earlier in most central European basins, in line with earlier summer snowmelt and higher summer evapotranspiration. Such

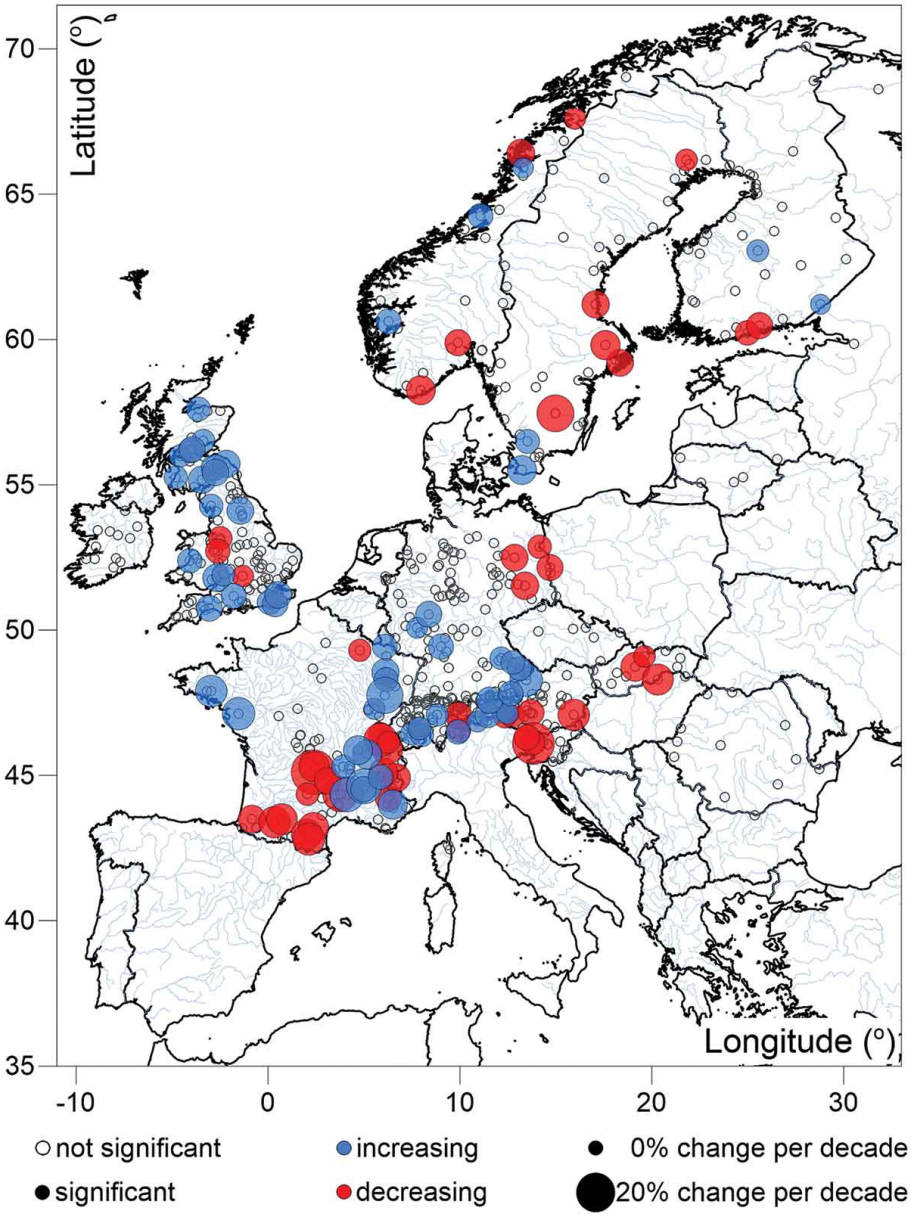

Figure 3.2: Trends in annual maximum flood series (AMF) for the period 1965 to 2005. Filled symbols indicate statistically significant positive (blue) and negative (red) trends at the 10% level of significance. Symbol size indicates the magnitude of change in the mean flood magnitude (% per decade). Source: adapted from Mangini et al. (2018).

shifts align with the overall trend of summer drying and winter wetting.

In the Alpine region, Bard et al. (2015) introduced a seasonal scale, which revealed reduced winter drought of lesser intensity and shorter duration for most regimes, except for snowmelt-rainfall regimes, where enhanced intensity was indicated. Snowmelt-driven high flows proceeded earlier and lasted longer, and percentiles of lower flow (Q_{10}–Q_{50}) were reduced in southern and eastern Alps, consistent with reduced summer and spring precipitation.

Long term Northern Italian records verify these results. Bocchiola et al. (2014) recognized general annual decreases in discharge and significant decreases in spring and summer flow. Within the Central Italian Alps, Balistrocchi et al. (2021) estimated significant reductions in annual mean runoff without significant trends in precipitation, and attributed the losses to rising temperatures and afforestation. Below these, in the Po Basin, Montanari et al. (2023) noted a long-term summer flow decrease over 80 years, resulting in record-low levels during the 2022 drought, due to reduced winter snowfall, earlier winter and spring snowmelt, rising evapotranspiration, and increased agricultural and domestic abstraction. It is clearly visible from the long Po River record in Figure 3.3.

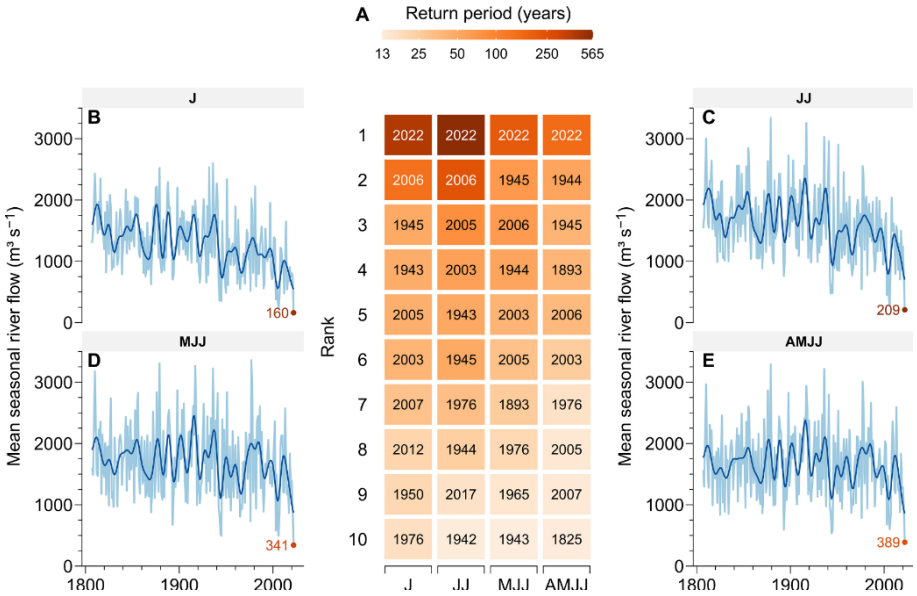

Figure 3.3: Long-term discharge series of the Po River at Pontelagoscuro (1807–2022), highlighting persistent summer flow decline and the record-low drought of 2022. Adapted from Montanari et al. (2023).

3.3 Part 2: Drivers of Hydrological Change

The second part of this chapter discusses the causes of the hydrological changes mentioned earlier, distinguishing between *climatic drivers*—variability in precipitation, temperature, snow cover, and evapotranspiration—and *non-climatic drivers*, which include land-use change, water abstraction, and regulation of flow. Such a split is intended to clarify the relative contributions of natural climatic variability, anthropogenic climatic change, and direct human interference.

3.3.1 Climatic Drivers of Streamflow

European-wide streamflow shifts can be closely linked to large-scale climatic processes that affect precipitation, air temperature, snow dynamics, and evapotranspiration. On a continental scale, as we discussed earlier, Stahl et al. (2010) demonstrated that the general summer decreases and winter increases in streamflow trends are analogous to trends in precipitation and temperature estimated by the European Climate Assessment dataset. Increases in winter precipitation, often in the form of rain in catchments affected by snow (snow-dominant), have resulted in summer and mid-winter flow increases in northern and central Europe, respectively. Meanwhile, low summer precipitation and increasing summer air temperatures resulted in reduced evapotranspiration and decreased summer flows, particularly in southern Europe.

A further pan-European study by Blöschl et al. (2019) indicated that shifts in the climatic drivers of seasonal precipitation and soil moisture were in accordance with changes in flood discharge. Flood growth in northwestern Europe was attributed to increased heavy rainfall and higher antecedent soil moisture, while flood declines in southern Europe, including Northern Italy, were explained by declines in winter rainfall and rising temperatures, resulting in significant reductions in flood sizes.

In the Alpine region, Bard et al. (2015) linked earlier snowmelt driven high flows with rising spring temperatures and a rising percentage of liquid precipitation. Reduced snow storage shortens the duration of the snowmelt period and shifts peak flows earlier, resulting in summer reductions in the southern and eastern Alps. Also, Zanchettin et al. (2014) found that in the Po River Basin, earlier spring discharge timing is strongly connected with precipitation seasonality shifts, through proportionally greater winter precipitation than spring and a rising ratio of liquid precipitation, which reflects regional warming.

Long-term analyses over northern Italy bring climatic variables into clearer contrast. Montanari et al. (2023) identified decreased winter snow accumulation, earlier timing of snowmelt, and increased evapotranspiration as key drivers of persistent summer flow decline in the Po River over the last eighty years, Figure 3.4. Over the Central Italian Alps, Balistrocchi et al. (2021) identified rising temperatures as a driver of increased hydrological losses, although here, temperature effects were supplemented by non-climatic drivers, such as land cover

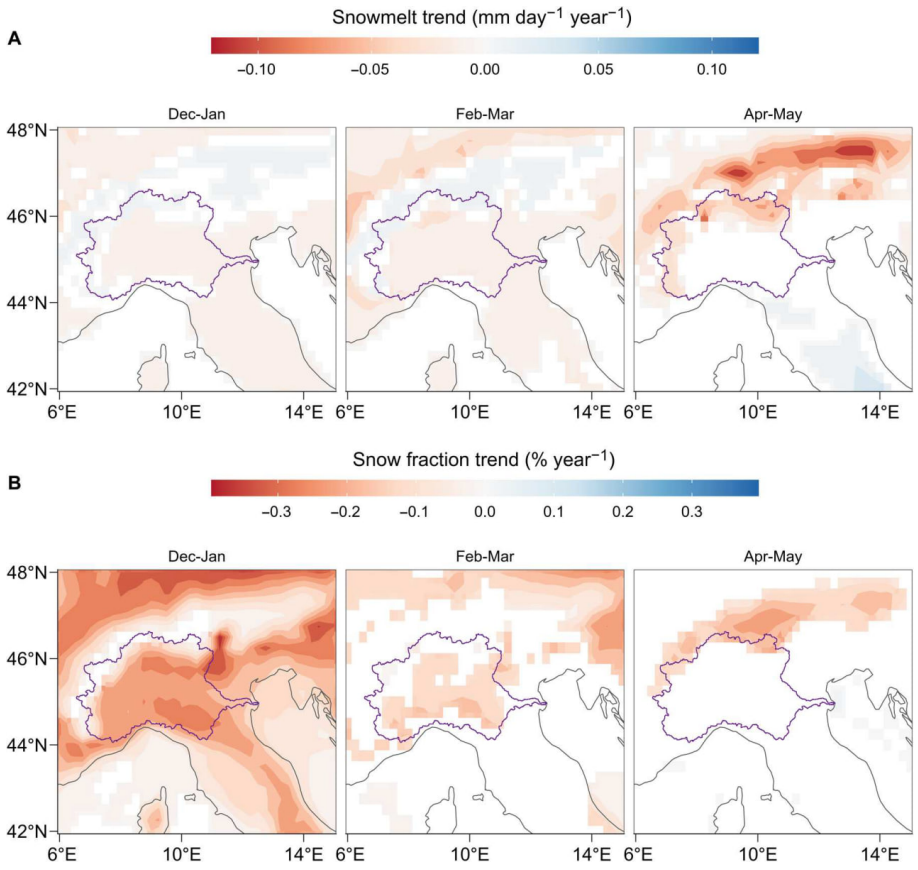

Figure 3.4: Change in Alpine snow regime, 1940–2022. (A) Snowmelt trend (mm day^{-1} year^{-1}). (B) Snow fraction trend (snowfall/total precipitation, % per year). Significant downward trends ($P < 0.1$) are evident across the Alpine headwaters of the Po Basin (boundary in purple), reflecting a shift from solid to liquid precipitation and reduced snowmelt during summer. Adapted from Montanari et al. (2023).

change. Overall, these analyses suggest that climatic forces—through precipitation regimes, snow dynamics, and evapotranspiration impacts—play a key role in controlling recent hydrological regime shifts in Europe and Northern Italy. A catalog of key climatic forces observed over Europe and Northern Italy, along with their associated hydrological consequences, is provided in Table 3.1.

3.3.2 Non-Climatic Drivers of Streamflow Change

Aside from climatic drivers, several studies have documented the role of non-climatic processes, such as land-use change, water abstraction, and flow regulation, on hydrological trends. Across Europe, Collignan et al. (2025) developed a methodological framework for distinguishing between climate-driven and human-driven discharge change across the region.

Table 3.1: Climatic drivers of observed streamflow changes in Europe and Northern Italy.

Driver	Observed impact on streamflow	Reference(s)
Increasing winter precipitation	Increased midwinter flows in northern and central Europe, especially in catchments affected by snow, in which the precipitation falls more in rain form	Stahl et al. (2010)
Declining summer precipitation	Reduced summer flows, increased likelihood of summer dryness in southern Europe	Stahl et al. (2010)
Rising air temperature	Increased evapotranspiration and reduced summer flows in southern Europe	Stahl et al. (2010)
Earlier snowmelt and more liquid precipitation	Earlier peak flows, shorter snowmelt period, reduced summer flows in the Alps	Bard et al. (2015); Zanchettin et al. (2014)
Flood-related climatic shifts	Increased summer floods in NW Europe linked with extreme precipitation and soil moisture; reduced flood peaks in southern Europe, Northern Italy included	Blöschl et al. (2019)
Decreased winter snow accumulation	Persistent summer flow decline in the Po River	Montanari et al. (2023)

By comparing a time series of discharge with the outputs of a physically based land surface model, they concluded that at most southern European stations, including parts of northern Italy, non-climatic processes dominate long-term trends. These were due to increasing irrigation demand, groundwater abstraction, and other water usage practices, which increase evaporation of the catchment and decrease the runoff.

In the Central Italian Alps, Balistrocchi et al. (2021) showed that statistically significant reductions in annual volumes of runoff were impossible to account for based only on precipitation variation. Comparison of land use from 1954 to 2018 indicated widespread afforestation, driven by abandonment of agriculture and diminishing woodland utilization, which resulted in increased evapotranspiration losses. This afforestation development was responsible for a significant percentage of hydrological losses not accounted for by the increase in temperature.

In the Adige River Basin, Mallucci et al. (2019) applied a multi-method attribution framework to distinguish human and climatic forcings. Lower summer streamflow in the lowlands was closely linked to lower winter snow accumulation, which is explained by increased water abstraction for agriculture since the 1970s. Winter increases in streamflow in the headwaters were accounted for by the more aquifer recharge in autumn, since the direct human

intervention at higher elevation is minimal.

Long-term Po River data suggest a strong anthropogenic influence. Montanari et al. (2023) suggest that the climatic forces of intense earlier snowmelt and rising evapotranspiration of water resources work together with increasing agricultural and domestic water abstractions to decrease summer low flows further and drive a continued seasonal decline in water availability. In the Central Italian Alps, land cover studies have verified wide-scale afforestation and cropland loss throughout the latter half of the twentieth century, linked with agricultural abandonment (Balistrocchi et al., 2021).Figure 3.5 presents the expansion of irrigated areas in the Po Basin and the land cover transition in the Central Alps.

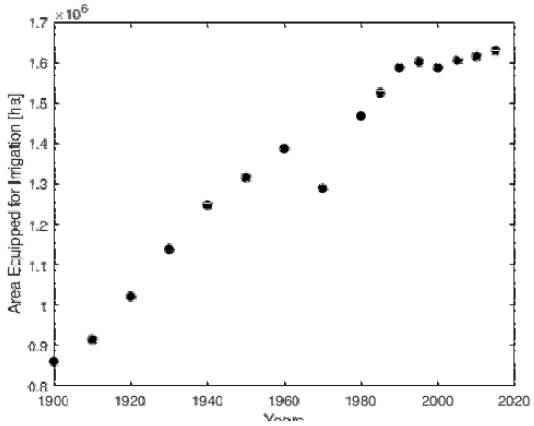

(a) Expansion of irrigated area in the Po River basin (1900–2015).

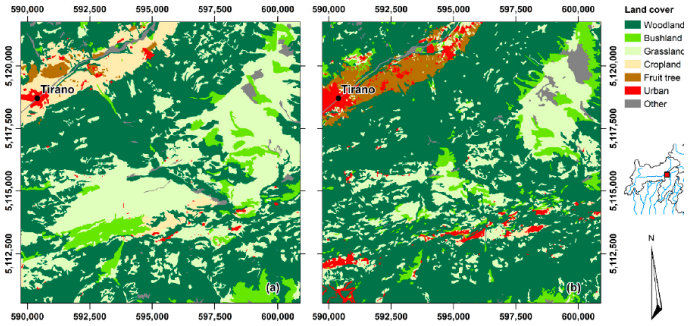

(b) Land cover change in the Central Italian Alps (1954 vs. 2018).

Figure 3.5: Non-climatic drivers of streamflow change in Northern Italy. (a) Irrigation area in the Po Basin more than doubled during the 20th century, increasing summer water withdrawals. (b) Extensive afforestation and urbanization in the Central Italian Alps reflect land use transitions that enhanced evapotranspiration and reduced runoff. Adapted from Montanari et al. (2023); Balistrocchi et al. (2021).

Table 3.2 summarizes the non-climatic influences on streamflow in the investigated studies.

Table 3.2: Non-climatic drivers of observed streamflow changes in Europe and Northern Italy.

Driver	Observed impact on streamflow	Reference(s)
Land use change (afforestation, agricultural abandonment)	Increased evapotranspiration losses and decreased annual runoff volumes in the Central Italian Alps	Balistrocchi et al. (2021)
Water withdrawals (agricultural and domestic)	Reduced summer low flows and exacerbated seasonal deficits in the Po River Basin	Montanari et al. (2023)
Irrigation and groundwater abstraction	Long-term discharge reductions in southern Europe, including parts of Northern Italy	Collignan et al. (2025)
Flow regulation and reservoirs	Altered seasonal distribution of flows, reduced natural variability, particularly in Alpine lowlands	Mallucci et al. (2019)

3.4 Conclusion

The literature reviewed here highlights the observation that the European, Alpine, and Northern Italian streamflow regimes have changed over the past few decades, revealing clear seasonal signatures. At the European scale, winters have been increasing in snow-dominated catchments, and summer flows have decreased over the majority of southern Europe, including Northern Italian regions. Alpine studies confirm an earlier start to snowmelt, shorter winter droughts in some regimes, and smaller summer baseflow. Flood amounts have decreased in southern and eastern Alpine basins, and their timing moved earlier in the hydrological year for some northern Italian rivers. Low-flow evaluation predicts more severe summer deficits, commonly linked to both climatic and human divers.

However, ongoing research indicates important gaps. Most of the studies have examined long-term hydrological changes in Europe, specifically in Alpine catchments and Northern Italy, and often at annual or seasonal scales, and large-scale syntheses. In Piedmont specifically, existing assessments tend to emphasize annual trends or seasonal totals. Although these are highly informative in the regional context, they may yield little insight into monthly dynamics. This leaves open basic questions about the timing of changes in monthly scales. For example, whether summer low-flow stress is localized in particular months, and whether flood-related indicators show coherent changes in autumn. This gap is the motivation of the present thesis, which will explore long-term patterns of monthly, seasonal, and annual river discharge data across the Piedmont region. By applying multi-scale analysis of the mean, maximum,

and minimum flows, the study will determine whether the patterns at the continental and Alpine scales extend locally, and explore potential climatic forcings specific to the region.

Chapter 4

Data and Methodology

In this chapter, we present the data sources, study area, and methodologies used to analyze long-term changes in the riverflow regime in Northern Italy, with a focus on the Piedmont region. Objective here is to introduce and characterize the used datasets, methods and procedures. In this way the resulting findings may be appropriately interpreted.

The chapter includes five different sections. Section 4.1 provides an introduction to the study area, describing its physiographic and climatic characteristics, as well as the distribution of available gauging stations across it. Section 4.2 explains the hydrological data sets that we used, which consist of discharge records and climatic drivers and their sources. Section 4.3 describes data processing procedures. Section 4.4 describes the selected statistical analysis method that we carried out for trend identification, of which the Modified Mann–Kendall and Sen's slope estimator are a main part. Section 4.5 describes the spatial analysis and visualization procedures listing the software environments and tools used in this study.

4.1 Study Area

Figure 4.1 shows our study region, Piedmont, which is an administrative area of Northwestern Italy and its key river networks. It spans a wide array of physiographic and climatic conditions, making it an ideal place for investigating hydrological changes. It encompasses Alpine headwaters at more than 3,000 m a.s.l. through the lowland plains of the Po River, and so includes both high-altitude mountain catchments, dominated by glacier and snowmelt, and lowland rivers supplied almost entirely through rainfall (Blöschl et al., 2019)

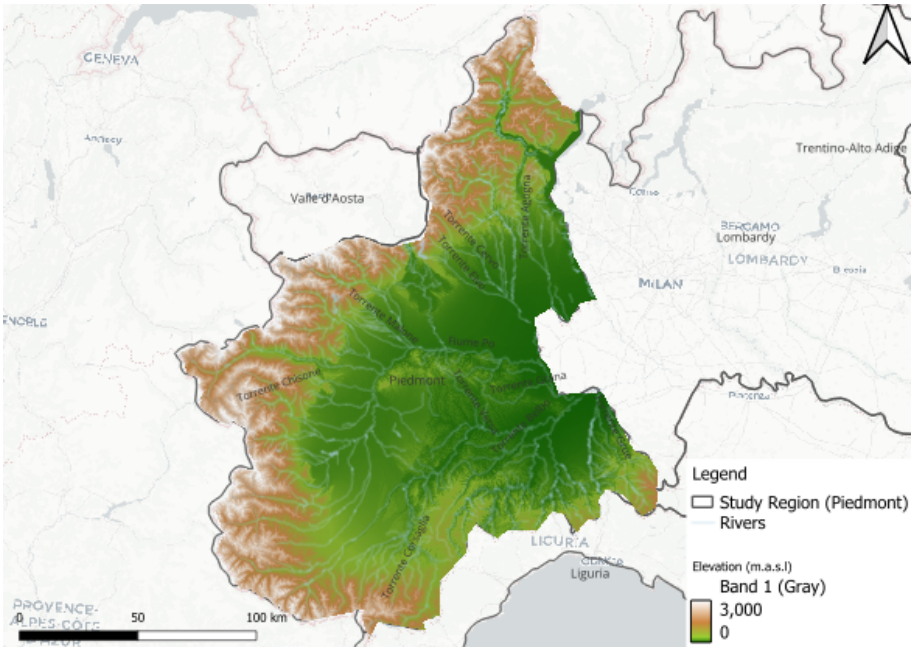

Figure 4.1: Map of the study area, administrative region of Piedmont.

Broad networks of rivers characterize the Piedmont region. They feed into the Po River. Its principal tributaries are including the Sesia, Tanaro, Dora Riparia, and the Dora Baltea (Autorità di Bacino del Fiume Po, 2021).

Hydroclimatic conditions of the studied basin are limited by Mediterranean and continental forces. Rainfall regimes range from summer convective storms over the Alpine basins up to autumn cyclonic rains over the Ligurian coast. Mean annual rainfall is usually higher than 1 500 mm over the Alps, while over the central Piedmont plain, it is lower, around 700–900 mm. Snow accumulation in winter plays an important control over runoff, especially over the Aosta Valley and over the upper Piedmont catchments. (Regione Piemonte and ARPA Piemonte, 2020; ISPRA, 2014).

Available gauging network for the Piedmont region includes 131 discharge stations (from ARPA), whose record lengths vary from the early 20th century up to the current time. Most of the stations, however, have less than 20 years of observation, due to gaps in data and a lack of digitization of previous paper reports, and some of the stations were built after the year 2000 or were displaced to another location.

To gain a reliable result that is representative of the long-term picture, we worked on the stations that have at least 25 years of data, resulting in the selection of 22 stations.

The recorded data for the Aosta Valley and Liguria regions (two neighbouring administrative

Table 4.1: Summary of discharge station characteristics and cumulative record-length classes.

Region	Total Stations	< 20 yrs	< 25 yrs	< 30 yrs	≥ 30 yrs
Piedmont	131	59	110	114	18

Note: Columns are cumulative counts by record length.

regions) were not considered because most of the downloaded time series were short, and the data were less than 25 years old for them.

4.2 Data

4.2.1 Hydrological Data

Our data series for this work consists of daily median discharge measurements at stations scattered across the Piedmont region. These time series date back to the mid-20th century, providing a long-term perspective on flows; however, most records contain gaps, as mentioned earlier. The long series of data forms a necessary condition for recognizing persistent changes in flow regimes and their potential climatic causes.

We obtained the discharge data from the regional environmental protection agency (ARPA Piemonte), which has the responsibility for hydrological observation and data custodianship, and from the SIREN project (Mazzoglio et al., 2025, 2024). Datasets were inspected pre-analysis for missing data and inconsistency, to be suitable for long-term trend analysis.

4.2.2 Physiographic classification of stations

We classified the Piedmont stations by elevation into three physiographic classes for simplicity in interpretation of discharge trends. Using ISTAT altimetric bands and adjusting them to reflect Alpine hydrological regimes (ISTAT, 2025; Stahl et al., 2010; Parajka and Blöschl, 2010; Mallucci et al., 2019), we classified Alpine headwaters for the stations at 800 m a.s.l. and higher (snow-dominated), foothill or transition for 300–800 m a.s.l., and lowlands for below 300 m a.s.l. Table 4.2 lists this classification, and Figure 4.2 shows the spatial location of the analysed stations in this study.

Table 4.2: Physiographic classification of the 22 Piedmont stations based on coordinates (reference system WGS84) and elevation thresholds (>800 m Alpine headwaters, 300–800 m foothill, <300 m lowland).

Station	X (Longitude)	Y (Latitude)	Classification
Bormida a Cassine (Caranzano)	8.54	44.74	Low land (123 m)
Chisone a Soucheres Basses	7.09	45.02	Alpine headwater (1466 m)
Chisone a S. Martino	7.22	44.95	Foothill (410 m)
Dora Baltea a Tavagnasco	7.83	45.54	Low land (270 m)
Dora Riparia a Ulzio (Oulx)	6.83	45.04	Alpine headwater (1080 m)
Grana a Monterosso	7.38	44.45	Foothill (720 m)
Po a Crissolo	7.13	44.70	Alpine headwater (1340 m)
Po a Carignano	7.68	44.90	Low land (240 m)
Scrivia a Serravalle	8.87	44.72	Low land (200 m)
Sesia a Campertogno	8.00	45.78	Alpine headwater (820 m)
Stura di Demonte a Gaiola	7.37	44.32	Foothill (650 m)
Stura di Lanzo a Lanzo	7.47	45.27	Foothill (454 m)
Tanaro a Ponte di Nava	7.95	44.11	Alpine headwater (820 m)
Tanaro a Farigliano	7.92	44.47	Low land (245 m)
Tanaro a Alba	8.03	44.70	Low land (172 m)
Tanaro a Montecastello	8.63	44.95	Low land (84 m)
Toce a Candoglia	8.46	45.95	Low land (201 m)
Isola S. Antonio Po	8.78	45.03	Low land (76 m)
Mombaldone Bormida	8.27	44.85	Low land (208 m)
Passobreve Cervo	8.05	45.56	Foothill (593 m)
Santino San Bernardino	8.55	45.42	Low land (250 m)
Moncalieri Po	7.68	45.00	Low land (220 m)

4.2.3 Climatic Drivers

In order to support hydrological change interpretation, we complemented the discharge records with gridded climate data from the ISPRA BigBang 90 dataset (Braca et al., 2025). BigBang 90 provides monthly and yearly fields of precipitation, mean temperature, and potential evapotranspiration (PET) and other hydrological variables on a grid of about 1 km for 1951–2024. PET follows the FAO–56 Penman–Monteith method. Data distributed as ASCII grids through the ISPRA BigBang portal. We selected these variables among our principal climatic forces governing discharge at interannual and seasonal scales to link the observed variation of flow and external forcing. Using the monthly data, we can create the seasonal data.

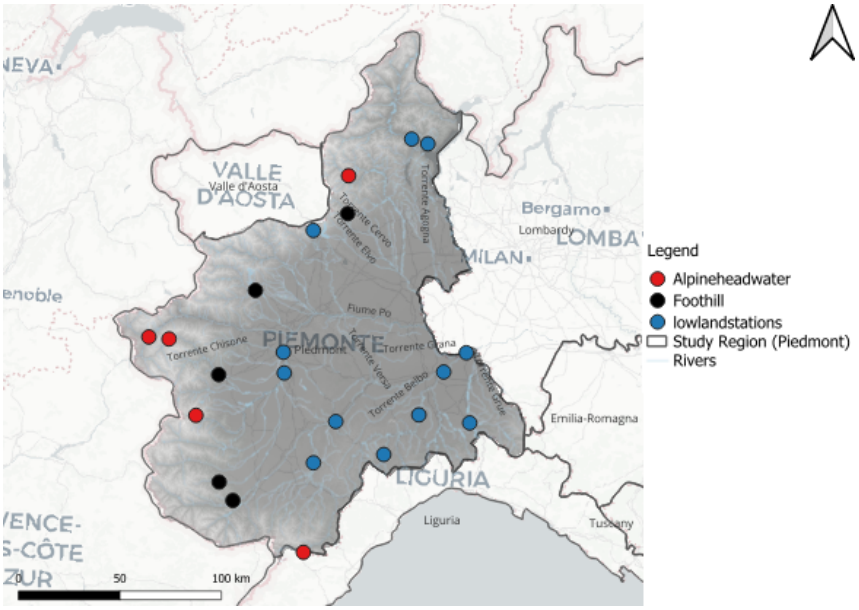

Figure 4.2: Locations of the 22 gauges in Piedmont by physiographic class: Alpine headwaters (>800 m), Foothill (300–800 m), and Lowland (<300 m).

Table 4.3: Datasets used in this study, with source and temporal coverage.

Dataset	Source	Coverage
Daily discharge records	ARPA Piemonte/SIREN	1940s–2020s (station scale)
Total precipitation	ISPRA BigBang 90 gridded dataset (1 km resolution)	1951–2024 (catchment scale)
Air temperature	ISPRA BigBang 90 gridded dataset (1 km resolution)	1951–2024 (catchment scale)
Potential evapotranspiration (PET)	ISPRA BigBang 90 gridded dataset (1 km, FAO-56 Penman–Monteith)	1951–2024 (catchment scale)

4.3 Data processing

The hydrological records, particularly the discharge records, were preprocessed to ensure consistency and comparability across stations, thereby preparing the data for statistical analysis. Preprocessing steps include quality control, temporal aggregation, and handling of missing values.

4.3.1 Quality control

We checked the raw time series of discharge for format and integrity in terms of station (and date) pairs, monotonic sequences of dates, and compatible units ($m^3\ s^{-1}$). Impossible

values (e.g., negative flows) are excluded or flagged as missing.

4.3.2 Handling Missing Data

The discharge records provided varying data gaps, particularly for historical series. Unfortunately, the majority of our time series have gaps due to sensor replacement, malfunction, and data loss around and after the I and II World Wars, among other factors. To address this, a two-step solution was implemented. First, missing components were filled in through the use of additional sources, e.g., the digitization of the Italian hydrological yearbooks performed within the SIREN project. The observations were then quality-checked. By doing so, partial reconstruction of some station records was feasible and we enhanced their usable length for long-term analysis.

Second, for those stations for which there were gaps after this reconstruction, missing values were retained as `NaN` entries. These Mann–Kendall and Sen's slope procedures used in this study can operate with incomplete time series, provided that gaps are non-extreme. Thus, we were able to conserve the statistical properties of the measured records. Through this method, we retained the maximum number of stations in the analysis. The resulting dataset represents a compromise between data completeness and spatial representativeness over the study region.

4.3.3 Temporal Aggregation

We aggregated daily discharge data into several temporal scales to capture different phenomena of river flow regimes:

- **Annual scale**: for each year and station, we computed the annual mean, annual maximum, and annual minimum discharge.
- **Seasonal scale**: mean, maximum, and minimum values were computed for four typical hydrological seasons (DJF, MAM, JJA, SON).
- **Monthly scale**: monthly averages and extremes were extracted to provide a higher resolution summary of shifts in flow timing and seasonality.

4.4 Trend Detection Methods

Detecting systematic changes in river flow regimes requires robust non-parametric techniques that are not overly sensitive to non-normality, outliers, or missing values in the dataset. As discussed in trend detection review Chapter, the analysis in this study relied on the Mann–Kendall (MK) test and the Sen's slope estimator, which are widely applied in hydrological trend analysis (Mann, 1945; Kendall, 1975; Kundzewicz and Robson, 2004). In order to approximate the magnitude of recognized trends, Sen's slope estimate was used alongside the MK test. Sen's slope is particularly suitable for hydrological applications, as it is unaffected by extreme values and can be applied to gappy data (Sen, 1968). Summaries of Sen's slopes (medians and interquartile ranges) are reported across stations without weighting by catchment area. These statistics, therefore, reflect the typical station response within the network rather than a regionally integrated signal. For true regional averages, discharges would need to be normalized (e.g., as specific discharge per unit area) or slopes weighted by catchment size.

We adopted a 5% level of significance for all tests, which corresponds to a 95% confidence interval. The threshold balances method's sensitivity to actual change against false identification of trends. Therefore, we have a general framework for assessing long-term change in discharge over our study region.

Another consideration is verifying whether the number of significant stations exceeds the expected number under spatial correlation. We applied a moving–block bootstrap with a block length of three years and $B = 1000$ replicates, while preserving temporal autocorrelation through the surrogate series. We calculated, for each driver and temporal scale (annual/seasonal/monthly), a null distribution of the number of significant trends at $alpha = 0.05$. We then compared the observed count of significant trends with the 95% interval of this null distribution. The result is field significance if the observed counts lay outside the two-sided 95% null interval and we provided a Monte Carlo p–value (Khaliq et al., 2009). Such corrections ensure that only spatially coherent and statistically robust climate signals are utilized in analysis.

4.5 Spatial Analysis

After completing the trend analysis for each station, we exported it into a geographic information system (GIS) for spatial analysis. It played a crucial role in transitioning from statistical end products at the point level to a basin-wide view of hydrological change within their physiographic context.

4.5.1 Station-Level Mapping

All stations were georeferenced using the official coordinates and indicated on regional Piedmont maps. Direction and meaning of identified trends were presented on station maps by using scaled and color-coded symbols. Increasing and decreasing trends, respectively, were accordingly indicated by positive and negative Sen's slope values. It allowed a direct visual verification of whether sets of similar trends existed at particular physiographic or climatic zones.

4.5.2 Programming Environment and GIS Tools

We carried out each step of data processing and statistical analysis using the Python programming language. The spatial analyses were done using QGIS software. Combining GIS and Python tools offered both reproducibility and good-quality cartographic outputs, ready for presentation and interpretation purposes. Corresponding analyses regarding discharge trend identification were executed and streamlined in Jupyter notebooks, All the notebooks follow the same sequence of steps: data ingestion, yearly, monthly, and seasonal summarization, and trend identification via the Mann–Kendall and Sen's slope and field significance tests. All the notebooks, intermediate CSV exports, and some plots provide a reader with the ability to reproduce all the outcomes of this chapter using the same raw data inputs.

4.5.3 Climatic Datasets and Processing

We used catchment boundaries and descriptions adopted from the FOCA (Italian FlOod and Catchment Atlas) dataset (Claps et al., 2024); downloaded at (Claps et al., 2023). We overlaid FOCA catchment boundaries and computed catchment means to generate time series compatible at each discharge station. As an aid to interpreting potential causes of

discharge trends, we present catchment mean precipitation, temperature, and PET, which correspond to catchment-integrated types of river flow. We do not compute minima and maxima, as these extrema tend to reflect local artifacts or inter–pixel variability at a pixel, rather than basin–wide forcing, and in other cases (most significantly PET minima) produce erratic or false signals. By averaging the climatic input over the entire catchment, the discharge becomes insensitive to the detailed spatial structure of the climatic variables; therefore, the spatially averaged mean value is the most physically sensible metric. Accordingly, the climatic trend analyses presented in this thesis are all catchment–mean value-based. It is notable here that all climatic trends were computed using the Mann–Kendall test and Sen's slope. We also checked for field significance. A moving block bootstrap of 3-year blocks, with replicates of $B = 1000$, created a surrogate series maintaining temporal autocorrelation. We generated, for each driver and season, a null distribution of the number of $\alpha = 0.05$ rejections and checked whether, for each data set, counts observed were outside of its 95% range.

Chapter Summary

We have briefly introduced this chapter by first describing our study area, the Piedmont region. The data and conceptual framework of the method for analysing long-term hydrological change were then explained. Our key data comprises a set of daily discharges for more than 22 diverse gauging stations (after simple cleaning and accessibility validation), as well as station coordinates (X, Y, and Elevation) for spatial analysis and possible interpretation based on catchment elevation classification.

Processing step included quality control and summation of the daily discharge data up to annual, seasonal (DJF, MAM, JJA, SON), and monthly aggregates for each station. Missing data were treated as NaNs: gaps left over were retained as `NaN`, since the employed trend tests operate on incomplete series.

Monotonic trends are assessed by the original Mann–Kendall test and estimated by Sen's slope for discharge and climatic driver values. Field significance was tested using a moving-block bootstrap to determine whether the number of significant stations exceeds what would be expected under the null hypothesis.

Outcomes of every station were visualized by trend direction and significance mapping at gauge points, and the Python notebook environment and supporting tools were documented.

.

Chapter 5

Results

This chapter presents the outcomes of the statistical analyses described in Chapter 4. The primary objective is to detect and quantify long-term trends in river discharge across the Piedmont and to compare these with changes in key climatic variables that we selected before. Results are structured first to describe hydrological changes and then extend the analysis to potential drivers.

First, we provide an overview of the discharge records, including data availability and general flow characteristics. Sections 5.2–5.3–5.4 report the results of the Mann–Kendall and Sen's slope analyses for discharge at annual, seasonal, and monthly scales. Section 5.5 presents the same trend-detection framework applied to precipitation, temperature, and potential evapotranspiration, enabling direct comparison with hydrological outcomes. The final section will summarize the main findings of this chapter to prepare the ground for interpreting and discussing the results in the next chapter.

5.1 Overview of Discharge Records

These discharge datasets include daily records of flow from 22 scattered gauging stations across the Piedmont. Series lengths vary across stations, with some spanning multiple decades and others covering recent periods only. Then, as mentioned in the previous chapter, the daily data were aggregated into annual, seasonal, and monthly series to carry out trend analysis, following elementary harmonization as well as integrity tests (Chapter 4).

5.1.1 Data Availability

To quantify temporal coverage, we counted the number of active stations for each year, defined as gauges with at least 90 percent valid daily observations in that year (i.e., a non-missing annual indicator after aggregation). The resulting series indicates a progressive densification of the network from the mid–20th century, with 22 stations in recent decades. Although record lengths vary across gauges, most stations did not provide adequate temporal extent for long-term trend analysis at the annual and seasonal scales; monthly analyses are more sensitive to data gaps and are interpreted accordingly (cf. Chapter 4). Figure 5.1 presents the spatial coverage of the available stations over the Piedmont region, which are scattered over Alpine Headwater Lowland and pre-Alpine areas.

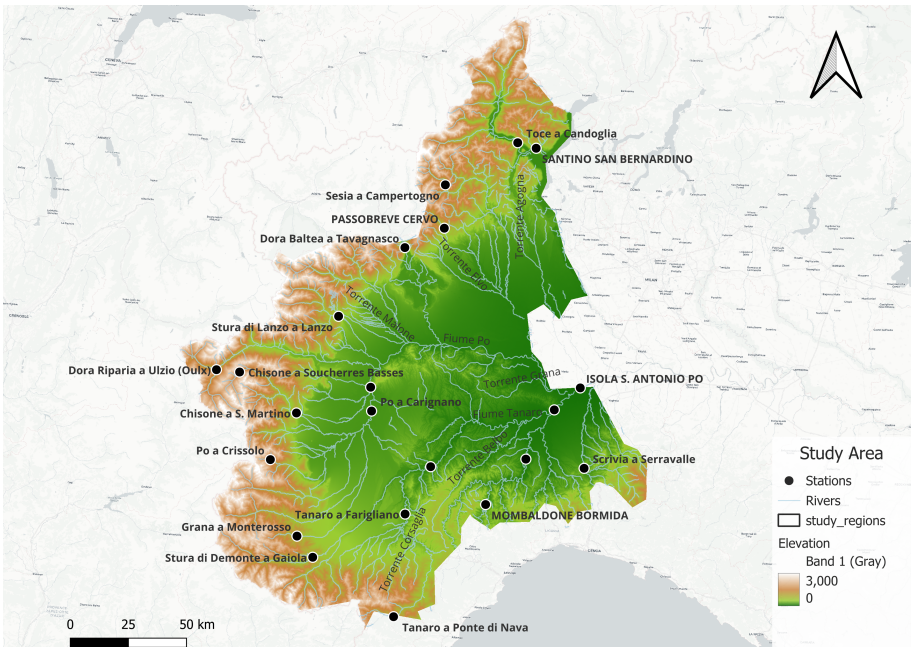

Figure 5.1: Locations of the 22 discharge gauging stations across Piedmont.

5.1.2 General Flow Characteristics

The stations have varied terrain and climates, and therefore, flow regimes also differ. Alpine basins, such as the Sesia at Campertogno, have a snowmelt regime with peaks in late spring and early summer. Bormida at Mombaldone has a flashy flow regime. October baselines in low flows have been a common occurrence. Sharp floods occur in autumn. The peaks are not due to snowmelt but possibly due to Mediterranean cyclonic storms. Compared to

Isola S. Antonio (basin outlet), baseflow, rainfall, and snowmelt come together, which damps extremes and produces seasonally mixed information.

Because regimes vary and records are irregularly scattered and contain gaps, we use non-parametric, rank-based tests (Mann–Kendall with Sen's slope).

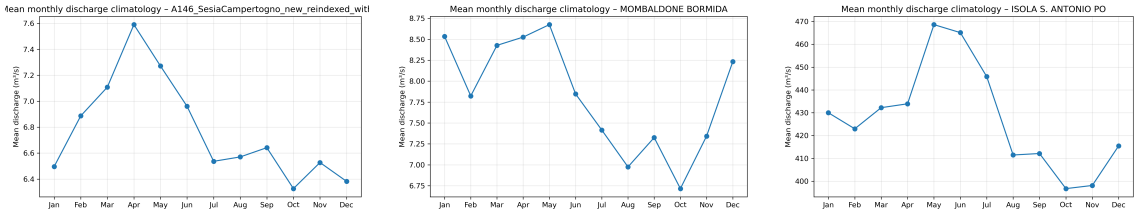

(a) Sesia at Campertogno (Alpine snowmelt)

(b) Bormida at Mombaldone (flashy)

(c) Po at Isola S. Antonio (lowland mixed)

Figure 5.2: Monthly discharge climatologies for three contrasting regimes in Piedmont: (a) Alpine snowmelt, (b) flashy Ligurian, (c) lowland mixed.

5.2 Annual Discharge Trends

Annual mean discharge, annual maximum discharge, and annual minimum discharge are analyzed. These three can represent different aspects of the flow regime, corresponding to overall water availability, flood potential, and low-flow conditions, respectively.

5.2.1 Annual Mean Discharge

Across 22 stations, 77.3% show decreasing annual mean discharge and 22.7% show increases, based on the sign of Sen's slope. At the 5% level, 3 stations are significant and all are decreases. Magnitudes of Sen's slope are generally small to moderate: the median Sen's slope is -0.044 $m^3\,s^{-1}\,yr^{-1}$ with an interquartile range of $[-0.110, -0.007]$ $m^3\,s^{-1}\,yr^{-1}$. Decreases occur across the network without clear geographic clustering.

5.2.2 Annual Maximum Discharge

For annual maxima, 10 stations show increasing trends and 11 stations decreasing trends, with only 3 of these changes being significant at the 5% level (all experienced decreases). Overall magnitudes are modest to moderate. The median Sen's slope is around -0.056 $m^3\,s^{-1}\,yr^{-1}$ with an interquartile range of $[-0.347, 0.574]$ $m^3\,s^{-1}\,yr^{-1}$. Spatially, increases and decreases

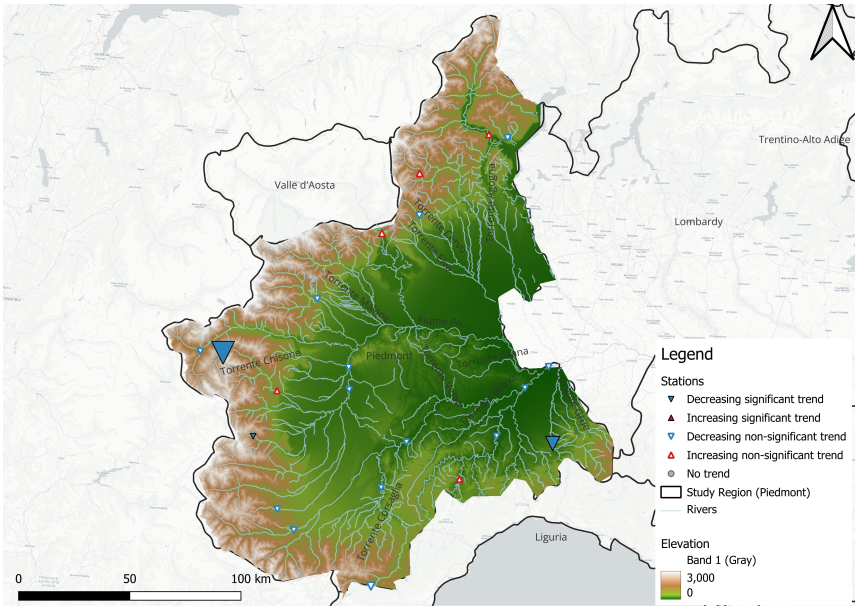

Figure 5.3: Map of Mann–Kendall test statistic for annual mean discharge across the study area. Positive values (red) indicate increases; negative values (blue) indicate decreases. Triangle size is inversely proportional to the p-value (larger symbols indicate stronger significance).

are interspersed across the Piedmont network, with no pronounced regional clustering evident at this scale.

5.2.3 Annual Minimum Discharge

Trends in annual minimum discharge contain information regarding low-flow condition evolutions. At the 22 Piedmont stations, 12 have a downward trend and 10 showed an upward trend. While the majority of shifts aren't significant, 7 stations have significance at 5% (all decreases) These results indicate a signal of increased drought risk in parts of the region. Magnitudes are small: median Sen's slope is -0.021 $\mathrm{m^3\,s^{-1}\,yr^{-1}}$ and interquartile range $[-0.056, 0.004]$ $\mathrm{m^3\,s^{-1}\,yr^{-1}}$.

5.3 Seasonal Discharge Trends

As an index of intra-annual variability, seasonal scale trends in discharges were examined. The usual month choices for seasons in hydrology were considered: winter (DJF), spring (MAM), summer (JJA), and autumn (SON). Again, for this case, Mean, max, and minimum discharge during each season were evaluated using the Mann–Kendall test and Sen's slope

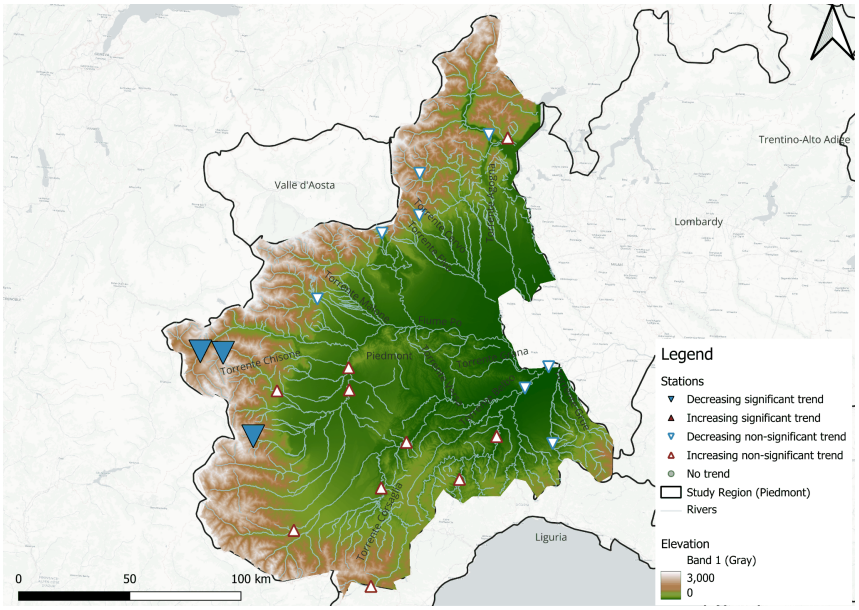

Figure 5.4: Map of Mann–Kendall test statistic for annual maximum discharge across the study area. Positive values (red) indicate increases; negative values (blue) indicate decreases. Triangle size is inversely proportional to the p-value (larger symbols indicate stronger significance).

estimator.

5.3.1 Winter (DJF)

Mean discharge. From the available 22 analysed stations, 9 (41%) show increasing trends and 13 (59%) decreasing trends in winter mean discharge. At the 5% level, 2 stations are significant, Po a Crissolo with decreasing trend and Sesia Campertogno with increasing trend. The Sen's slope magnitudes are skewed toward increases: the median Sen's slope is 2.15 $m^3\,s^{-1}\,yr^{-1}$, with an interquartile range of $[-0.23, 7.43]$ $m^3\,s^{-1}\,yr^{-1}$.

Maximum discharge. Winter maxima increase at 12 of 22 stations (54%), while 10 (46%) show decreases. Only 1 station is significant at the 5% level, which is Sesia Campertogno with a Sen's slope of 0.027 $m^3\,s^{-1}\,yr^{-1}$.

Minimum discharge. By contrast, winter minima decrease at 17 of 22 stations (77%), while 4 (23%) of them increase, and one of them has a flat Sen's slope. 4 stations are significant at the 5% level, all of which decrease, including Dora Baltea, Santino San Bernardino, Passobreve Cervo, and Po a Crissolo.

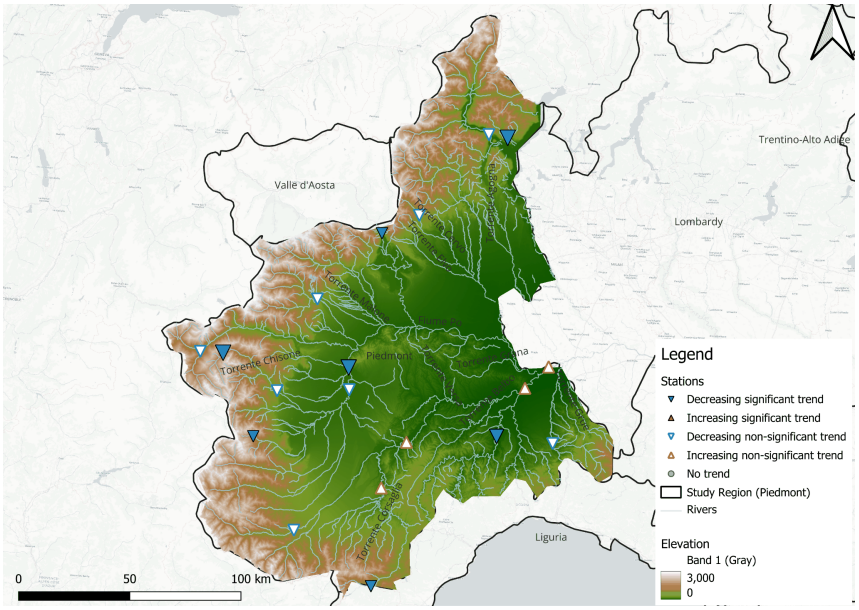

Figure 5.5: Map of Mann–Kendall test statistic for annual minimum discharge across the study area. Positive values (red) indicate increases; negative values (blue) indicate decreases. Triangle size is inversely proportional to the p-value (larger symbols indicate stronger significance).

5.3.2 Spring (MAM)

Mean discharge. Out of the 22 stations analyzed, 5 (23%) show increasing trends and 17 (77%) decreasing trends in spring mean discharge. At the 5% level, 5 stations are significant: Scrivia Serravalle, Chisone, Tanaro Ponte Nava, and Po a Crissolo with a decreasing trend, while only Dora Baltea has an increasing trend. The distribution of slopes is skewed toward decreases, with a median Sen's slope of -0.025 $\mathrm{m^3\,s^{-1}\,yr^{-1}}$ and an interquartile range of $[-0.133, -0.005]$ $\mathrm{m^3\,s^{-1}\,yr^{-1}}$.

Maximum discharge. Spring maxima increase at 7 of 22 stations (32%), while 15 (68%) show decreases. 5 stations are significant at the 5% level: Scrivia Serravalle, Chisone, Dora Riparia, with decreasing trends, and Passobreve Cervo, Dora Baltea, with increasing trends.

Minimum discharge. Spring minima decrease at 15 of 22 stations (68%), while 6 (27%) increase (1 flat). 3 stations of Passobreve Cervo, Po a Crissolo, and Dora Baltea have a decreasing significant trend at the 5% level.

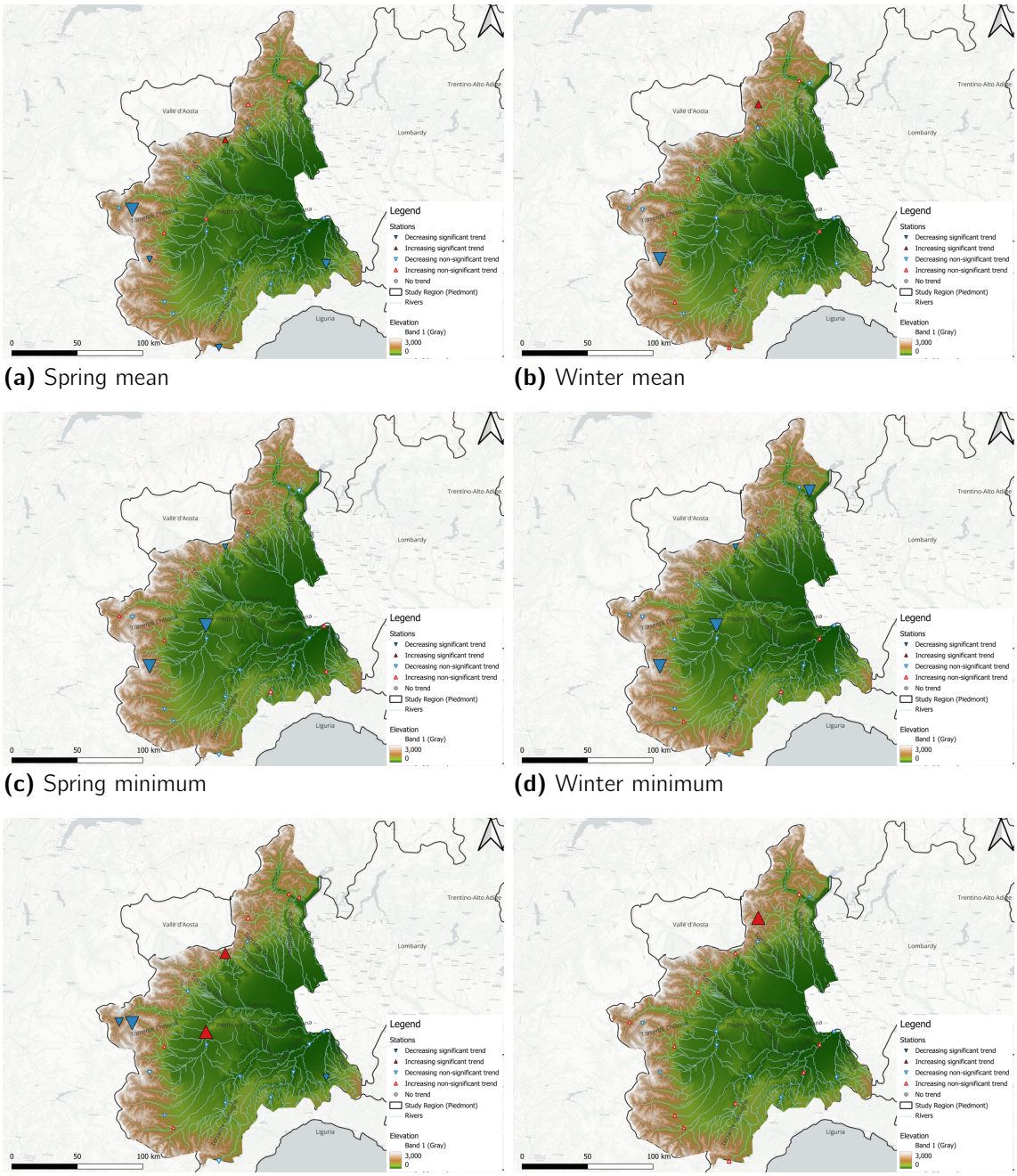

(a) Spring mean **(b)** Winter mean

(c) Spring minimum **(d)** Winter minimum

(e) Spring maximum **(f)** Winter maximum

Figure 5.6: Mann–Kendall test statistic for seasonal discharge (Spring vs. Winter). Blue indicates increases; red indicates decreases. Triangle size is inversely proportional to the p-value (larger symbols mark stronger significance).

Table 5.1: Summary of Mann–Kendall results for spring (MAM) discharge in Piedmont (22 stations).

Metric	Increasing trends	Decreasing trends	Significant ($p<0.05$)
Mean	5	17	5
Max	7	15	5
Min	6	15	3

5.3.3 Summer (JJA)

Mean discharge. Out of the 22 stations, Mann–Kendall results for seasonal climate variables and 9 (41%) increasing trends in summer mean discharge. At the 5% level, 3 stations are significant

Maximum discharge. Summer maxima decrease at 17 of 22 stations (77%), while 5 (23%) show increases. 4 stations are significant at the 5% level with decreasing trends.

Minimum discharge. Summer minima decrease at 15 of 22 stations (68%), while 6 (27%) increase and 1 flat. 5 stations are significant at the 5% level that have decreasing trends This emphasizes a signal of declining summer low flows. Table 5.2 and Figure 5.7 show the result of trend analysis.

Table 5.2: Summary of Mann–Kendall results for summer (JJA) discharge in Piedmont (22 stations).

Metric	Increasing trends	Decreasing trends	Significant ($p<0.05$)
Mean	9	13	3
Max	5	17	4
Min	6	15	5

5.3.4 Autumn (SON)

Mean discharge. Across 22 stations, 2 (9%) increase and 20 (91%) decrease. At the 5% level, 3 stations are significant, all decreases.

Maximum discharge. Autumn maxima rise at 9 of 22 stations (41%) and fall at 13 (59%). Only 1 station is significant at 5% (a decrease).

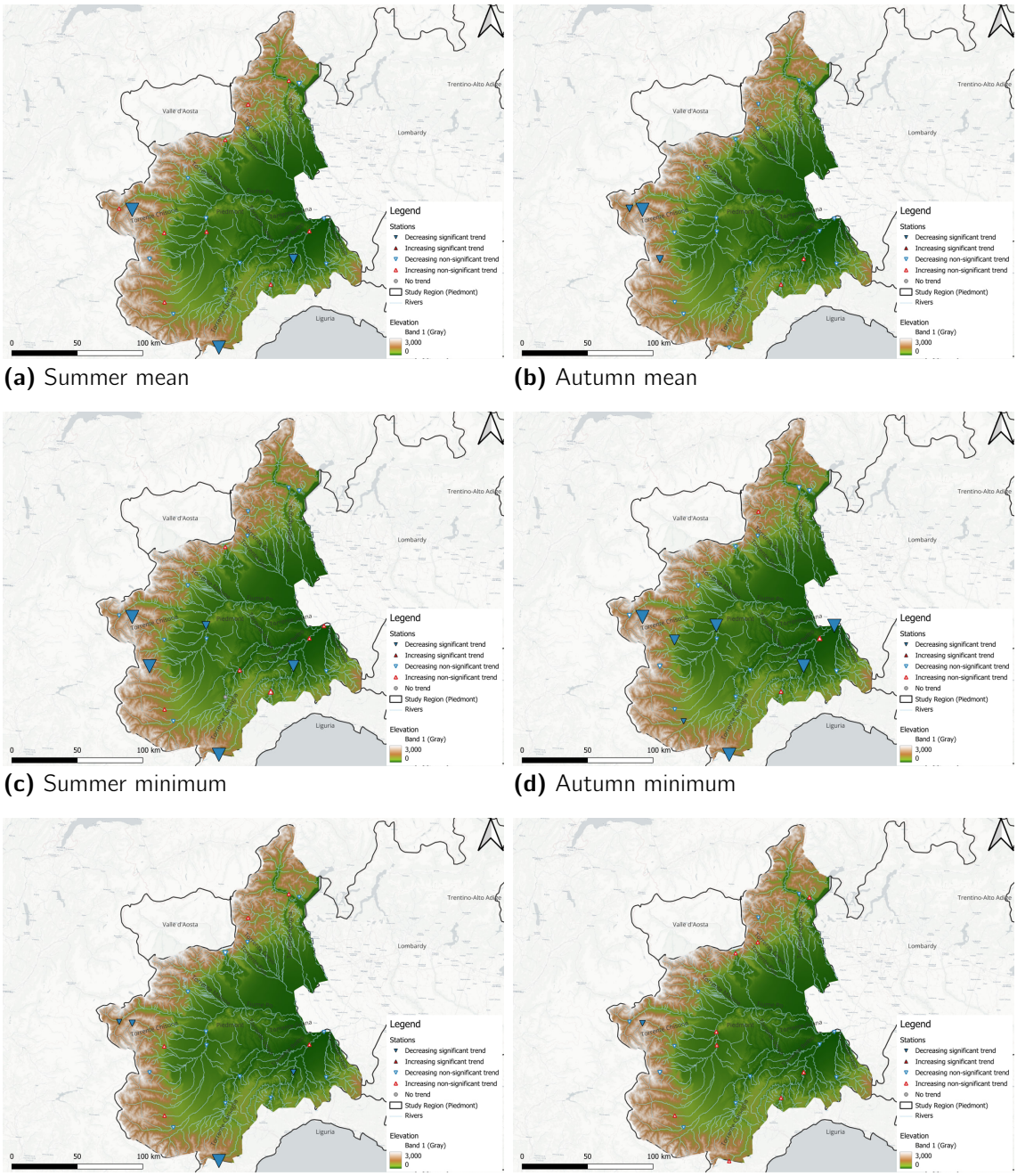

(a) Summer mean **(b)** Autumn mean

(c) Summer minimum **(d)** Autumn minimum

(e) Summer maximum **(f)** Autumn maximum

Figure 5.7: Mann–Kendall test statistic for seasonal discharge (Summer vs. Autumn). Positive values (blue) indicate increases; negative values (red) indicate decreases. Triangle size is inversely proportional to the p-value (larger symbols show stronger significance).

Minimum discharge. Autumn minima increase at 3 of 22 stations (14%) and decrease at 19 (86%). 7 stations are significant at 5%, all reductions.

Table 5.3: Mann–Kendall results for autumn (SON) discharge in Piedmont (22 stations).

Metric	Increasing trends	Decreasing trends	Significant ($p<0.05$)
Mean	2	20	3
Max	9	13	1
Min	3	19	7

As a short summary, autumn mean and minimum discharges mostly decline across the network, and Minima have the strongest significant trends. Maxima are more balanced but still lean toward decreases. Figure 5.7 shows the spatial locations of the stations with their trend analysis results.

5.4 Monthly Discharge Trends

We analyzed monthly-scale trends to have temporal detail of flow changes. We apply the Mann–Kendall test and Sen's slope to the monthly mean, maximum, and minimum discharge at each station. This view can also help reveal and understand the causes of changes within-year behavior and seasonality changes, which could be lost in annual or seasonal trends.

5.4.1 Monthly Mean Discharge

Monthly means show mixed behavior through the year. In winter (January to February), decreases dominate, at 54% and 74% of stations, respectively. Although significance is weak, Chisone and Po show a decreasing trend for both months, and Santino San Bernardino, only in February, has experienced a significant decrease. From March to May, declines remain prevalent (74–82%), and in May 3 stations are significant. June is mixed (9 increasing, 14 decreasing), of which only two stations have a significant trend, and both are declining. In July and August, the balance shifts back toward decreases (16–18 stations), and significance is highest then: four stations each month at the 5% level, all with a declining trend. Po a Crissolo decreases in August, Cassine Bormida, Chisone, Tanaro at Ponte Nava decrease in both July and August, and Passobreve Cervo decreases in July.

September provides the strongest evidence. All 22 stations experience a decreasing trend of mean discharge, of which 11 are significant at 5% level. The stations are Chisone, Chisone San Martino, Dora Riparia, Po a Crissolo, Sesia at Campertogno, Stura di Lanzo, Tanaro at Ponte Nava, Tanaro at Alba, Toce at Candoglia, Isola S. Antonio (Po), and Passobreve Cervo. October also has 19 stations with decreases, three of which are significant, including Chisone, Chisone San Martino, and Dora Riparia. November and December were mostly negative, but without strong accompanying support, and there was just one significant station in December at Santino San Bernardino. All in all, there is seasonality to this trend: slight declines in winter, stable spring declines, drought signals in late summer, and a dramatic decline in September.

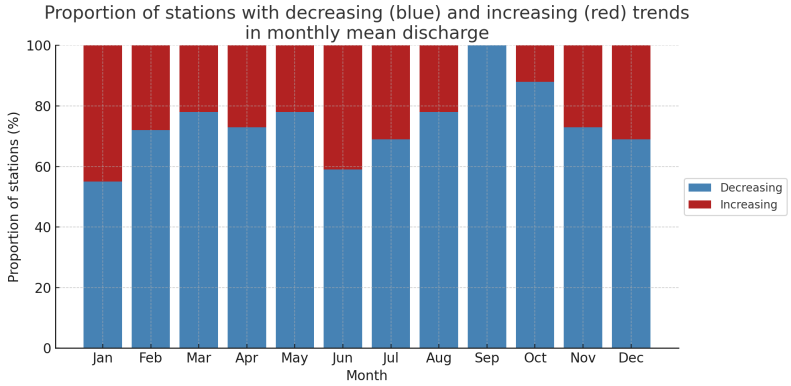

Figure 5.8: Proportion of stations with increasing (red) and decreasing (blue) trends in monthly mean discharge across the study area.

Typically, decreases in monthly mean discharge are happening during the year but with a small number of significant trends. Figure 5.9 shows the July and August spatial results of trend detection across the Piedmont, which are management relevance (summer stress window) months. The most stable signal occurs during early autumn, specifically in September, with persistent and significant decreases at most stations.

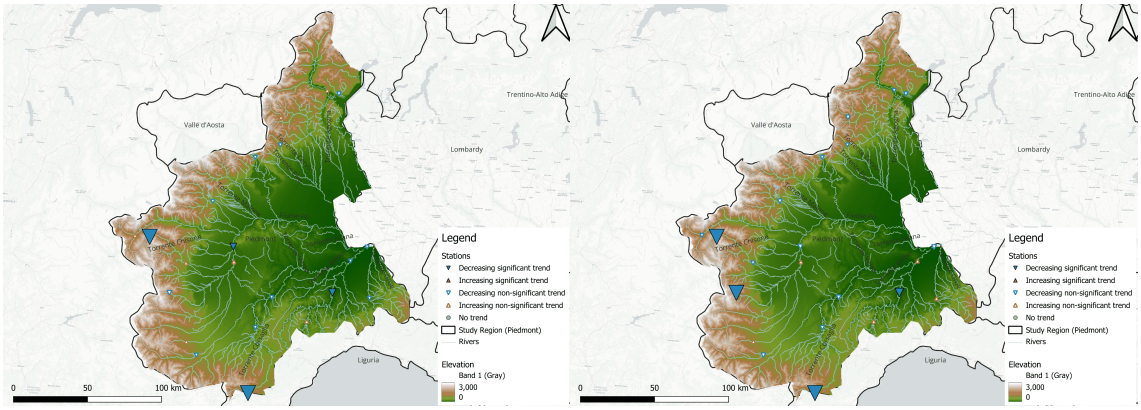

(a) July — Monthly Mean discharge **(b)** August — Monthly Mean discharge

Figure 5.9: Mann–Kendall trends (station-level) and Sen's slopes per decade for Monthly Mean discharge in July and August. Symbols scale inversely with p-value; blue = decreases, red = increases.

5.4.2 Monthly Maximum Discharge

For monthly maximum discharge, increasing trends are most frequent in winter months such as January, while decreases dominate in late winter and throughout most of spring and summer. Two stations increase (Dora Baltea, Toce Candoglia) and one decreases (Po a Crissolo) in January, all are significant. Sesia at Campertogno increases, and Po a Crissolo decreases in February, both of which are significant. March had no significant trend. April had three significant decreases (Chisone, Scrivia Serravalle, Tanaro Montecastello). May had one increase (Dora Baltea) and two decreases (Chisone, Dora Riparia) that were significant. The summer months, June–August are characterized by widespread decreases (17 stations each month), for peak discharge none had significance increases during June to August months. In June, there were three stations, which saw a significant decrease (Chisone, Dora Riparia, Tanaro Ponte Nava).

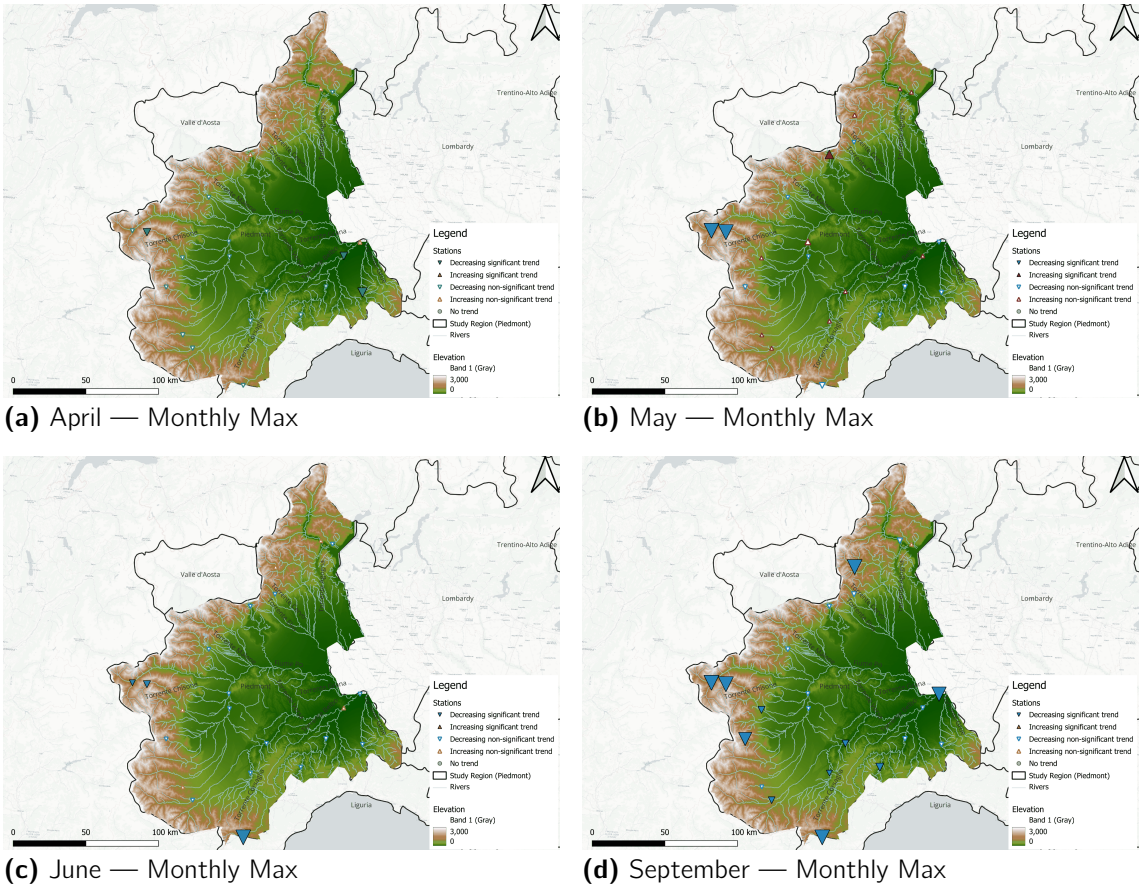

(a) April — Monthly Max **(b)** May — Monthly Max

(c) June — Monthly Max **(d)** September — Monthly Max

Figure 5.10: Mann–Kendall trends (station-level) and Sen's slopes per decade for Monthly Maximum discharge in April, May, June, (late spring and early summer) and September. Symbols scale inversely with p-value; blue = decreases, red = increases. (All panels share identical legend and symbol scaling.)

In July, two significant stations decreased (Chisone, Tanaro Ponte Nava), and in August, two stations decreased (Chisone, Po a Crissolo). In September, 21 of 22 stations exhibit decreasing maxima, with 11 significant at the 5% level (Chisone, Chisone San Martino, Dora Riparia, Po a Crissolo, Sesia Campertogno, Stura di Demonte Gaiola, Tanaro Ponte Nava, Tanaro Farigliano, Tanaro Alba, Isola S. Antonio Po, Mombaldone Bormida). October continues with mostly negative trends, none of them significant, whereas November and December show more balanced patterns. At the 5% level, considering only significant stations, October and November exhibit no significant maximum trends, whereas in December, one station (Tanaro Ponte Nava) shows an increase.

Overall, most monthly maximum discharge trends are decreasing across months, particularly in late summer and early autumn, with only a few cases showing an increase. All trends for each month are mapped and reported in the appendix for a better understanding of the

Table 5.4: Summary of Mann–Kendall results for monthly maximum discharge in 22 Piedmont stations(increasing and decreasing is based on Sen's slope sign).

Month	Increasing	Decreasing	Significant ($p<0.05$)
Jan	13	9	3
Feb	4	17	2
Mar	6	16	0
Apr	5	17	3
May	11	11	3
Jun	5	17	3
Jul	5	17	2
Aug	5	17	2
Sep	1	21	11
Oct	8	14	0
Nov	11	10	0
Dec	10	11	1

spatial occurrence of the trends.

5.4.3 Monthly Minimum Discharge

Monthly minima are a tracking index to monitor changes in low-flow conditions. In winter and spring, most stations trend downward, with 14 to 17 sites falling and only a few reaching significance at the 5% level. In terms of significant trends, January saw two stations decrease (Passobreve Cervo, Po Crissolo); in February, two decreased (Chisone, Po Crissolo); in March, three decreased (Dora Baltea, Passobreve Cervo, Po Crissolo); in April, two decreased (Passobreve Cervo, Santino San Bernardino); and in May, Dora Baltea increased while Santino San Bernardino decreased. June and July are more balanced between increases and decreases. Taking into account the significant trends, in June, Dora Baltea increased while Chisone, Santino San Bernardino, and TanaroPonte Nava decreased. In July, four stations showed a significant decrease (Cassine Bormida, Chisone, Passobreve Cervo, Tanaro Ponte Nava. In August, the pattern turns toward decline, 18 of 22 stations, and 5 are showing significant at the 5% level (Cassine–Bormida, Chisone, Passobreve–Cervo, Po–Crissolo, Tanaro Ponte Nava). Early autumn shows the clearest signal.

In September, 19 stations declined, with eight stations showing a significant decrease (Cas-

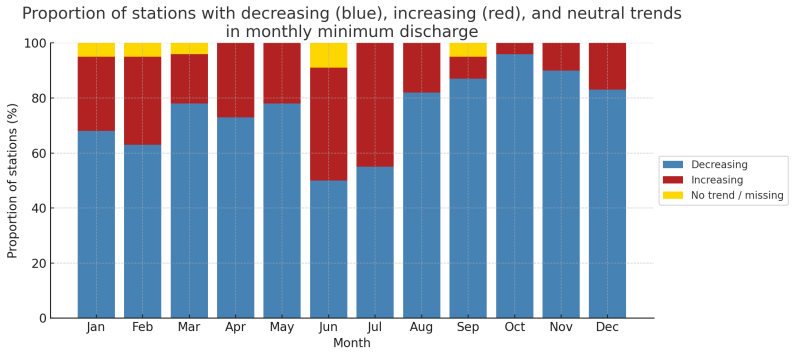

(a) Proportion of stations with increasing (red), decreasing (blue), or neutral (yellow) monthly minimum discharge.

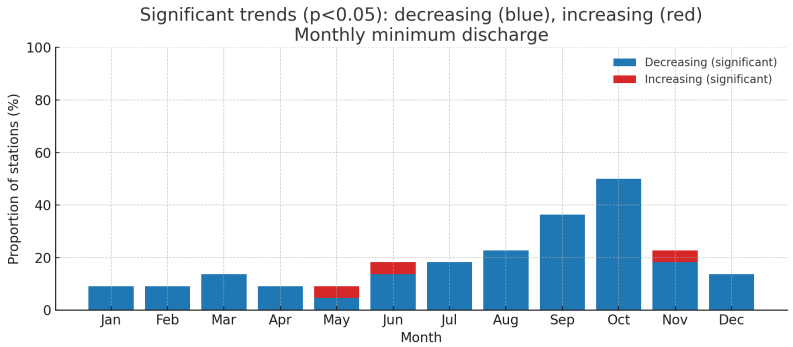

(b) Stations with significant trends ($p < 0.05$) in monthly minimum discharge.

Figure 5.11: Monthly minimum discharge trends across the Piedmont stations. (a) shows only significant results, (b) shows all detected trends. Together, they highlight the strong dominance of decreasing low flows in late summer and autumn.

sine Bormida, Chisone, Chisone San Martino, Passobreve Cervo, Po a Crissolo, Sesia Campertogno, Tanaro Ponte Nava, and Toce Candoglia). In October, we had 21 declines with 11 significant (Cassine Bormida, Chisone, Chisone San Martino, Dora Riparia, Isola S. Antonio Po, Mombaldone Bormida, Po a Crissolo, Passobreve Cervo, Stura Demonte Gaiola, Tanaro Farigliano, Tanaro Ponte Nava, and Toce Candoglia). November and December again lean negative, though with fewer significant cases. November witnessed an increase by Cassine Bormida but a drop by Chisone, Chisone San Martino, Isola S. Antonio Po, and Passobreve Cervo. In December, the minima of three stations decreased (Passobreve Cervo, Po a Crissolo, and Santino San Bernardino). Overall, the results indicate increasing drought risk from late summer into autumn months. Figure 5.12 presents these drought risk shifts from critical months of water availability in the region to the autumn months.

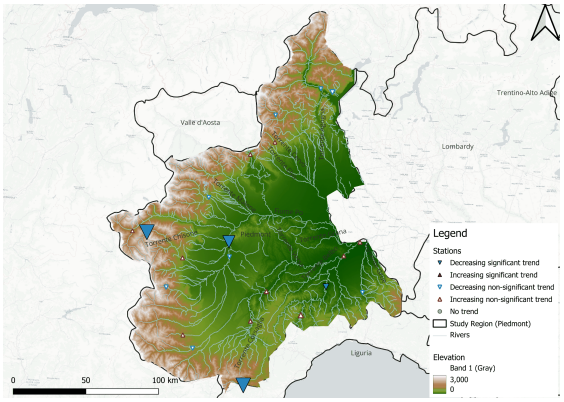

(a) July — Monthly Min

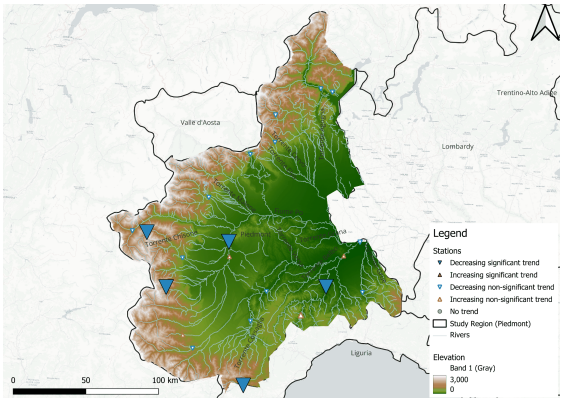

(b) August — Monthly Min

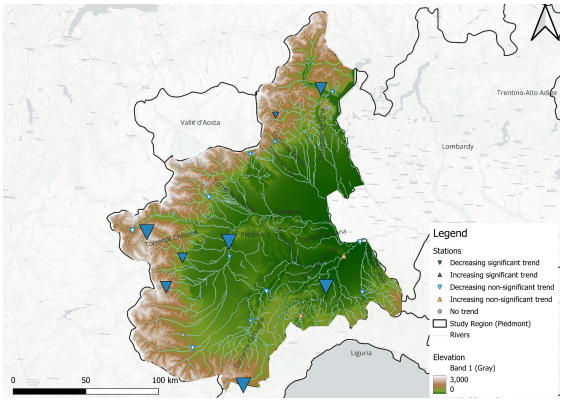

(c) September — Monthly Min

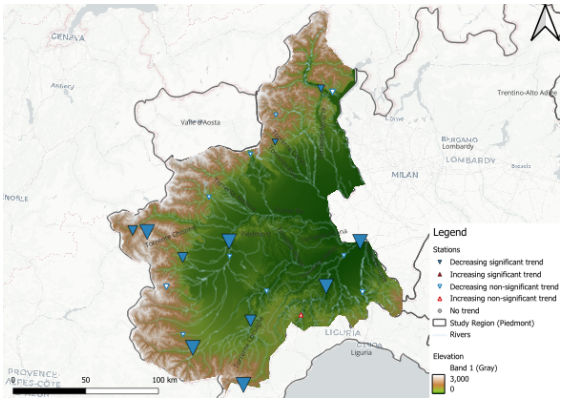

(d) October — Monthly Min

Figure 5.12: Mann–Kendall trends (station-level) and Sen's slopes per decade for Monthly Minimum discharge in July–October. Symbols scale inversely with p-value; blue = decreases, red = increases. Panels share identical legend and symbol scaling.

Synthesis

Monthly results have a clear within-year structure. Winter shows mixed but generally negative, modest trends. From spring onwards, reductions continue, with May starting widespread reductions. Summer keeps the downward pressure: means and maxima reduce at many sites, and minima fall sharply, suggesting drought stress. The evident signal appears in early autumn. September and October show network-wide reductions in the mean and minimum flow, with widespread cases significant. Overall, hydrological change is most significant during the transition from summer to autumn, indicating a growing vulnerability of autumn and late summer low flows. As mentioned before, monthly trend result maps can be found in the Appendix.

Table 5.5: Monthly **minimum** discharge trends across 22 stations. Increasing/Decreasing count *all* gauges by the sign of Sen's slope; the last column reports gauges with significant trends by the Mann–Kendall test (p¡0.05).

Month	Increasing (all)	Decreasing (all)	Significant (p< 0.05)
Jan	6	15	2
Feb	7	14	2
Mar	4	17	3
Apr	6	16	2
May	5	17	2
Jun	9	11	4
Jul	10	12	4
Aug	4	18	5
Sep	2	19	8
Oct	1	21	11
Nov	2	20	5
Dec	4	18	3

5.5 Climatic Drivers of Discharge Trends

To support hydrological change, the same trend detection framework was applied for three climatic variables: total precipitation, mean temperature, and potential evapotranspiration (PET). These variables represent the main factors of the water balance and are crucial for interpreting the connection between climate variability and the river discharge. The analyses were conducted for the annual, seasonal, and monthly timescales as described in chapter-4 by using gridded data.

5.5.1 Annual Trends

The annual mean precipitation trend records a small and mostly non-significant decrease over the study region, with a median catchment-mean trend of -11 mm decade^{-1}. Based on the results, none of the analysed catchments reports a significant increase. The magnitudes are moderate, and their spatial distribution is not coherent.

The mean annual temperature exhibits a clear and persistent warming trend. The catchments all have positive Sen's slopes and all are significant at the 5% level. The median rate of these changes is 0.37 °C decade^{-1} (IQR = 0.25–0.40 °C decade^{-1}) which agree with regional and global patterns ((SNPA/ISPRA, 2024; European Environment Agency, 2025)).

The result of the Potential evapotranspiration (PET) trend analysis also shows a wide rise

with strong support. Catchment-mean PET increases significantly in all catchments, with a median Sen's slope of +16.5 mm decade^{-1} (IQR= 12.3–19.1 mm decade^{-1}).

5.5.2 Seasonal Trends

Precipitation shows weak seasonal trends and is, for the most part, not significant. Winter and spring registered some falls (4 and 1 stations), none of which were significant. Summer and autumn show no consistent direction. Temperature shows rises during all seasons. All stations show positive Sen's slopes, with 16–17 significant cases for each season, and the maximum warming during summer. Potential evapotranspiration (PET) shows a similar trend to mean temperature, with large and statistically significant increases. Summer shows maximum rates: all 22 stations trend upward and are significant, suggesting increased water demand from the atmosphere for the warm months. Taken together, seasonal change is maximum for temperature and PET, whereas precipitation is weak and spatially scattered.

Table 5.6: Mann–Kendall results for seasonal climate variables (counts of stations with increasing or decreasing trends, based on mean values). Only significant trends are tallied.

Season	Precipitation		Temperature		PET	
	Increasing	Decreasing	Increasing	Decreasing	Increasing	Decreasing
DJF	0	0	16	0	20	0
MAM	0	0	17	0	21	0
JJA	0	0	17	0	22	0
SON	0	0	16	0	19	0

Table 5.7: Median Sen's slope estimates (with interquartile range, IQR) for seasonal climatic variables across all stations. Temperature is expressed in °C per decade; precipitation and PET in mm per decade.

Season	Precipitation	Temperature	PET
DJF	−7.3 (−8.6 to −5.4)	+0.41 (0.25–0.53)	+0.47 (0.16–0.54)
MAM	−0.7 (−3.1 to +5.0)	+0.34 (0.27–0.38)	+1.65 (1.16–1.85)
JJA	−2.7 (−3.3 to −1.3)	+0.38 (0.34–0.44)	+2.31 (1.77–2.72)
SON	+1.0 (−0.1 to +1.8)	+0.25 (0.19–0.31)	+1.04 (0.67–1.30)

The seasonal time series (Table 5.6) indicate that strong increases in temperature and PET

occur across all seasons, whereas precipitation does not exhibit strong signals. The slope magnitudes (Table 5.7) also emphasize regular warming of 0.3–0.4 °C decade^{-1} throughout the seasons, strong PET increases in particular summer (+2.3 mm decade^{-1}), and negative precipitation trends in winter and summer, contrasted with a slight positive trend in autumn.

5.5.3 Monthly Trends

Monthly results show finer-scale variations of the climatic driving signals. Precipitation is weak over the record and does not have a significant trend often. A seasonal pattern is present, the median change is least positive during January to March, reverses back towards losses during June to August, and shows moderate positive medians during May and during October–November, but these positives are not significant. Figure 5.14 shows the total precipitation trend results for July–October.

The temperature increases every month. Significant warming takes place at between 12 and 17 stations for most of the month, with summer and later winter maxima and medians close to 0.35–0.47 °C decade^{-1}. Potential evapotranspiration (PET) increases during nearly all months and usually attains significance. Medians are largest during summer (+2.1 to +2.5 mm decade^{-1}) and smaller but positive during winter. Together, these signals suggest summer heat, atmospheric demand compounding, and, with diminishing summer precipitation, a rising risk of warm-season water stress.

Table 5.8: Number of stations with significant increasing and decreasing trends in monthly climatic variables (Mean metric, 1951–2024).

Month	Precipitation		Temperature		PET	
	Increasing	Decreasing	Increasing	Decreasing	Increasing	Decreasing
Jan	0	0	16	0	19	0
Feb	0	3	16	0	19	0
Mar	0	0	17	0	21	0
Apr	0	0	17	0	20	0
May	2	0	14	0	14	0
Jun	0	0	17	0	21	0
Jul	0	1	17	0	20	0
Aug	0	0	17	0	22	0
Sep	0	0	1	0	2	0
Oct	0	0	17	0	20	0
Nov	0	0	15	0	19	0
Dec	0	0	12	0	16	0

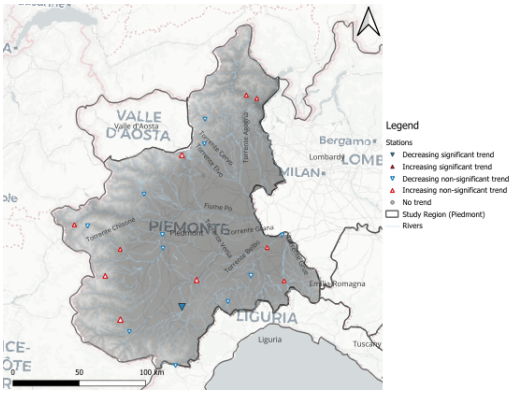

(a) July

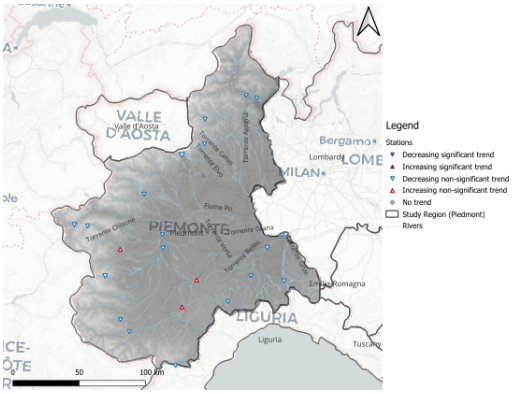

(b) August

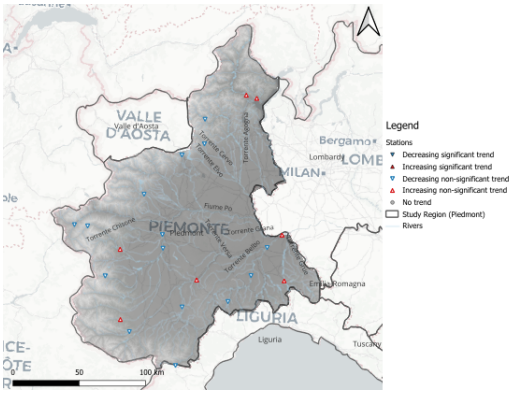

(c) September

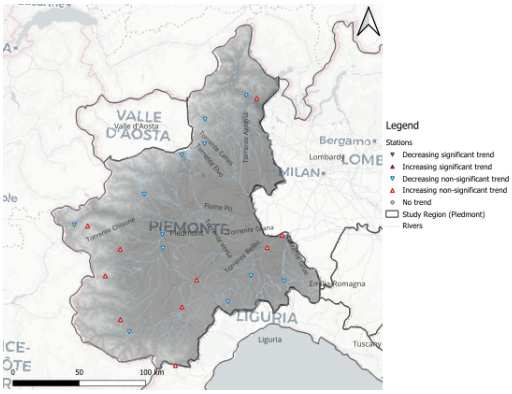

(d) October

Figure 5.14: Mann–Kendall test statistic for monthly **precipitation** from July to October across the study area. Positive values (red) indicate increases; negative values (blue) indicate decreases. Triangle size is inversely proportional to the p value.

Table 5.9: Median Sen's slopes (with interquartile range, IQR) for monthly climatic variables across all stations. Temperature in °C per decade; precipitation and PET in mm per decade.

Month	Precipitation	Temperature	PET
Jan	-1.40 (-1.78 to -1.09)	0.41 (0.27 to 0.52)	0.22 (0.09 to 0.45)
Feb	-2.87 (-3.35 to -2.55)	0.47 (0.33 to 0.56)	0.41 (0.29 to 0.62)
Mar	-3.16 (-4.11 to -2.60)	0.43 (0.33 to 0.46)	1.12 (0.73 to 1.28)
Apr	-2.26 (-2.89 to -1.69)	0.35 (0.28 to 0.39)	1.68 (1.32 to 2.03)
May	4.88 (3.89 to 6.54)	0.25 (0.21 to 0.31)	1.69 (1.12 to 2.29)
Jun	-1.65 (-2.34 to -0.92)	0.40 (0.35 to 0.43)	2.53 (1.93 to 2.85)
Jul	-0.04 (-1.31 to 1.43)	0.35 (0.31 to 0.39)	2.06 (1.55 to 2.39)
Aug	-1.28 (-1.98 to -1.05)	0.41 (0.37 to 0.44)	2.33 (1.82 to 2.50)
Sep	-0.77 (-1.28 to 0.34)	0.12 (0.11 to 0.16)	0.58 (0.23 to 0.76)
Oct	-0.17 (-0.55 to 1.88)	0.31 (0.26 to 0.34)	1.63 (1.11 to 1.96)
Nov	0.06 (-0.66 to 1.01)	0.27 (0.20 to 0.33)	0.62 (0.52 to 0.92)
Dec	-1.32 (-1.78 to 0.19)	0.34 (0.15 to 0.42)	0.28 (0.06 to 0.34)

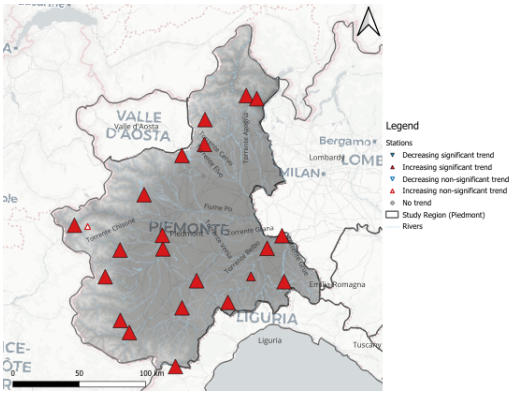

(a) July

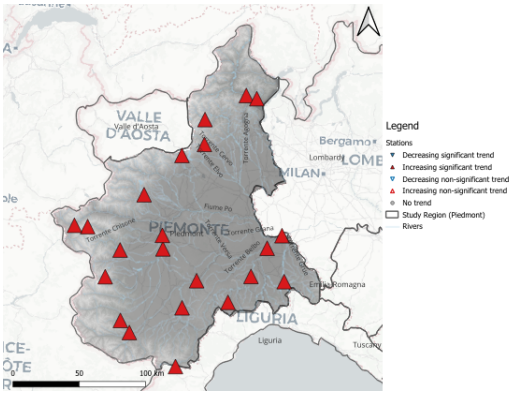

(b) August

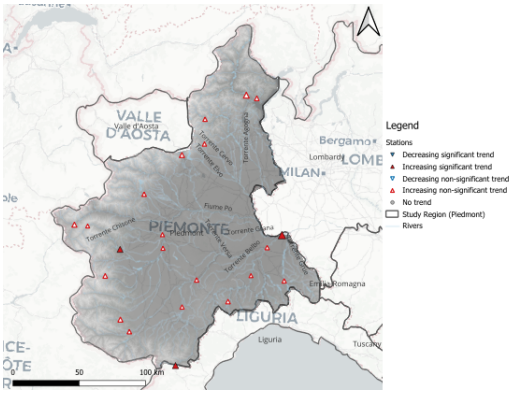

(c) September

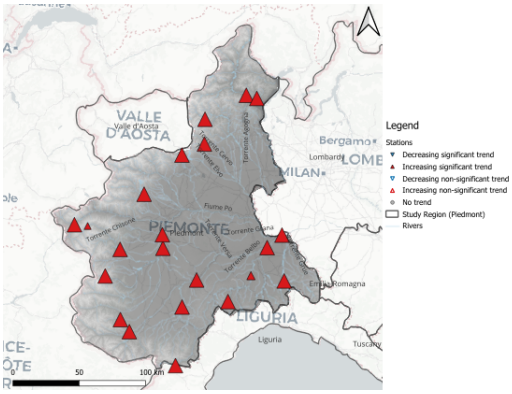

(d) October

Figure 5.15: Mann–Kendall test statistic for monthly **temperature** from July to October across the study area. Positive values (red) indicate increases; negative values (blue) indicate decreases. Triangle size is inversely proportional to the p value.

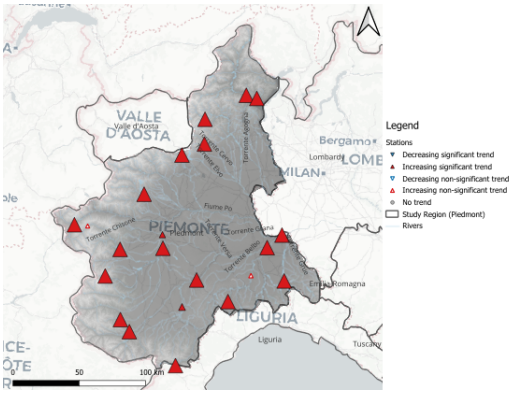

(a) July

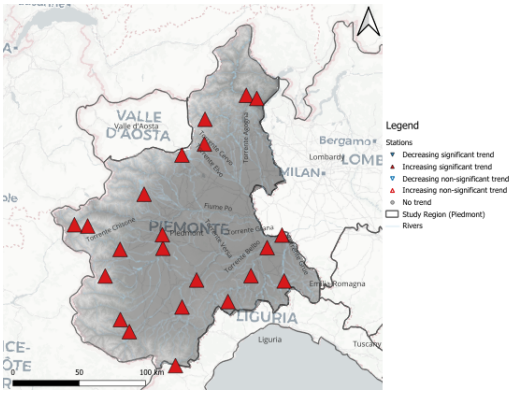

(b) August

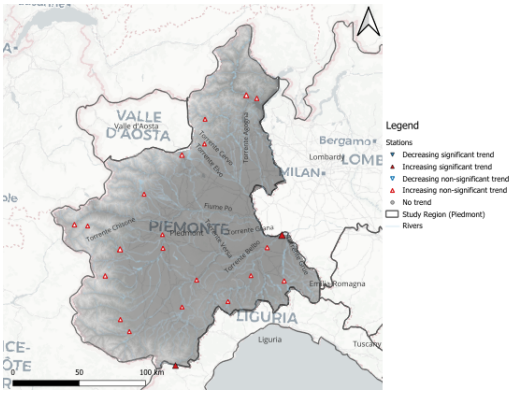

(c) September

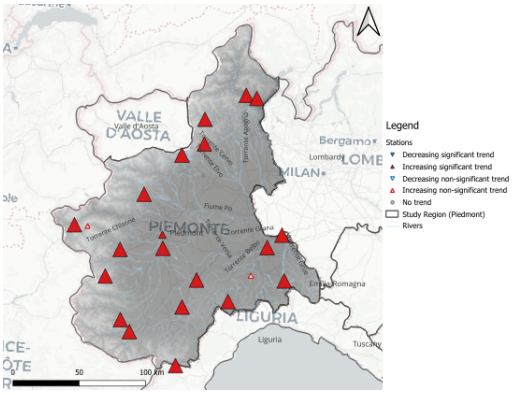

(d) October

Figure 5.13: Mann–Kendall test statistic for monthly **potential evapotranspiration (PET)** from July to October across the study area. Positive values (red) indicate increases; negative values (blue) indicate decreases. Triangle size is inversely proportional to the p value, so larger symbols mark stronger significance.

5.6 Summary of Results

This chapter provides trend analyses of the river discharge and key climatic variables over the Piedmont region in Italy. The main findings are:

- **Annual scale:** River discharge shows mixed trends. Annual means decline at many stations, while annual maxima increase at some localized stations, and annual minima are variable, but show a significant decrease at more stations across all metrics. Temperature increases substantially and spatially consistently (median $+0.37\,^{\circ}\mathrm{C}$ decade^{-1}). Precipitation trends are generally weak and not significant. Potential evapotranspiration (PET) significantly increases by all stations (median $+16$ mm)

- **Seasonal scale:** Characteristic seasonal contrasts emerge. The winter and spring flows suggest snowmelt impacts, and summer discharges fall widely and often sig-

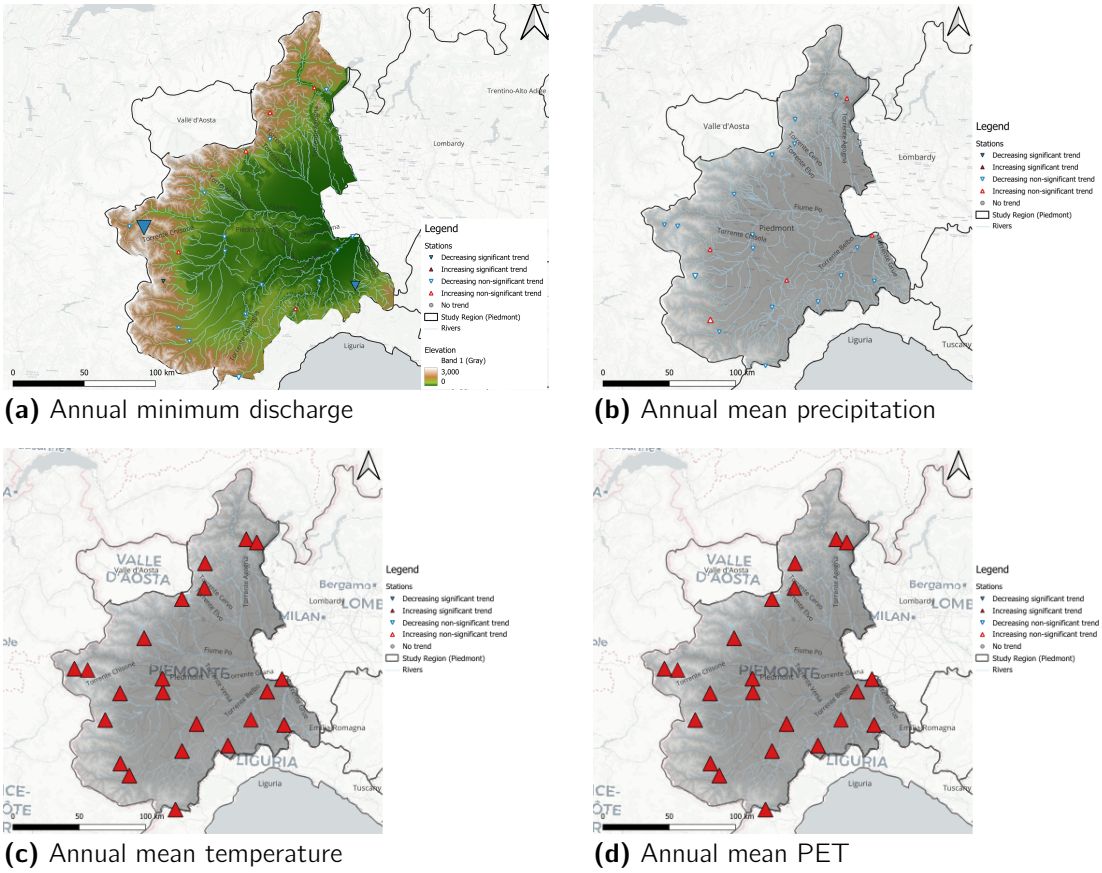

(a) Annual minimum discharge

(b) Annual mean precipitation

(c) Annual mean temperature

(d) Annual mean PET

Figure 5.16: Mann–Kendall test statistic maps for (a) annual minimum discharge, (b) annual mean precipitation, (c) annual mean temperature, and (d) annual mean potential evapotranspiration (PET) across the study area. Positive values (red) indicate increases; negative values (blue) indicate decreases. Triangle size is inversely proportional to the p value.

nificantly, as expected given warming and high evaporative demand. Autumn shows localized increases for maximum flows. Climatic drivers suggest summer precipitation decreases (median $-2.7\,\text{mm}\,\text{decade}^{-1}$), ongoing warming across the year ($+0.3$–$0.4\,^{\circ}\text{C}\,\text{decade}^{-1}$)

- **Monthly scale:** monthly results highlight critical windows. Summer (June–August) low flows dominate the negative trend in discharge signals, even in early autumn (September), while other autumn months show mixed results. Climatic patterns align: robust warming in every month except September, reduced rainfall in summer (e.g., $-1.7\,\text{mm}\,\text{decade}^{-1}$ in June and $-1.3\,\text{mm}\,\text{decade}^{-1}$ in August) but not significant, and enhanced PET during the warm season ($+2$–$3\,\text{mm}\,\text{decade}^{-1}$ in June–August).

In general, discharge regimes are shifting. Late autumn flood maxima do not show amplifi-

cation, and summer low-flow conditions have become more intense earlier in autumn. These changes primarily follow observed trends in temperature, precipitation, and PET, highlighting the interconnections between river flow and climate in our study area. Figure 5.17 shows the monthly mean Sen's slope for precipitation, temperature, and PET. Chapter 6 discusses these further, as well as their implications.

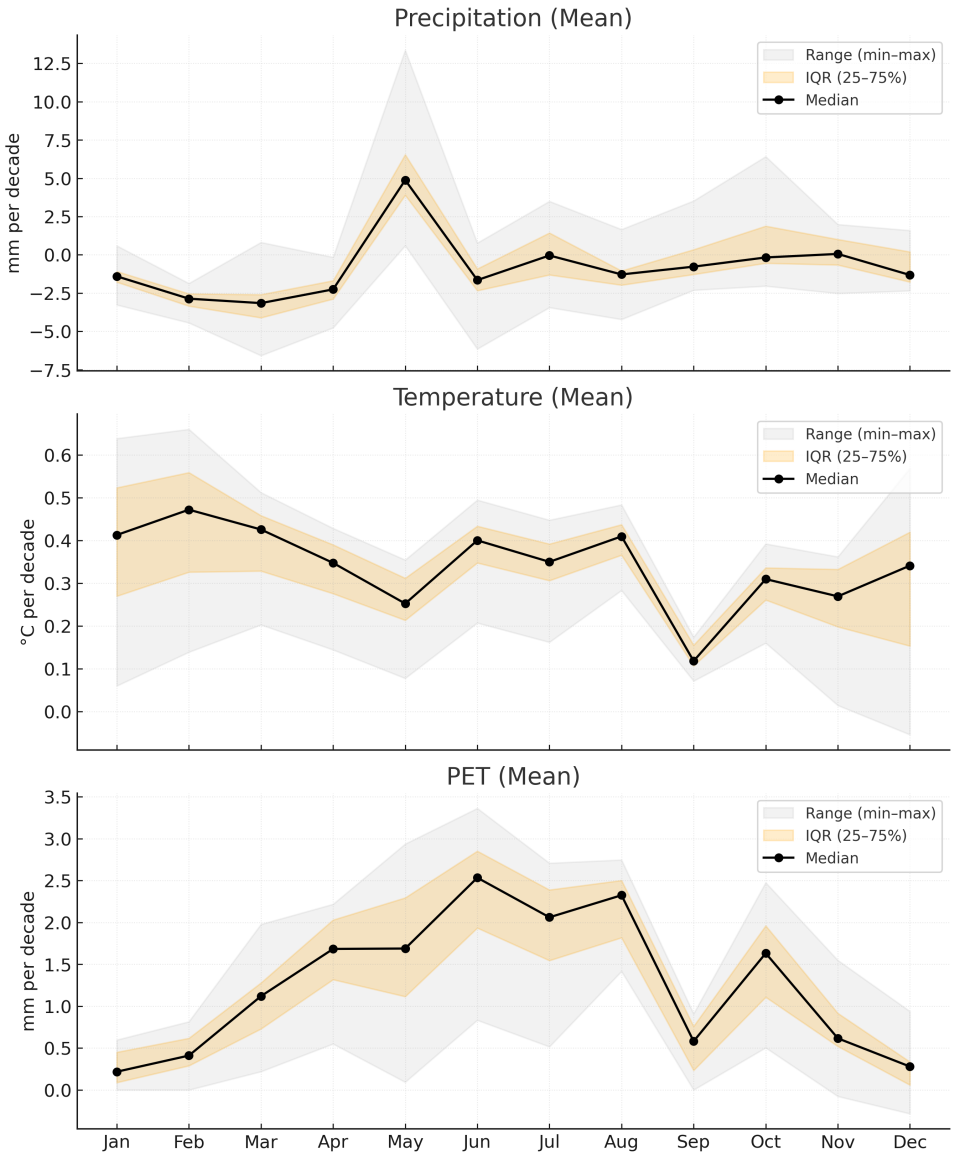

Figure 5.17: Monthly median Sen's slopes (1951–2024) for catchment-mean precipitation, temperature, and PET. The black line shows the median across stations, the orange band indicates the interquartile range (25th–75th percentile), and the light gray band marks the full range (minimum to maximum) across stations. Units: precipitation and PET in mm decade^{-1}; temperature in °C decade^{-1}.

Chapter 6

Discussion

6.1 Introduction

The earlier chapter presented long-term trends in Piedmont river discharges and the transformation of main climate indicators. The Sen's slope and the Mann-Kendall test revealed the direction and magnitude of the trend. The chapter has three purposes. First, we interpret the discharge trends at annual, seasonal (DJF, MAM, JJA, SON), and monthly timescales. Second, the results are compared with trends for precipitation, mean temperature, and potential evapotranspiration (PET) to relate probable causes. Third, the results are compared to the published literature and outline implications for a water management approach, while being transparent with respect to uncertainties and limitations.

6.2 Discharges

6.2.1 Annual Trends

At the station level, few of the trends of the mean discharge are significant (3/22). The area shows a broad, mainly non-significant slope towards lower annual means, indicating a gradual decrease in the supply of water. Similar behaviour is also reported for European catchments, especially those from the Mediterranean region and the Alps, which signals a shift in the hydro-climatic regimes (Stahl et al., 2010; Mallucci et al., 2019; Masseroni et al., 2021). Significant trends also for annual maxima are few (3 of 22 in Alpine) and spatially dispersed, in other words, not field significant. Some stations increase, while others decrease, without

a clear spatial pattern. So, high flows have thereby not increased consistently at the annual time-scale, as would be expected by European syntheses explaining flood change by regional storm dynamics and catchment properties, but not a single continental forcing (Blöschl et al., 2019; Hall and Blöschl, 2014).

For annual minima, strong trends occur more regularly and almost all of them are negative. The annual picture is a mixed but slightly declining one for both Alpine and lowland areas, reflecting stronger drought stress as well as weaker base flow. Large-scale European research for nearly natural basins report matching low-flow reductions under warming conditions (Stahl et al., 2010). In total, the annual view shows a decrease in mean discharges and an increase in low flow stress, while high flow extremes do not show a consistent annual increase.

Although we observed a general decline in discharge, it was not significant at the regional level. The annual maxima also lack a regional signal. However, annual minima exhibit more stations with decreasing trends. Our tests, which preserved temporal autocorrelation (via a moving–block bootstrap), still did not find the minima to be field significant.

6.2.2 Seasonal Trends

The Piedmont network shows seasonal flow shifts, but not a single and specific pattern for all the catchments.

- **Winter (DJF):** station-level significance for means (2/22) and maxima (1/22) and more requent for minima (4/22, all decreases). Majority of slopes also are negative for means and minima. This aligns with reduced snowpack and altered cold-season storage. Some smaller increases almost indicate a larger contribution of liquid runoff. The same type of variability is also observed elsewhere in the Alps (Birsan et al., 2005; Mallucci et al., 2019).

- **Spring (MAM):** significant trends occur across metrics (mean 5/22, max 5/22, min 3/22), mostly decreases. This can be related to the fact that snowmelt-dominated basins show earlier runoff and weaker late spring flows, in line with reports of advancing melt timing (shift in timing) (Stahl et al., 2010; Mallucci et al., 2019; Parajka and Blöschl, 2010; Bertola et al., 2020).

- **Summer (JJA):** significant negative trends are exist in analyzed metrics (mean 3/22,

maximum 4/22, minimum 5/22, essentially all declines). Most of the non-significant trends are also almost negative. The trend confirms rising warm-season drought stress and supports pan-European syntheses describing summer low-flow declines because of warming and increasing potential evapotranspiration in lowlands and possibly decreasing the snow reserves, which contribute to river flow at snow-dominated catchments in (Montanari et al., 2023; Stahl et al., 2010).

- **Autumn (SON):** significant minimum discharge reductions are more (7/22, all decreases), also some of the mean discharges had significant decreases (3/22). Maxima have lower significance (1/22), so autumn maxima do not experience a network-wide rise. The overall picture is that the deficit from summer continues into autumn.

6.2.3 Monthly Trends

The seasonal comparison reveals the summer and early autumn months as the period with the coherent decreases. Mean flow shows a significant losses during July–September, while minimum flow shows an even stronger and longer signal from June to December. Maximum flow recordings exhibit spatially localized signals, of which the month with the highest significance (11 of 22 stations declining) is the month of September. This seasonal connection implies a regional summer boost, drought stress, and declining baseflows, which corresponds with more general European and northern Italy evidence (Stahl et al., 2010; Hannaford et al., 2013; Bard et al., 2015; Mallucci et al., 2019).

September also seems to be a transitional month and links summer to autumn; also, field significance is detected for mean and minimum flows, and maxima show their only field-significant signal of the year. This indicates that summer drought stress (low water availability and baseflow decline) probably extends into autumn. By contrast, later autumn (October–November) shows significant decreases in minima at many stations. But the pattern is not mirrored in maxima and it is more heterogeneous. Overall, summer flows, especially minima, decline into the autumn. Other months vary more, which is probably shaped by basin properties and local controls. This agrees with large-sample European studies that find seasonal signatures rather than uniform annual shifts (Stahl et al., 2010; Hannaford et al., 2013; Floriancic et al., 2021). In summary, the monthly scale helps clarify what was observed

at the annual and seasonal scales: persistent summer drought stress is the clearest expression of discharge change in the Piedmont, with extensions into early autumn.

Synthesis

From annual to monthly resolution, discharge changes almost have a consistent story. Mean flows go downward and low flow stress occurs more often at the annual scale, while high flow extremes show no uniform rise. By investigating seasonal results, we can say that winter and spring river flows in Alpine basins probably reflect reduced snow storage and earlier melt. Summer records declines in every metric (minima, maxima, mean). Autumn remains mixed, with no coherent flood signal in the Piedmont network. Downscaling into monthly, the July–August discharges decline and extend into September–October, which can lead to intensifying warm-season drought stress.

6.3 Climatic Drivers and Their Consistency

We compare precipitation, temperature, and potential evapotranspiration (PET) to evaluate whether the observed change in flow corresponds to these forcings. This comparison can help to decide whether reduced water availability and changing regimes indicate consistent climatic signals or whether those results are mainly due to other factors like local variability, catchment characteristics, and other non-climatic factors, which we are not going to discuss in this research.

6.3.1 Precipitation

The precipitation does not show a single long-term pattern at the annual timescale over the Piedmont catchments. Some basins slope downward, others tends upward, and the region does not show a coherent signal. At a seasonal timescale, summer (JJA) shows a general pattern of decreasing mean precipitation. Autumn (SON) shows scattered, mainly small increases are recorded. The winter and the spring are scattered. overall, we couldn't see a significant trend.

On a monthly scale, most of the declines cluster in July and August. October and November, with some rises at individual catchments, but still the pattern is not significant. This

mixed picture aligns with Alpine and European assessments. They reported modest, spatially variable precipitation change compared with stronger temperature-driven signals (Bocchiola et al., 2014; Stahl et al., 2010). Based on our analysis, we can state that the weak or mixed precipitation signal suggests that precipitation alone cannot explain the full magnitude of riverflow changes in the study region.

6.3.2 Temperature

Temperature is rising in all the Piedmont catchments, across all time scales, including annual, seasonal, and monthly. The signal is spatially coherent (i.e., field significant). Warming is continuous throughout the year, including during the summer. This can increase the seasonal asymmetry in discharge values. Slopes of trends are positive on a month by month basis in each case. We observed the largest increases in February and mid-summer, July–August. The trend is consistent with regional and continental trends that record intense European warming and intensification of summer and minimum temperatures, as Europe is warming and Italy is warming faster (SNPA/ISPRA, 2024; European Environment Agency, 2025; Mallucci et al., 2019). Warming trends in snow-affected Alpine basins can be linked to earlier runoff peaks and reduced spring snow storage.

6.3.3 Potential Evapotranspiration (PET)

Mean potential evapotranspiration rises across all Piedmont catchments. Summer rises are the largest. Seasonal and monthly results confirm warm-season dominance: PET rises more from June to August, and also with a smaller slope, but still significant trends for spring and autumn. These rises are consistent across the system and indicative of basin-wide intensification of atmospheric water demand, probably independent of catchment size or setting.

6.3.4 Consistency Between Climatic and Hydrological Trends

The analysis of Climatic drivers, including precipitation, temperature, and PET, provided a clear context for the shifts in discharge. Precipitation has an erratic and geographically uneven nature, with just a feature, less summer rainfall, only with respect to Sen's slope

magnitudes. PET and temperature are consistently rising at all the catchments. June-August shifts are the largest. The trend corresponds with the hydrologic response, with flows reducing during the summer and ongoing low-flow stress. September river flow has a wide field significant decline in almost all the metrics, the two climate forcing of PET and temperature trends for this month are increasing mostly, but they are not significant. So, it seems that the coherent decline may be influenced by other climatic or non climatic drivers. Non-significant autumn peak of rainfall over Piedmont results in autumn high-flow indicators not increasing consistently, despite the Mediterranean coastal basin showing such signals (Blöschl et al., 2019; Hall and Blöschl, 2014). Declining summer discharge with demand motivated by warming reflects European syntheses of intensifying drought, strengthening (Stahl et al., 2010; Mallucci et al., 2019). Regional precipitation trend for the Piedmont also reflects Alpine outcomes, indicating that temperature and evapotranspiration are dominant and widespread signals (Stahl et al., 2010; Bocchiola et al., 2014). Overall, the main climate signals that can be seen are strengthening summer drought intensification as the primary regional footprint of forcing; in contrast, the flood-related responses remain local and weaker.

6.4 Comparison with Previous Studies

The results for Piedmont mostly agree with European and Alpine findings. The study adds finer and sharper temporal and spatial detail. Stahl et al. (2010) reported widespread summer low flow declines and changes in flood responses regionally on a European scale. The concentration of significant summer low flows in our analysis agrees with the mentioned broader pattern. Blöschl et al. (2019) showed that flood changes are strongly regional, with clearer signals in Mediterranean catchments than in the Alps. Therefore, the lack of a consistent autumn increase at our stations fits it.

Italian studies such as Mallucci et al. (2019) list snowmelt and warm-season drought stress at Alpine basins that point in the same direction. Castellarin et al. (2024) reported regime shifts in northern Italy that reduce warm-season water availability. We provided a monthly scale approach, and it helps to investigate finer timing of increasing droughts in the Piedmont region.

Our methodological approach followed practice like (Kundzewicz and Robson, 2004), employ-

ing the Mann–Kendall test and Sen's slope applied to discharge and climate forcings. Similar techniques are employed in large-scale Alpine and European studies (Parajka and Blöschl, 2010; Bard et al., 2015), although monthly resolution with a Piedmont focus is rare. We link long-term climatic forcing with discharge responses from Alpine through foothill and plain catchments of Piedmont and relate at the continental scale with the local scale for future water-management needs.

6.5 Implications for Water Management

Our study indicates a persistent decline in summer low flows extending into early autumn in the long term, whereas flood extremes show no significant increase. Both signals have practical implications for water management. Climatic drivers (temperature, precipitation, PET) condition these changes, while the response can also vary with physiography. Alpine headwaters, lowland basins, and foothill catchments require specific methods for water management.

6.5.1 Managing Summer Low Flow Decline and Drought Risk

The urgent issue is the drop in summer low flows. Earlier snowmelt in Alpine headwaters and reduced summer runoff weaken the natural storage capacity of these systems. The high PET in the lowland intensifies the seasonal deficits. The 2022 Po drought, stated as the most severe extreme in two centuries (Montanari et al., 2023), demonstrates how climatic stress and increasing demand together can produce severe stress. Allocation rules must account for a declining and less reliable summer supply.

Effective measures include demand management for urban and irrigation uses, leakage control, and drought risk planning. Combined use of surface water and groundwater can stabilise supplies. Alpine reservoir operations are worth consideration to balance hydropower supplies and late season environmental flows, as proposed in Alpine assessments (Mallucci et al., 2019). Environmental flow standards will also need seasonal adjustment to protect ecosystems during critical months.

6.5.2 Flood Risk and Autumn Extremes

Piedmont rivers do not have regular autumn rise in floods. The Alpine–lowland system tends to dampen maxima. Without a sharp autumn rise in rainfall, major structural adaptation to flood risk is not supported; however, climate change can cause extreme weather events and continued monitoring is necessary (Blöschl et al., 2019; Hall and Blöschl, 2014).

6.5.3 Monitoring, Design, and Governance

Adaptation applications need to have strong foundations. Long-term monitoring of discharge and climate drivers is essential. Denser gauging in underrepresented basins and careful metadata curation. This enable robust reanalysis (Kundzewicz and Robson, 2004).

Piedmont must prepare for increased summer water restrictions, be flexible and ready for floods, but strike a balance. This differentiated, evidence-informed approach is consistent with previous studies and recent European guidance on managing water (Stahl et al., 2010; European Commission, 2025).

6.6 Chapter Summary

This chapter shows that annual means of Piedmont's river flows are mostly declining, and magnitudes of floods are not rising coherently. The seasonal–monthly view reveals a regional summer–early autumn signal: July–September decreases are more (extending to October for mean flows and to November–December for minima); Alpine headwaters responding most (reduced snow storage and earlier melt), foothill tributaries responding intermediately, and lowland rivers having larger summer deficits with increasing PET. These patterns confirm continent-wide decreases in Alpine snowmelt shifts in low-flow, and no rise in autumn floods consistent with regional findings of the Alps Management implications are increased summer demand management, conjunctive use of groundwater–surface water, adaptive reservoir use, and proportional flood preparation, consistent with European guidance about nonstationarity.

Chapter 7

Conclusion

7.1 Key Findings

This thesis examined long-term changes in river discharge across the Piedmont region in northern Italy and compared them with trends in precipitation, temperature, and potential evapotranspiration (PET). Using the Mann–Kendall test and Sen's slope on annual, seasonal, and monthly scales, two conclusions follow:

1. **Summer low flows are dropping in the study region.** The largest declines are clearest in monthly minima and are seen in Alpine and low-land basin areas (Po plain). The seasonality almost matches high temperature and high PET conditions, and summer rainfall does not have a compensating rise.

2. **There is no coherent increase in high-flow indicators.** Annual maxima are not field significant, and maxima for months are only isolated, field significant *decreases* in *September*, and it is not significantly consistent with the investigated drivers. Therefore, the flood change is less consistent than the signals of drought.

7.2 Contributions of the Thesis

The study adds:

- A hydroclimatic framework that uses the same tests for discharge and three climate drivers, including precipitation, temperature, and PET. This allows direct comparison and first-order assessment.

- A regional view that included three different types of catchments, including Alpine headwaters, foothills, and lowland rivers, within a consistent workflow.
- Using a multiscale analysis (annual, seasonal, monthly) that can help to clarify timing, build confidence, and support decisions.

7.3 Limitations

This research relies on monotonic trend tests. In this case, changes in steps, accelerations, and cycles may be missed. Site-level *p*-values were not adjusted for serial correlation, which can lead to overstate significance at individual stations. We used a field significance test to assess the regional coherence, but it still does not replace autocorrelation-robust tests at each site. Data gaps can reduce the power of trend detection methodology, especially when these gaps are clustered in certain decades. In addition to data gaps, a serious limitation was the smaller number of usable stations for conducting a trend test, which lowers the power and makes it very difficult to reach a confident field significance result. Influences (such as operations, abstractions, and land use changes) were not investigated in this study, but they can shape local responses. These limits motivate the future work below.

7.4 Future Work

- **Extended detection.** Combine change-point tools with monotonic trend tests. Apply autocorrelation-robust significance and stronger multiplicity control across stations, months, and metrics.
- **Human–water processes.** Incorporate abstractions, reservoir-operating rules, irrigation, land use change, and environment-flow policies to distinguish climate from management signals.
- **Attribution analysis.** Quantify how climate drivers, physiographic setting, and water operations contribute to monthly and seasonal trends to distinguish climate signals from human and catchment effects.

Bibliography

Noor Ahmad Akhundzadah. Analyzing temperature, precipitation, and river discharge trends in afghanistan's main river basins using innovative trend analysis, mann–kendall, and sen's slope methods. *Climate*, 12(12):196, 2024.

Hans Alexandersson. A homogeneity test applied to precipitation data. *Journal of climatology*, 6(6):661–675, 1986.

Autorità di Bacino del Fiume Po. Po river basin district management plan. https://www.adbpo.it/PianoAcque2021/PdGPo2021_22dic21/Elaborato_00_RelGEn_22dic2021/PdGPo2021_Elab_0_RelGen_22dic21.pdf, 2021. Accessed 2025-09-21.

Jushan Bai and Pierre Perron. Computation and analysis of multiple structural change models. *Journal of applied econometrics*, 18(1):1–22, 2003.

Alessandro Balistrocchi et al. Hydroclimatic variability and land cover transformations in the central italian alps. *Water*, 13(7):963, 2021. doi: 10.3390/w13070963.

Alain Bard, Bastien Renard, Michel Lang, et al. Trends in the hydrologic regime of alpine rivers. *Journal of Hydrology*, 529:1823–1837, 2015. doi: 10.1016/j.jhydrol.2015.07.052.

Miriam Bertola, Alberto Viglione, David Lun, Julia Hall, and Günter Blöschl. Flood trends in europe: are changes in small and big floods different? *Hydrology and Earth System Sciences*, 24(4):1805–1822, 2020.

M.-V. Birsan, P. Molnar, P. Burlando, and M. Pfaundler. Streamflow trends in switzerland. *Journal of Hydrology*, 314:312–329, 2005. doi: 10.1016/j.jhydrol.2005.06.008.

Günter Blöschl, J. Hall, J. Parajka, B. Perdigão, A. Merz, B. Arheimer, and G. Viglione. Changing climate both increases and decreases european river floods. *Nature*, 573:108–111, 2019. doi: 10.1038/s41586-019-1495-6.

Günter Blöschl et al. Changing climate both increases and decreases european river floods. *Nature*, 573:108–111, 2019. doi: 10.1038/s41586-019-1495-6.

Daniele Bocchiola et al. Long-term (1921–2011) hydrological regime of alpine catchments in northern italy. *Advances in Water Resources*, 67:10–22, 2014. doi: 10.1016/j.advwatres.2014.04.017.

G. Braca, M. Bussettini, M. Casaioli, B. Lastoria, S. Mariani, F. Piva, and R. Tropeano. Elaborazioni modello bigbang versione 9.0. https://groupware.sinanet.isprambiente.it/bigbang-data/library/bigbang_90, 2025. Istituto Superiore per la Protezione e la Ricerca Ambientale (ISPRA) [data set]. Last access: 2025-03-31.

Elisa Brussolo, Elisa Palazzi, Jost von Hardenberg, Giulio Masetti, Gianna Vivaldo, Maurizio Previati, Davide Canone, Davide Gisolo, Ivan Bevilacqua, Antonello Provenzale, and Stefano Ferraris. Aquifer recharge in the piedmont alpine zone: historical trends and future scenarios. *Hydrology and Earth System Sciences*, 26:407–427, 2022. doi: 10.5194/hess-26-407-2022.

T. A. Buishand. Tests for detecting a shift in the mean of hydrological time series. *Journal of Hydrology*, 73(1–2):51–69, 1984. doi: 10.1016/0022-1694(84)90032-5.

Attilio Castellarin, Andrea Magnini, Kay Khaing Kyaw, Filippo Ciavaglia, Miriam Bertola, Gunter Blöschl, Elena Volpi, Pierluigi Claps, Alberto Viglione, Alberto Marinelli, et al. Frequency of italian record-breaking floods over the last century (1911–2020). *Atmosphere*, 15(7):865, 2024.

Pierluigi Claps, Giuseppe Evangelista, Daniele Ganora, Paola Mazzoglio, and Silvia Monforte. Foca italian flood and catchment atlas, 2023. URL https://doi.org/10.5281/zenodo.10446258. Data set.

Pierluigi Claps, Giuseppe Evangelista, Daniele Ganora, Paola Mazzoglio, and Silvia Monforte. Foca: a new quality-controlled database of floods and catchment descriptors in italy.

Earth System Science Data, 16:1503–1522, 2024. doi: 10.5194/essd-16-1503-2024. URL https://doi.org/10.5194/essd-16-1503-2024.

Martine Collaud Coen, Elisabeth Andrews, Alessandro Bigi, Giovanni Martucci, Gonzague Romanens, Frédéric P. A. Vogt, and Laurent Vuilleumier. Effects of the prewhitening method, the time granularity, and the time segmentation on the mann–kendall trend detection and the associated sen's slope. *Atmospheric Measurement Techniques*, 13:6945–6964, 2020. doi: 10.5194/amt-13-6945-2020. URL https://doi.org/10.5194/amt-13-6945-2020.

Jean-Baptiste Collignan et al. Identifying and quantifying the impact of climatic and non-climatic drivers on river discharge in europe. *Water Resources Research*, 2025. doi: 10.1029/2024WR038220.

Norman R. Draper and Harry Smith. *Applied Regression Analysis*. Wiley-Interscience, 3rd edition, 1998.

European Commission. Water framework directive (2000/60/ec) - river basin management. https://environment.ec.europa.eu/topics/water/water-framework-directive_en, 2025. Accessed: 2025-09-25.

European Environment Agency. Global and european temperatures, 2025. URL https://www.eea.europa.eu/en/analysis/indicators/global-and-european-temperatures. Europe has warmed faster than the global average in recent decades.

Marius G. Floriancic, Wouter R. Berghuijs, Peter Molnar, and James W. Kirchner. Seasonality and drivers of low flows across europe and the united states. *Water Resources Research*, 57(9):e2019WR026928, 2021. doi: 10.1029/2019WR026928.

Richard O. Gilbert. *Statistical Methods for Environmental Pollution Monitoring*. John Wiley & Sons, 1987. URL https://www.scirp.org/reference/referencespapers?referenceid=1997064.

Julia Hall and Günter Blöschl. Understanding flood regime changes in europe: A state-of-the-art assessment. *Hydrology and Earth System Sciences*, 18:2735–2772, 2014. doi: 10.5194/hess-18-2735-2014.

K.H. Hamed and A.R. Rao. A modified mann–kendall trend test for autocorrelated data. *Journal of Hydrology*, 204(1–4):182–196, 1998. doi: 10.1016/S0022-1694(97)00125-X.

Jamie Hannaford, Gabriel Buys, Christel Svensson, Kerstin Stahl, and Ben Lloyd-Hughes. Trends in long european streamflow records. *Hydrology and Earth System Sciences Discussions (HESSD)*, 10:1859–1911, 2013. doi: 10.5194/hessd-10-1859-2013.

Dennis R. Helsel and Robert M. Hirsch. *Statistical Methods in Water Resources*. U.S. Geological Survey, 2002.

Robert M. Hirsch and James R. Slack. A nonparametric trend test for seasonal data with serial dependence. *Water Resources Research*, 20(6):727–732, 1984.

Robert M. Hirsch, James R. Slack, and Richard A. Smith. Techniques of trend analysis for monthly water quality data. *Water Resources Research*, 18(1):107–121, 1982. doi: 10.1029/WR018i001p00107.

IPCC. Climate change 2021: The physical science basis. contribution of working group i to the sixth assessment report of the ipcc, 2021. URL https://www.ipcc.ch/report/ar6/wg1/. Intergovernmental Panel on Climate Change.

ISPRA. Valori climatici normali del periodo 1981–2010. Rapporto 55/2014, ISPRA — Istituto Superiore per la Protezione e la Ricerca Ambientale, Roma, Italia, 2014. URL https://www.isprambiente.gov.it/files/pubblicazioni/SA_55_14_Valori_climatici_normali.pdf. Vedi p. 11, Sec. 4.4 *Precipitazione cumulata*.

ISTAT. Principali statistiche geografiche sui comuni, 2025. URL https://www.istat.it/classificazione/principali-statistiche-geografiche-sui-comuni/.

Maurice G. Kendall. *Rank Correlation Methods*. Griffin, 4th edition, 1975.

M. N. Khaliq, T. B. M. J. Ouarda, D. H. Burn, and P. Gachon. Identification of hydrological trends in the presence of serial and cross correlations: A review of selected methods and their application to annual flow regimes of canadian rivers. *Hydrological Sciences Journal*, 54(4):711–727, 2009. doi: 10.1623/hysj.54.4.711.

Rebecca Killick, Paul Fearnhead, and Idris A Eckley. Optimal detection of changepoints with a linear computational cost. *Journal of the American Statistical Association*, 107(500): 1590–1598, 2012.

Roger Koenker and Gilbert Bassett. Regression quantiles. *Econometrica*, 46(1):33–50, 1978. doi: 10.2307/1913643.

Zbigniew W. Kundzewicz and Arthur J. Robson. Change detection in hydrological records–a review of the methodology. *Hydrological Sciences Journal*, 49(1):7–19, 2004. doi: 10.1623/hysj.49.1.7.53993.

R. E. Livezey and W. Y. Chen. Statistical field significance and its determination by monte carlo techniques. *Monthly Weather Review*, 111:46–59, 1983.

Stefano Mallucci, Bruno Majone, and Alberto Bellin. Detection and attribution of hydrological changes in a large alpine river basin. *Journal of Hydrology*, 576:25–41, 2019. doi: 10.1016/j.jhydrol.2019.05.023.

W. Mangini, A. Viglione, J. Hall, et al. Detection of trends in magnitude and frequency of flood peaks across europe. *Journal of Hydrology*, 559:373–384, 2018.

H. B. Mann. Nonparametric tests against trend. *Econometrica*, 13(3):245–259, 1945.

Davide Masseroni et al. The 63-year changes in annual streamflow volumes across europe with a focus on the mediterranean basin. *Hydrology and Earth System Sciences*, 25: 5589–5601, 2021. doi: 10.5194/hess-25-5589-2021.

Paola Mazzoglio, Miriam Bertola, Luca Lombardo, Chiara Sacco, Alberto Viglione, Francesco Laio, and Pierluigi Claps. Increasing the availability of italian daily hydrological measurements with a citizen science approach: the siren project. In *EGU General Assembly Conference Abstracts*, page 2080, 2024.

Paola Mazzoglio, Miriam Bertola, Alvise Mattozzi, Tommaso Listo, Luca Princivalle, Chiara Sacco, Luca Lombardo, Alberto Viglione, Francesco Laio, Pierluigi Claps, et al. Siren: a citizen science project for the recovery of the italian hydrological data. In *Titolo volume non avvalorato*. Copernicus GmbH, 2025.

Alberto Montanari. Hydrology of the po river: looking for changing patterns in variability and persistence. *Hydrology and Earth System Sciences*, 16(11):3739–3747, 2012. doi: 10.5194/hess-16-3739-2012. URL https://hess.copernicus.org/articles/16/3739/2012/.

Andrea Montanari et al. Why the 2022 po river drought is the worst in the past two centuries. *Science Advances*, 9(32):eadg8304, 2023. doi: 10.1126/sciadv.adg8304.

Francesco Di Nunno, Carlo Giudicianni, Enrico Creaco, and Fabio Granata. Exploring streamflow dynamics: trends and abrupt changes in major european rivers. *Stochastic Environmental Research and Risk Assessment*, 38:5019–5038, 2024. doi: 10.1007/s00477-024-02848-3.

F. Ouassanouan et al. Multi-decadal analysis of water resources and agricultural production in piedmont. *Science of The Total Environment*, 857:159404, 2022. doi: 10.1016/j.scitotenv.2022.159404.

Julija Parajka and Günter Blöschl. Seasonal characteristics of flood regimes across the alpine–carpathian range. *Journal of Hydrology*, 394:78–89, 2010. doi: 10.1016/j.jhydrol.2010.05.015.

A. N. Pettitt. A non-parametric approach to the change-point problem. *Applied Statistics*, 28(2):126–135, 1979. doi: 10.2307/2346729.

Regione Piemonte and ARPA Piemonte. Analisi del clima regionale del periodo 1981–2010 e tendenze negli ultimi 60 anni (sintesi). Technical report, Regione Piemonte & ARPA Piemonte, Torino, Italia, 2020. URL https://www.regione.piemonte.it/web/sites/default/files/media/documenti/2020-07/analisi_clima_regionale_1981-2010.pdf. Vedi p. 5, sezione "Precipitazioni".

Rajkumar Sakamuri et al. Trends due to climate change in precipitation and stream flows: A case study of italy. In *Climate Change Impact on Water Resources, Lecture Notes in Civil Engineering, Vol. 561*, pages 127–148. Springer, 2025. doi: 10.1007/978-981-97-9180-4_9.

Pranab Kumar Sen. Estimates of the regression coefficient based on kendall's tau. *Journal of the American Statistical Association*, 63(324):1379–1389, 1968.

SNPA/ISPRA. Ambiente in italia 2024 — 10. clima. https://indicatoriambientali.isprambiente.it/sites/default/files/pdf/Ambiente%20in%20Italia%202024/10%20Clima.pdf, 2024. Sezione *Temperatura media*, p. 112.

Klaus Stahl et al. Streamflow trends in europe: Evidence from a dataset of near-natural catchments. *Hydrology and Earth System Sciences*, 14:2367–2382, 2010. doi: 10.5194/hess-14-2367-2010.

Garth Tarr. Small sample performance of quantile regression confidence intervals. *Journal of Statistical Computation and Simulation*, 82(1):81–94, 2012. doi: 10.1080/00949655.2010.527844.

Hans von Storch and Francis W. Zwiers. *Statistical Analysis in Climate Research*. Cambridge University Press, 1999.

Shaoqiang Yue and Chiew Wang. The mann–kendall test modified by effective sample size to detect trend in serially correlated hydrological series. *Water Resources Management*, 18(3):201–218, 2004a. doi: 10.1023/B:WARM.0000043140.61082.60.

Shaoqiang Yue and Chiew Wang. The mann–kendall test modified by effective sample size to detect trend in serially correlated hydrological series. *Water Resources Management*, 18(3):201–218, 2004b.

D. Zanchettin, P. Traverso, and M. Tomasino. Earlier spring discharge in alpine rivers: the role of precipitation seasonality and liquid precipitation ratio. *Hydrology and Earth System Sciences*, 18(11):4655–4668, 2014.

Appendix A

Supplementary Maps and Figures

A.1 River flow time series

A017 CASSINE BORMIDA

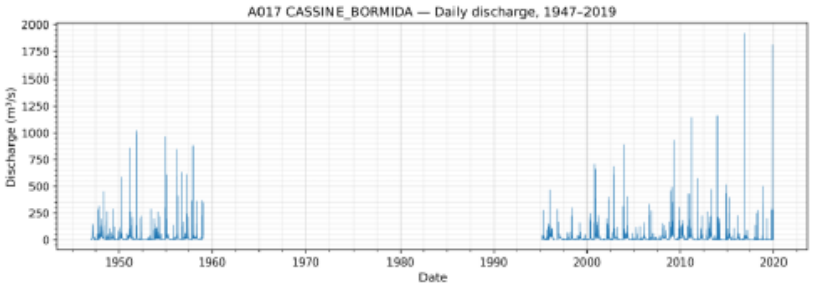

A022 MOMBALDONE BORMIDA

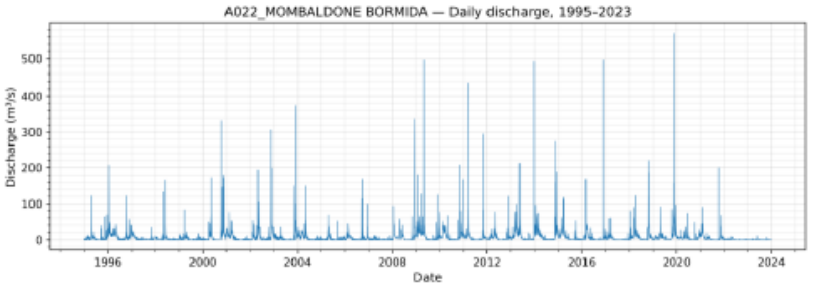

A030 PASSOBREVE CERVO

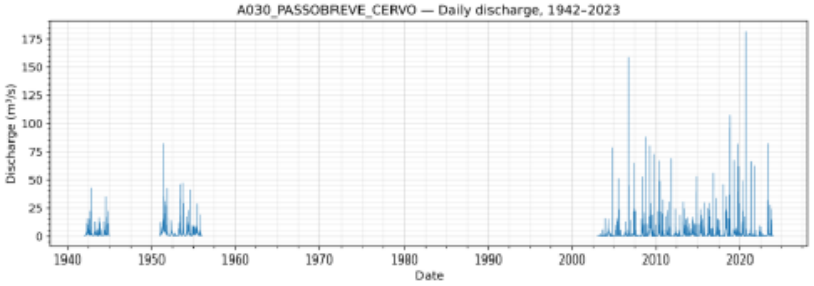

A038 Chisone

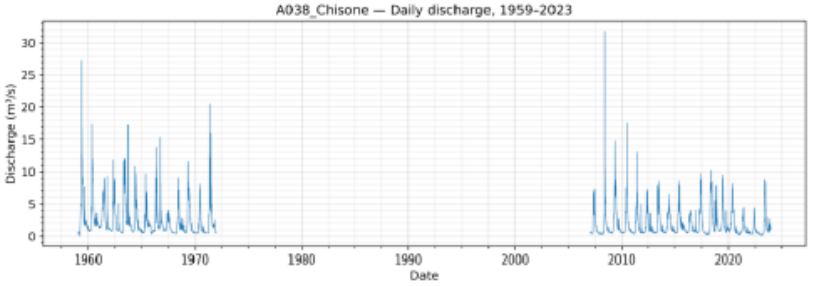

A040 ChisoneSanMartino

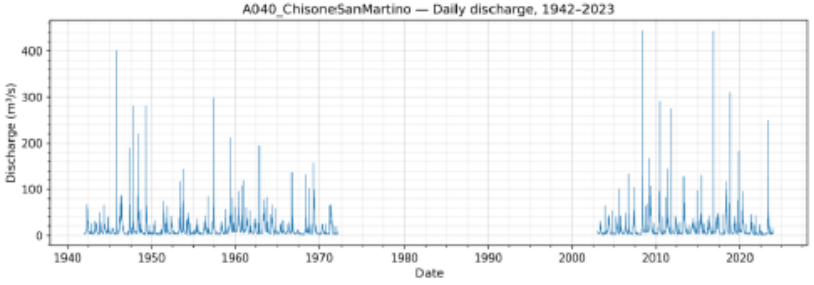

A049 DoraBaltea

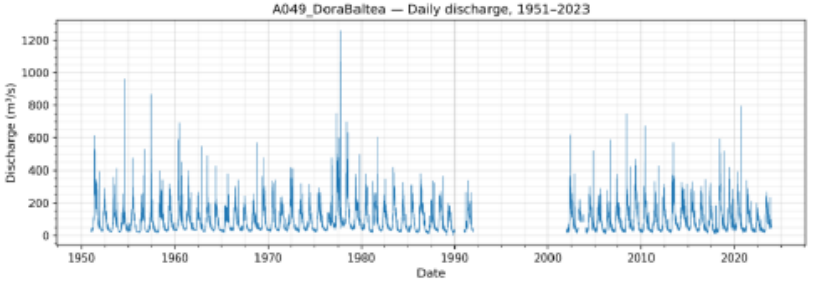

A057 DoraRiparia

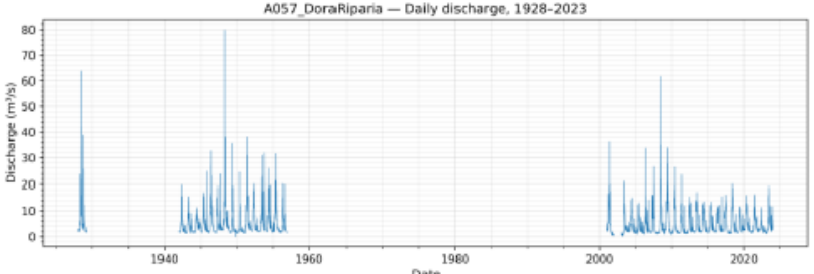

A073 GranaMonterosso

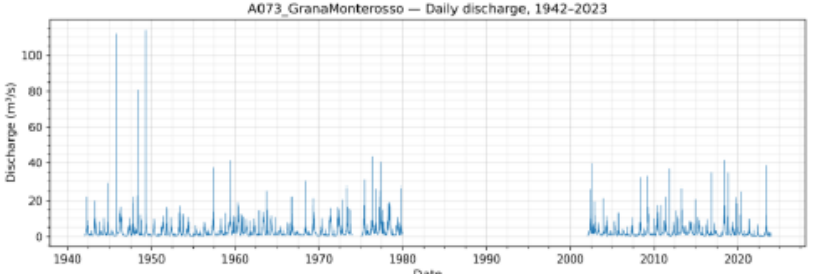

A106 PoCrissolo

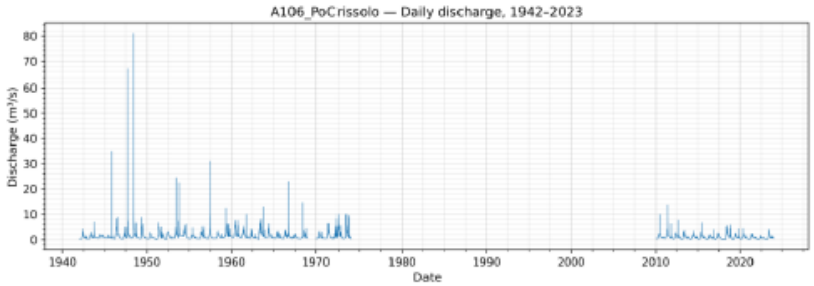

A107 PoCarignano

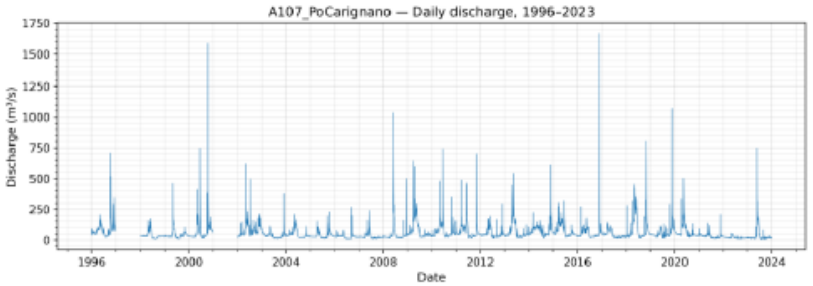

A108 MONCALIERI PO

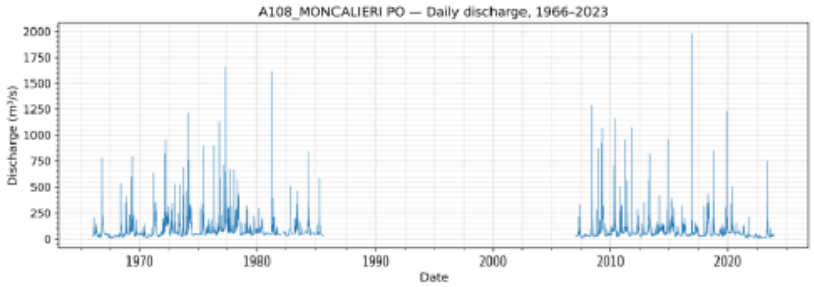

A113 ISOLA S ANTONIO PO

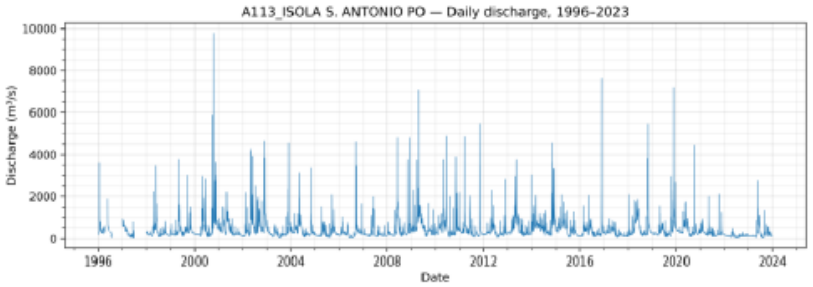

A129 SANTINO SAN BERNARDINO

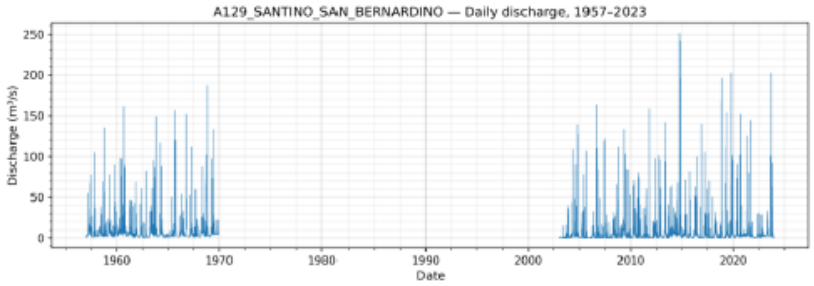

A141 ScriviaSerravalle

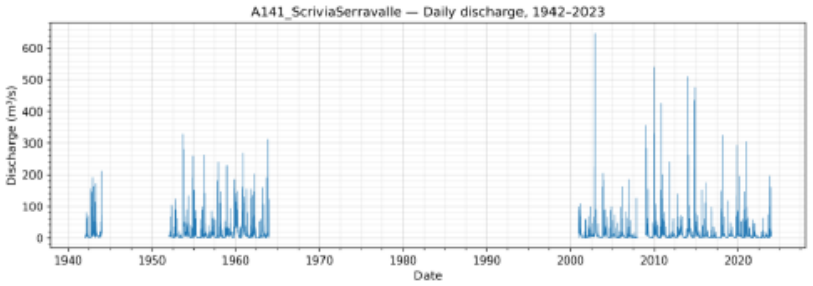

A146 SesiaCampertogno

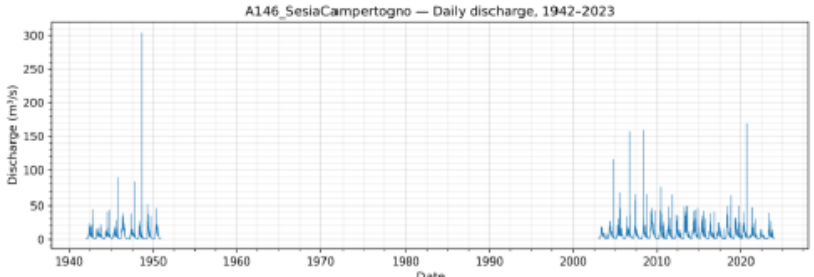

A152 SturaDemonteGaiola

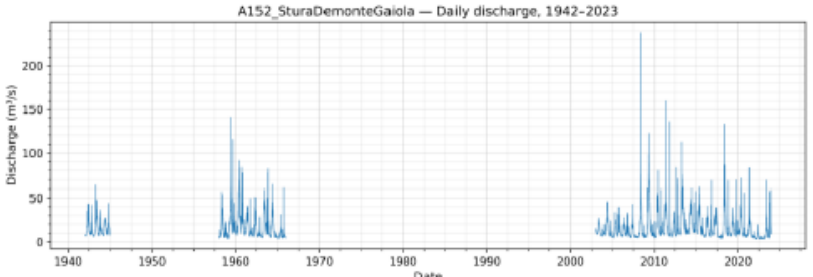

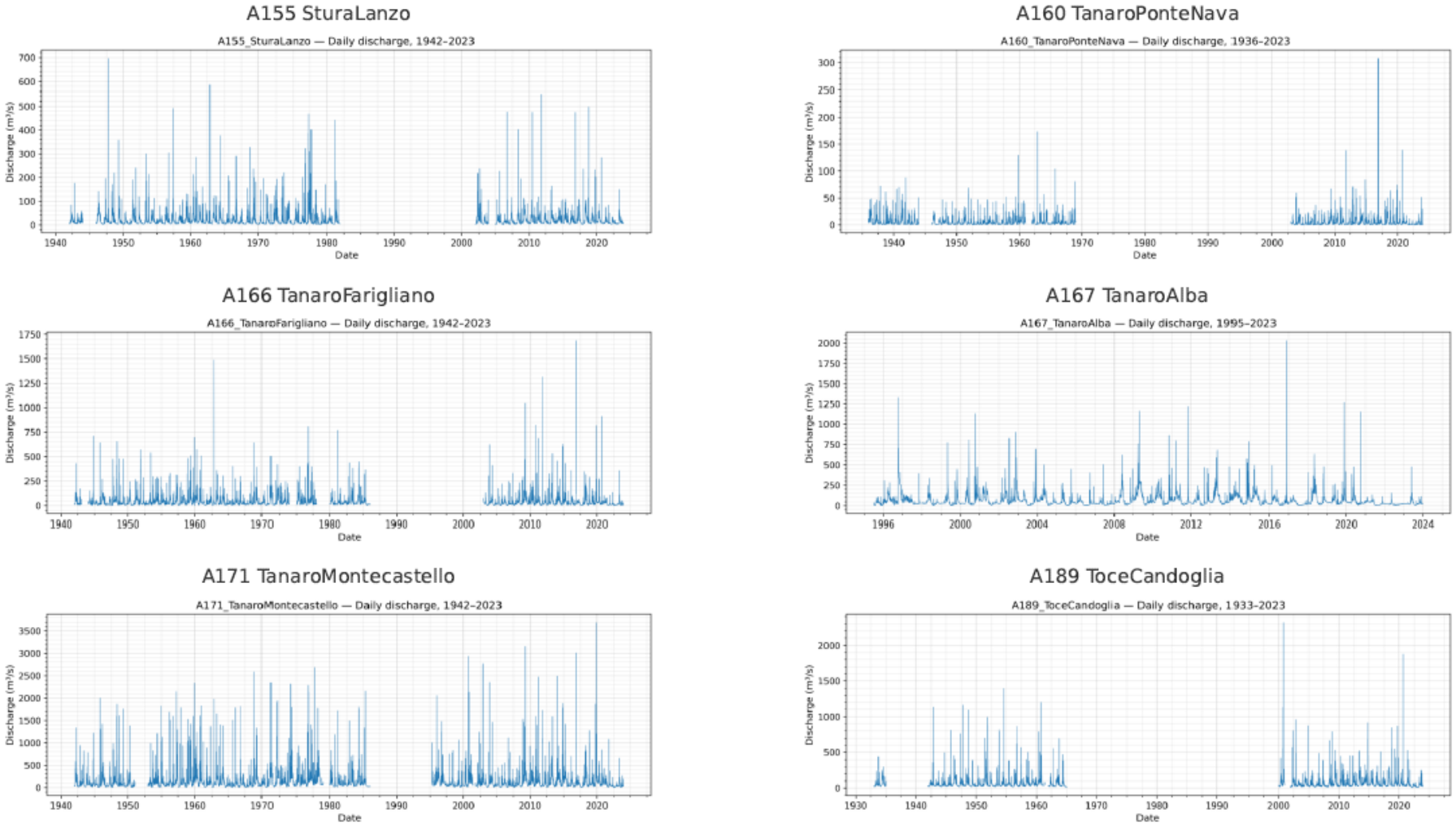

Figure A.3: River flow time series — Figure 3

A.2 Station Trend Map

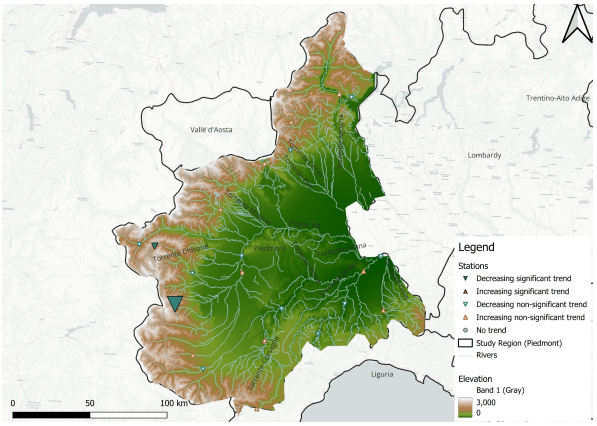

(a) January mean

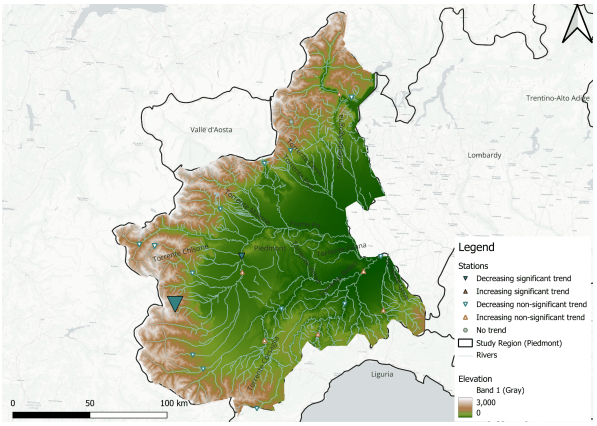

(b) January minimum

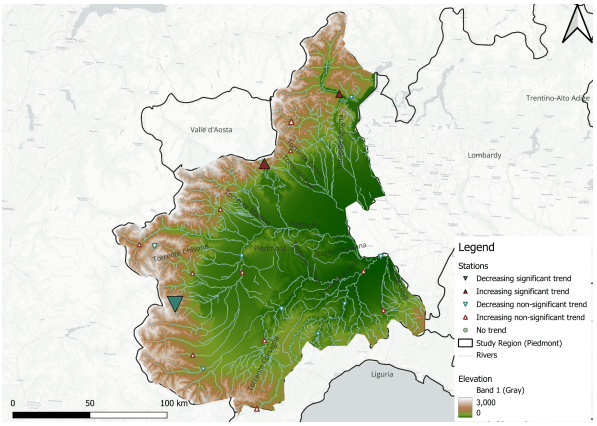

(c) January maximum

Figure A.4: Mann–Kendall test statistic for January discharge across the study area. Positive values (red) indicate increases; negative values (blue) indicate decreases. Triangle size is inversely proportional to the p-value (larger symbols indicate stronger significance).

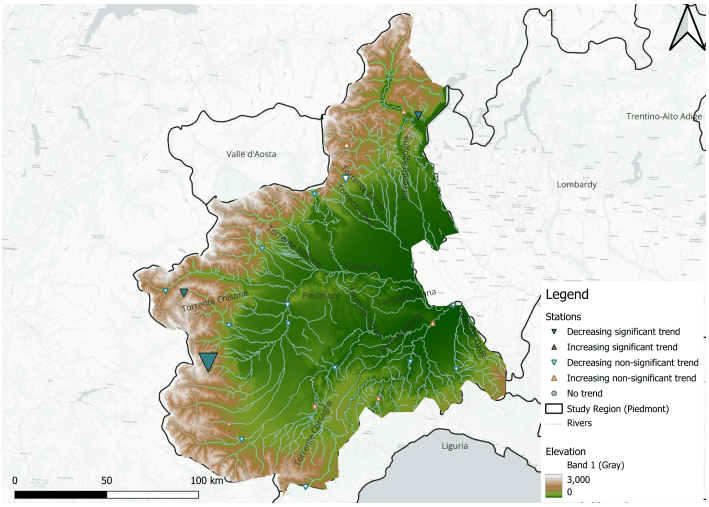

(a) February mean

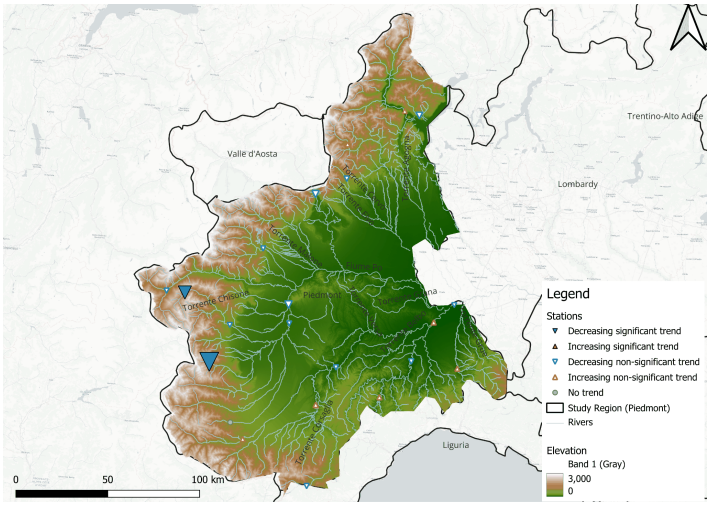

(b) February minimum

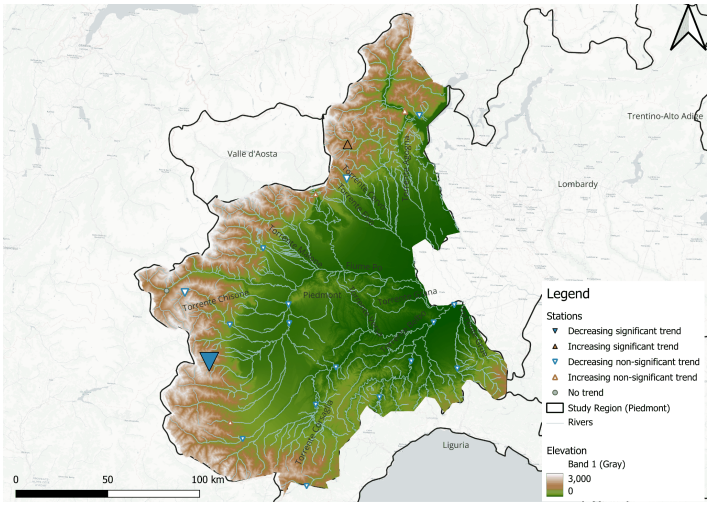

(c) February maximum

Figure A.5: Mann–Kendall test statistic for February discharge across the study area. Positive values (red) indicate increases; negative values (blue) indicate decreases. Triangle size is inversely proportional to the p-value (larger symbols indicate stronger significance).

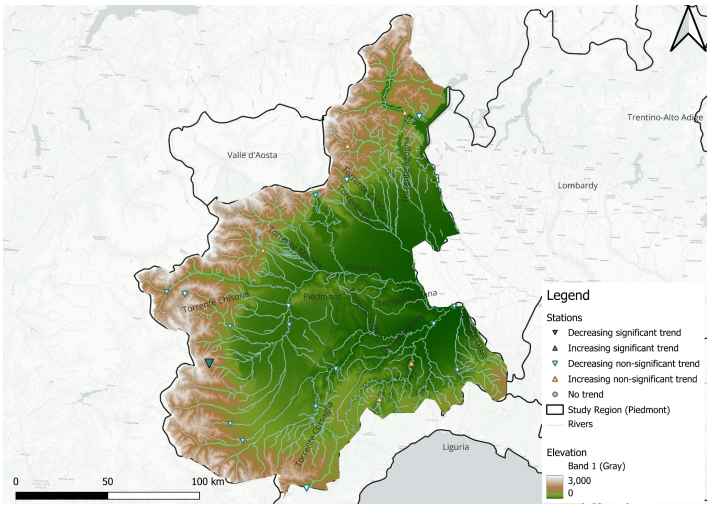

(a) March mean

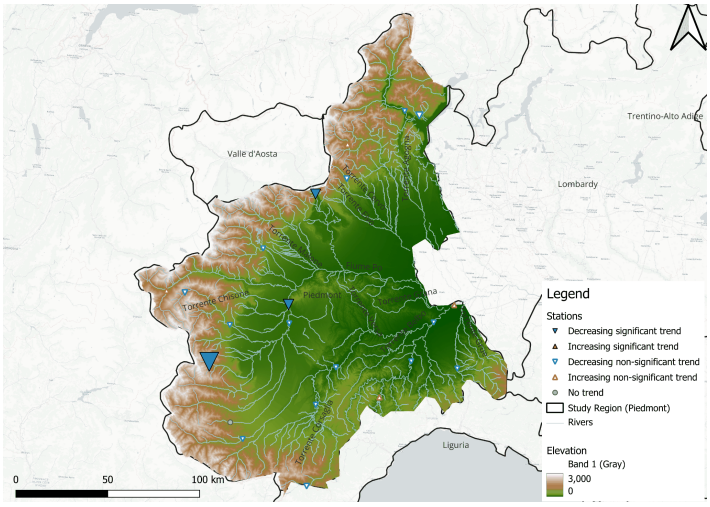

(b) March minimum

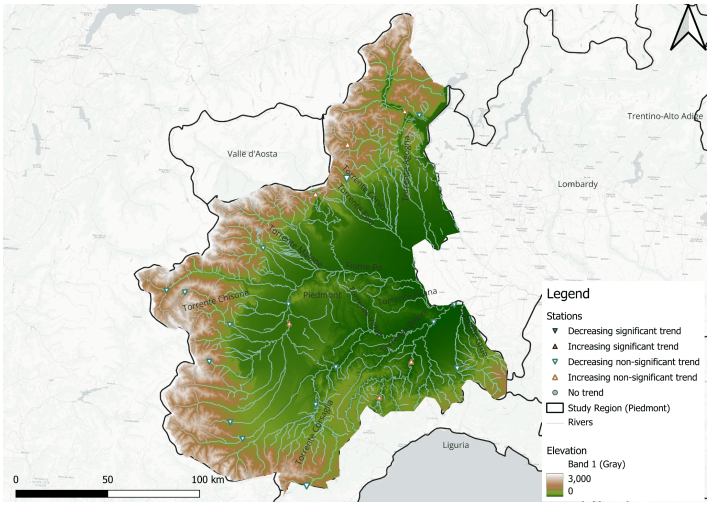

(c) March maximum

Figure A.6: Mann–Kendall test statistic for March discharge across the study area. Positive values (red) indicate increases; negative values (blue) indicate decreases. Triangle size is inversely proportional to the p-value (larger symbols indicate stronger significance).

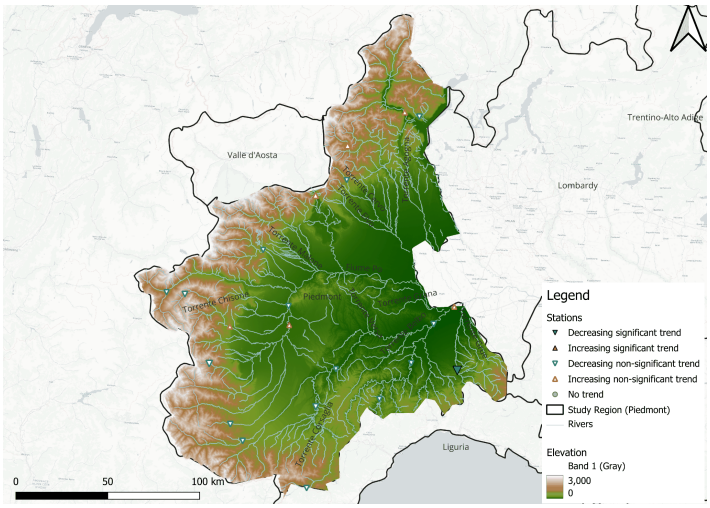

(a) April mean

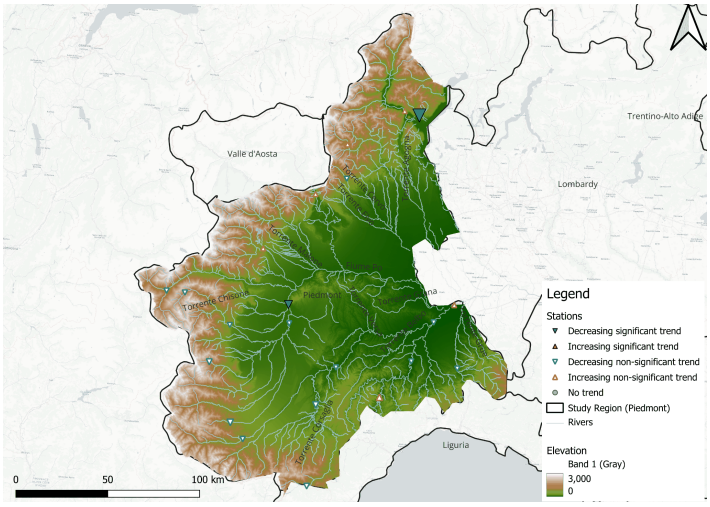

(b) April minimum

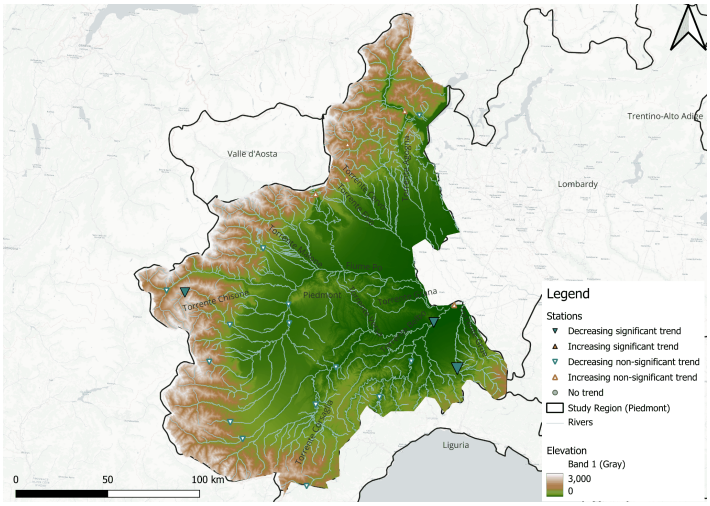

(c) April maximum

Figure A.7: Mann–Kendall test statistic for April discharge across the study area. Positive values (red) indicate increases; negative values (blue) indicate decreases. Triangle size is inversely proportional to the p-value (larger symbols indicate stronger significance).

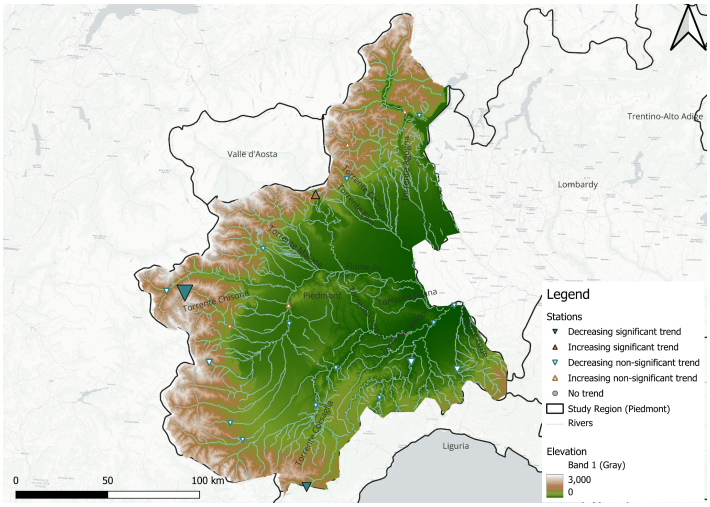

(a) May mean

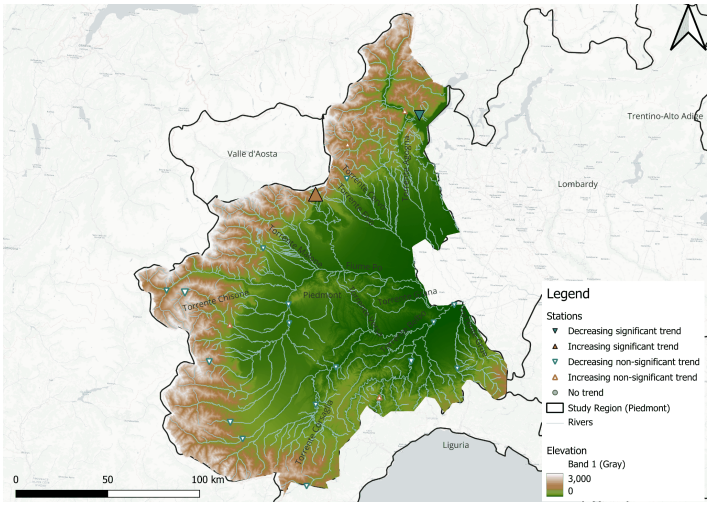

(b) May minimum

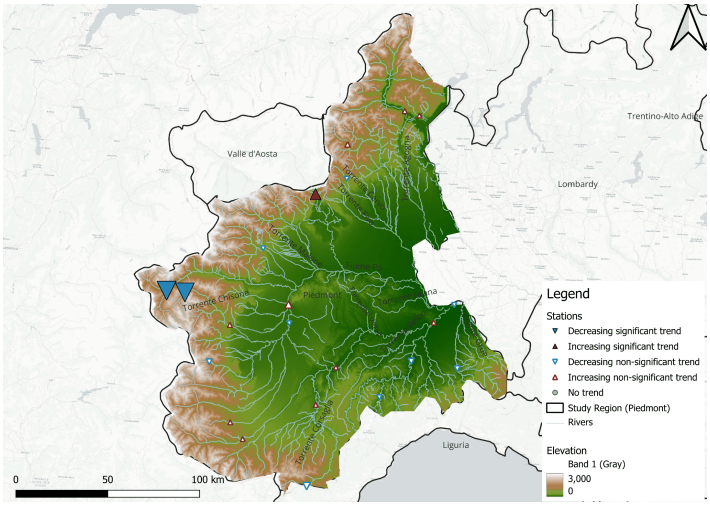

(c) May maximum

Figure A.8: Mann–Kendall test statistic for May discharge across the study area. Positive values (red) indicate increases; negative values (blue) indicate decreases. Triangle size is inversely proportional to the p-value (larger symbols indicate stronger significance).

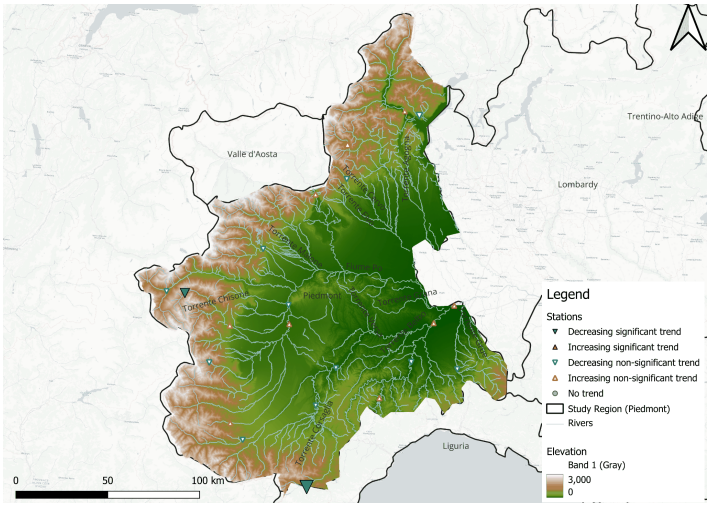

(a) June mean

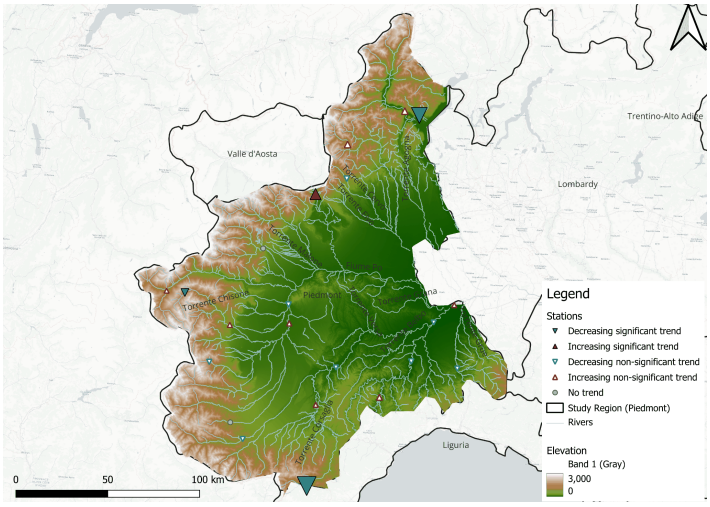

(b) June minimum

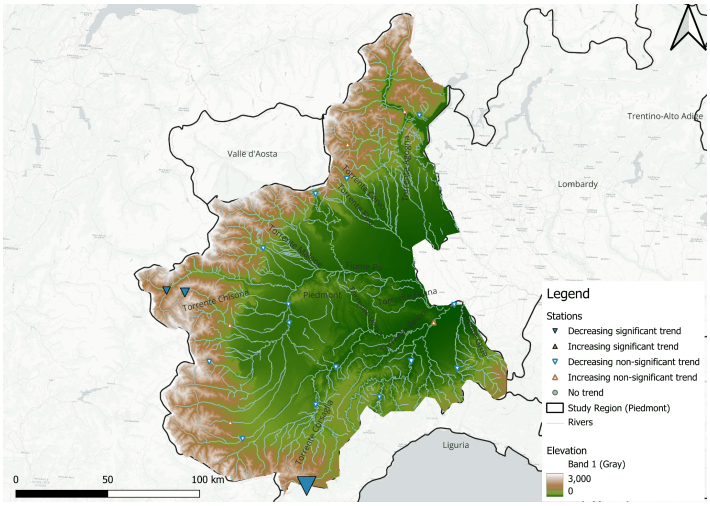

(c) June maximum

Figure A.9: Mann–Kendall test statistic for June discharge across the study area. Positive values (red) indicate increases; negative values (blue) indicate decreases. Triangle size is inversely proportional to the p-value (larger symbols indicate stronger significance).

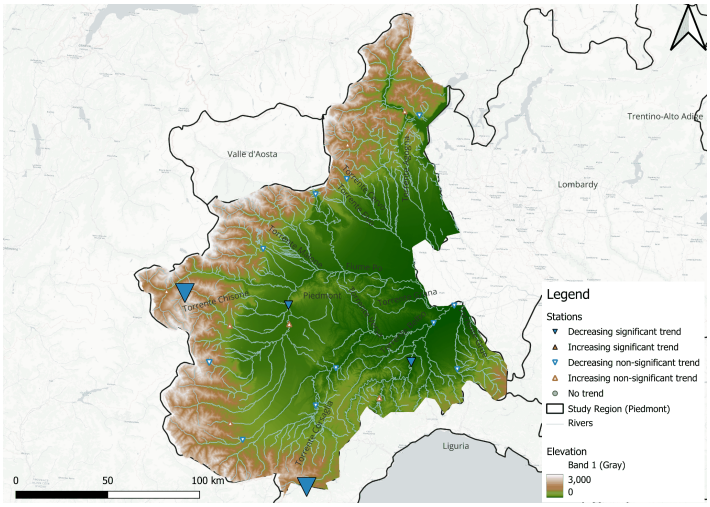

(a) July mean

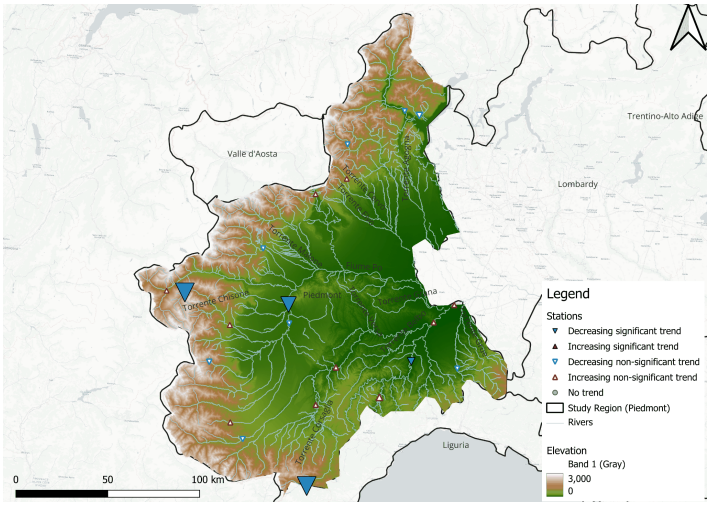

(b) July minimum

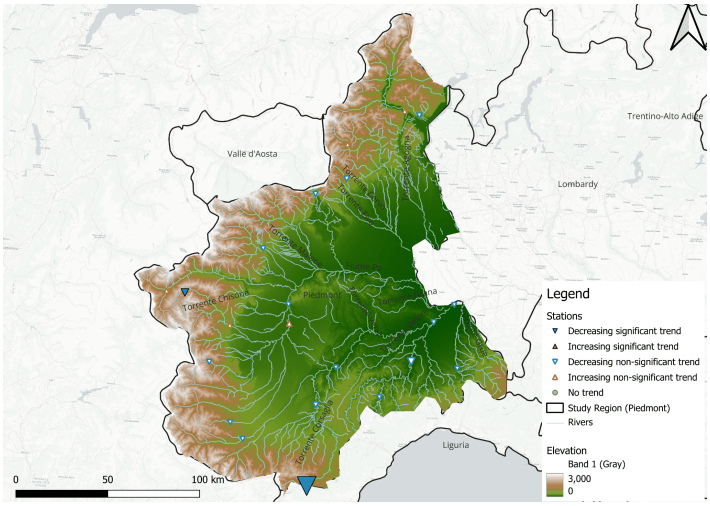

(c) July maximum

Figure A.10: Mann–Kendall test statistic for July discharge across the study area. Positive values (red) indicate increases; negative values (blue) indicate decreases. Triangle size is inversely proportional to the p-value (larger symbols indicate stronger significance).

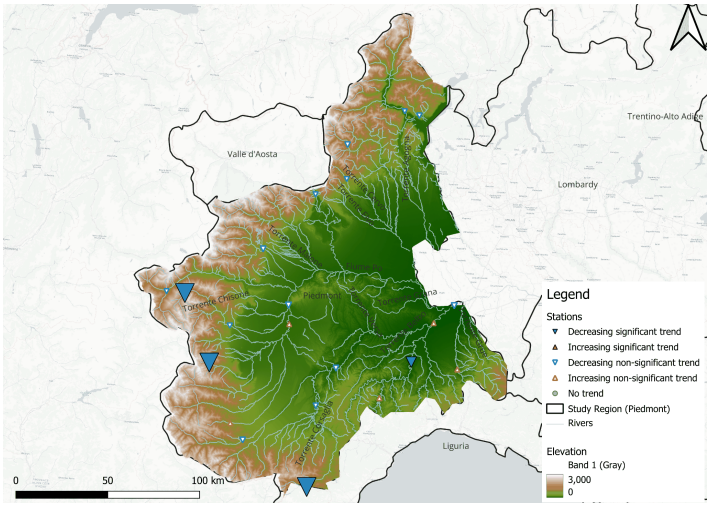

(a) August mean

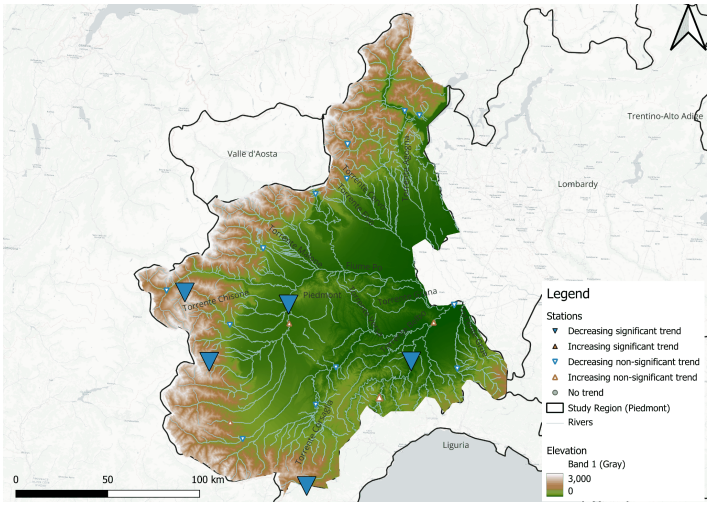

(b) August minimum

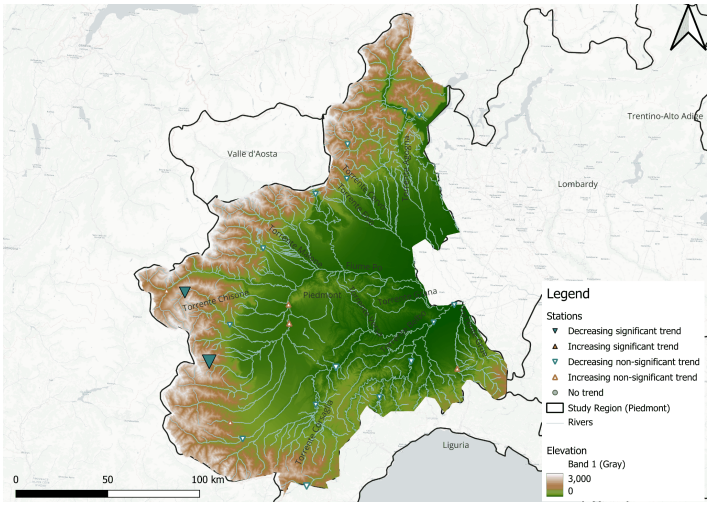

(c) August maximum

Figure A.11: Mann–Kendall test statistic for August discharge across the study area. Positive values (red) indicate increases; negative values (blue) indicate decreases. Triangle size is inversely proportional to the p-value (larger symbols indicate stronger significance).

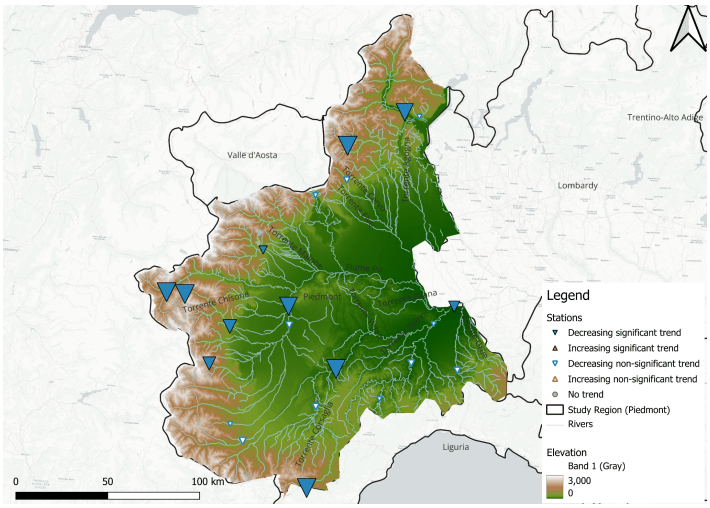

(a) September mean

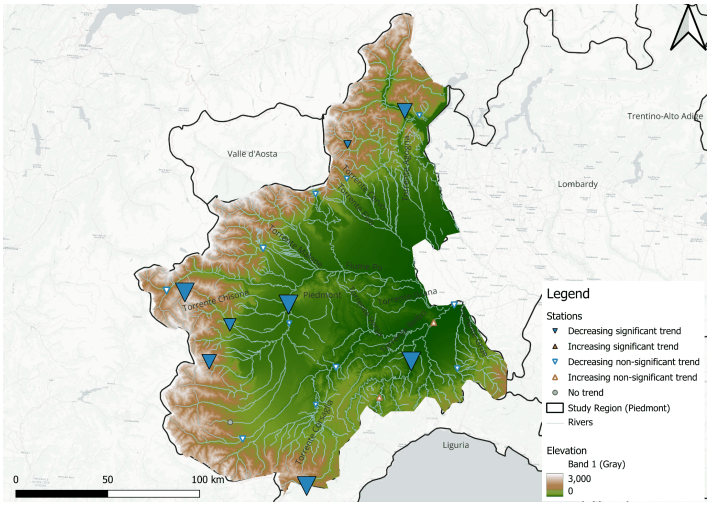

(b) September minimum

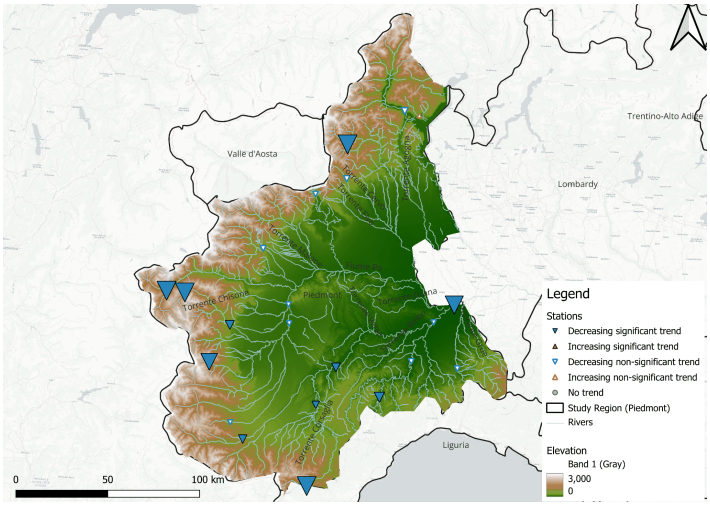

(c) September maximum

Figure A.12: Mann–Kendall test statistic for September discharge across the study area. Positive values (red) indicate increases; negative values (blue) indicate decreases. Triangle size is inversely proportional to the p-value (larger symbols indicate stronger significance).

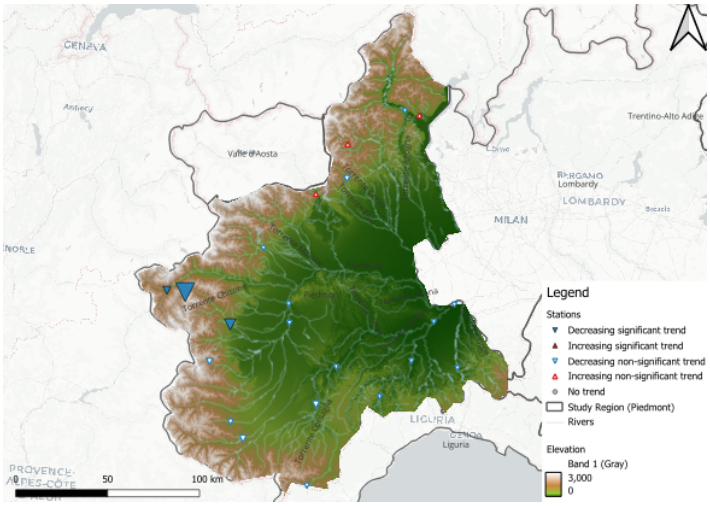

(a) October mean

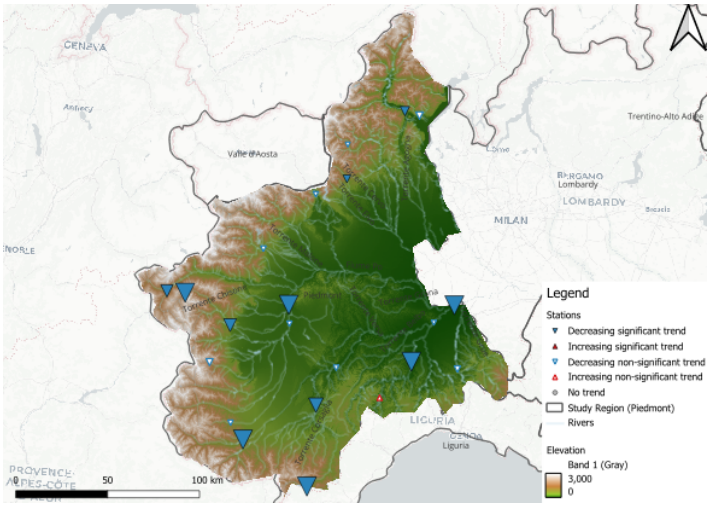

(b) October minimum

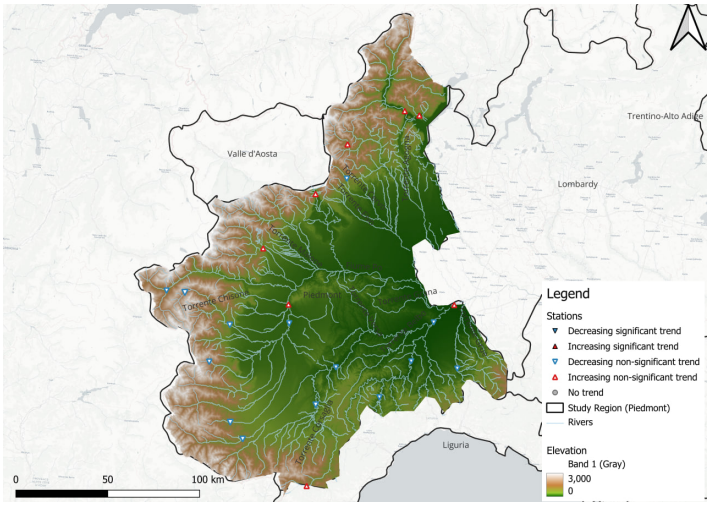

(c) October maximum

Figure A.13: Mann–Kendall test statistic for October discharge across the study area. Positive values (red) indicate increases; negative values (blue) indicate decreases. Triangle size is inversely proportional to the p-value (larger symbols indicate stronger significance).

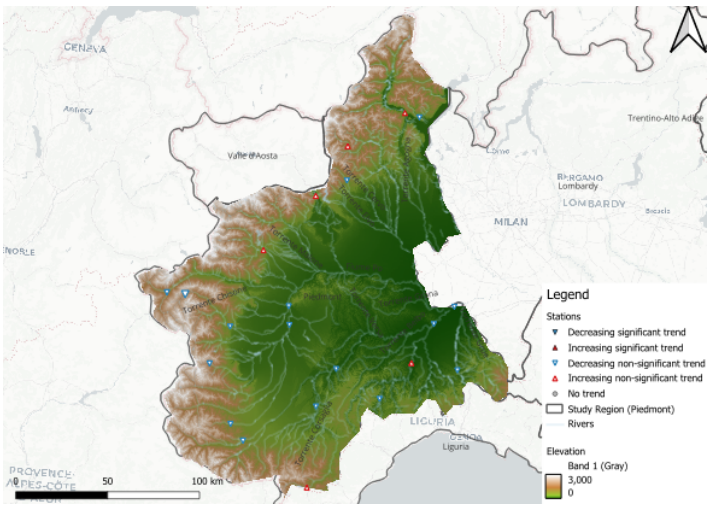

(a) November mean

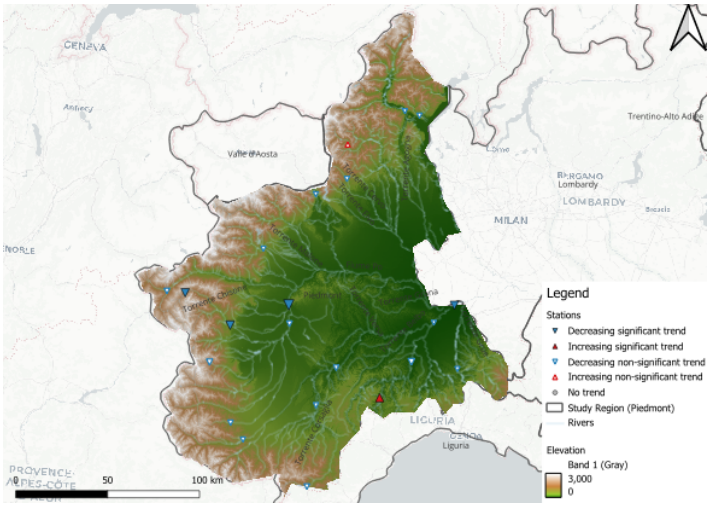

(b) November minimum

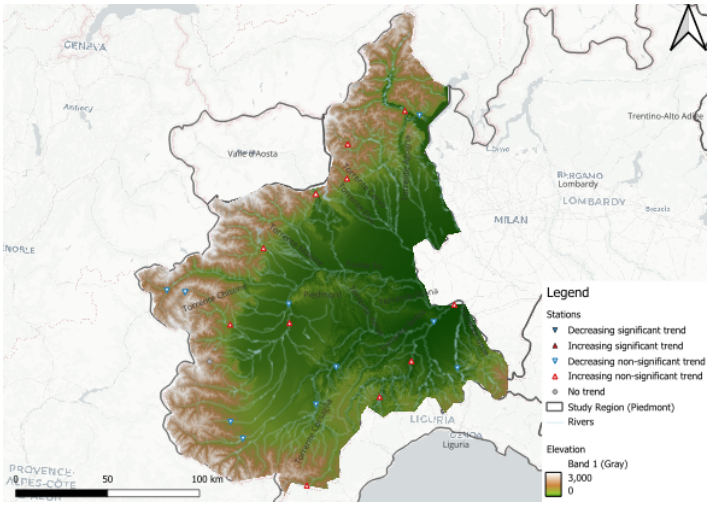

(c) November maximum

Figure A.14: Mann–Kendall test statistic for November discharge across the study area. Positive values (red) indicate increases; negative values (blue) indicate decreases. Triangle size is inversely proportional to the p-value.

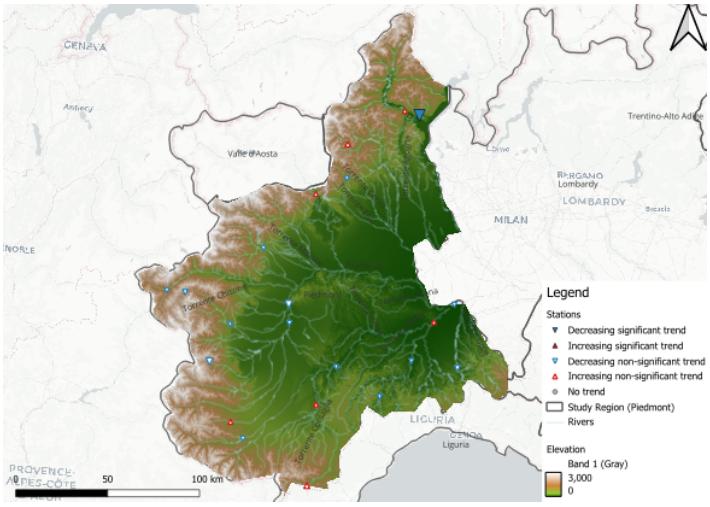

(a) December mean

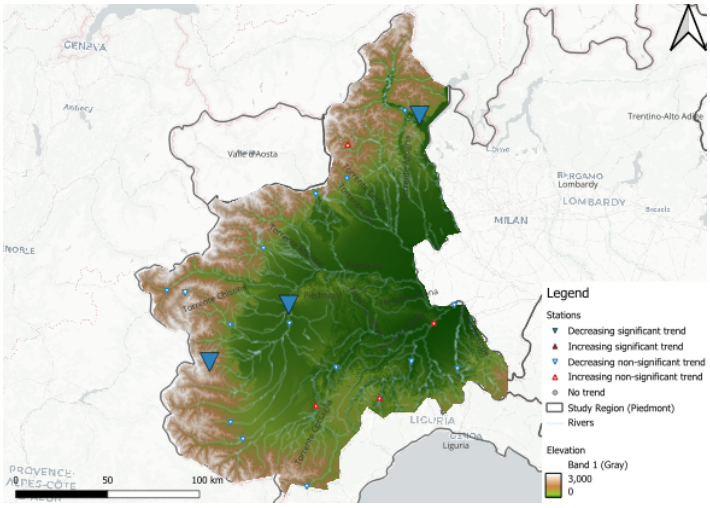

(b) December minimum

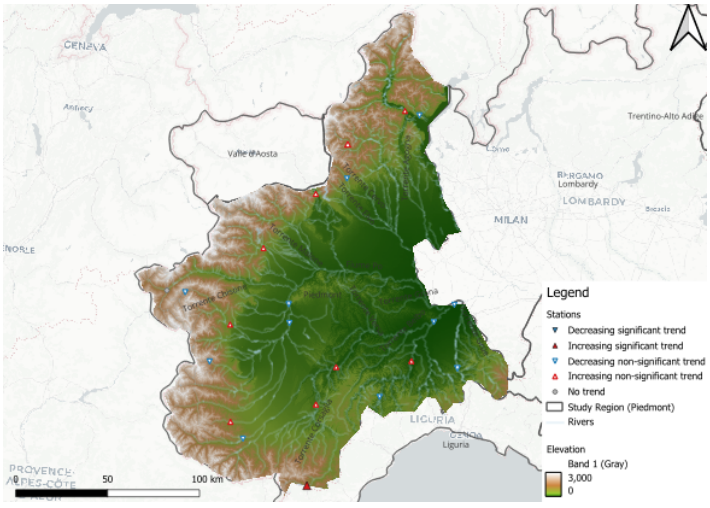

(c) December maximum

Figure A.15: Mann–Kendall test statistic for December discharge across the study area. Positive values (red) indicate increases; negative values (blue) indicate decreases. Triangle size is inversely proportional to the p-value.